



Technische Universität München
Fakultät für Medizin

The entthesis: nature's solution to a hard-soft interface

Lara Angelika Dorothee Kuntz

Vollständiger Abdruck der von der Fakultät für Medizin der Technischen Universität
München zur Erlangung des akademischen Grades eines

Doktors der Naturwissenschaften (Dr. rer. nat.)

genehmigten Dissertation.

Vorsitzender: Prof. Dr. Gil G. Westmeyer

Prüfende der Dissertation:

1. apl. Prof. Dr. Rainer Burgkart
2. Prof. Dr. Andreas Bausch
3. Prof. Dr. Felix Eckstein

Die Dissertation wurde am 10.05.2017 bei der Technischen Universität München
eingereicht und durch die Fakultät für Medizin am 21.02.2018 angenommen.

Prefix

This dissertation was part of the biomaterials focus group project “The entheses: Nature’s solution to a hard-soft junction“ funded by the International Graduate School of Science and Engineering (IGSSE) of the Technical University of Munich. It was a collaborative project between the Technical University of Munich Clinics of Orthopedics/Sports Orthopedics and the Chair of Cellular Biophysics.

Herewith I would like to thank everybody who contributed to this thesis directly or indirectly. It was a very lively, interesting time and many have contributed to it being fun and productive. I thank my advisors Professor Rainer Burgkart and Professor Andreas Bausch for supervision and guidance. Thank you, Rainer, for keeping me motivated to dig deep into the Achilles heel with your positive attitude and your passion for the entheses. Thank you, Andreas, for your scientific advice and for important lessons for life. Thank you both for giving me the freedom to develop project ideas on my own, yet giving me guidance and direction when I felt stuck. I have learned very much on the scientific as well as personal level from both of you.

I would like to thank my colleagues from the orthopedic research lab as well as the biophysics lab for a great working environment. Especially, I thank Jutta Tübel, Carmen Marthen, Peter Föhr, and Constantin von Deimling for a great and warm working atmosphere. I thank Leone Rossetti for showing me how to cook Italian style pasta and for great scientific collaboration. We tackled the entheses together¹ and I greatly appreciate what we learned from each other. Many thanks to Elena Kunold and Jonathan Schock for helping me with their expertise in mass spectrometry and computed tomography, respectively. I learned very much during the work side by side with you and the collaboration greatly fostered the entheses project. I would like to acknowledge my working students Elena Vehns and Katharina Kümpel. Thanks to Almut Glinzer for proofreading my thesis and for many fun lunch breaks in the clinics.

Further, I would like to acknowledge the International Graduate School of Science and Engineering (IGSSE) for their support. I greatly benefitted not only from the funding, but also from many interesting seminars that were offered.

Lastly and very importantly, thanks to my family and Philipp for their loving care, encouragement, and support.

Summary

Designing resilient interfaces between mechanically dissimilar materials is very challenging; high stress concentrations occur at these hard-soft interfaces resulting in their susceptibility to rupture^{2,3}. Especially hard-soft interfaces that are loaded in different directions undergo extraordinary high mechanical demands. Tackling the challenge of creating resilient hard-soft interfaces plays a role in all disciplines, in which interfaces between mechanically dissimilar materials occur. These are, for example, junctions between bone and tendon/ligament tissue in orthopedic surgeries or junctions between steel and concrete in mechanical engineering. Biomimicry is an emerging field that aims to learn from and imitate nature's solution to complex challenges. Biomimicry is a promising approach to the design of resilient hard-soft interfaces.

The musculoskeletal system exhibits hard-soft material junctions that are highly interesting with regard to biomimicry of hard-soft interfaces. The insertion site between Achilles tendon and bone, named Achilles tendon enthesis, is an outstandingly resilient hard-soft interface and bears high tensile load. It exhibits a complex tissue organization that allows for stress transfer between mechanically dissimilar materials⁴. Biomimicry of the Achilles tendon-bone interface's outstanding properties is a promising approach to design attachment sites between mechanically dissimilar materials. This thesis aimed to characterize this outstanding biological hard-soft interface to provide guidelines and design criteria for biomimicry of hard-soft interfaces.

A broad spectrum of characterization methods was used to analyze the biomolecular key structures of the Achilles tendon enthesis using pig as animal model. Firstly, the structural arrangement of fibers at the tendon-bone interface was investigated using scanning electron microscopy, confocal microscopy, and high-resolution micro-computed tomography. A geometrical transition of fibers was observed at the interface region between tendon and bone. Thicker tendon fibers with a diameter of $(105 \pm 21) \mu\text{m}$ splayed and subdivided into thinner interface fibers with a diameter of $(13 \pm 4) \mu\text{m}$ before attaching to bone. Wave-like crimp pattern of fibers was observed within the tendon region, but not within the interface region. Secondly, the molecular composition of the enthesis' extracellular matrix was analyzed using confocal microscopy, tandem mass spectrometry, and energy dispersive X-ray spectroscopy. Confocal microscopy showed that there was not only a geometrical transition of fibers, but also a compositional transition of fibers; the predominant composition of fibers was collagen type I in the tendon region and collagen type II in the interface region with splayed

fibers. A chemical difference of interface region and tendon was indicated by different X-ray absorption properties using micro-computed tomography. Tandem mass spectrometry revealed the full complexity of enthesis and tendon extracellular matrix proteomes. More than 400 proteins were detected in total, of which 26 proteins were statistically significant enriched in tendon and 22 proteins in the enthesis. Histology indicated that the tendon region contained adipose depots while the interface region did not.

Thirdly, morphological differences were observed between interface cells and tendon cells. Enthesis cells were characterized and biomarkers were identified using next generation sequencing. Due to the identification of many cartilage-like molecules within enthesis in the proteome study, in the transcriptome analysis enthesis was not only compared to tendon, but also to cartilage. Transcriptomics identified 34468 transcripts in total in enthesis, tendon, and cartilage. The transcriptome comparisons identified 3980 differentially regulated candidates for enthesis and tendon, 395 for enthesis and cartilage, and 946 for cartilage and tendon. Comparison of transcriptomes and proteomes of enthesis and tendon identified biomarkers that were statistically significant at least twofold upregulated on transcript level and protein level. Ten biomarkers were identified for enthesis and six biomarkers for tendon. Additionally, two applied tissue engineering approaches for musculoskeletal hard-soft interfaces were investigated. Firstly, cartilage regeneration using fibrin scaffolds was histologically analyzed using immunofluorescence. Secondly, decellularization of entheses as scaffolds for tissue engineering was evaluated.

Here, biomolecular key structures of the tendon-bone interface were identified such as the compositional transition of fibers as well as the geometrical transition which reduces tensile stresses at the interface. The matrix protein composition of the tendon-bone insertion was characterized and several proteoglycans were detected with crucial function for compressive stress reduction. Biomarkers of enthesis cell differentiation were identified to provide guidelines for enthesis tissue engineering. Further, a first step towards application of tissue engineering approaches was taken with decellularization of enthesis scaffolds and end-point determination of cartilage scaffolds. The presented data provide deep insights into the nature of an outstanding biological hard-soft interface and pave the way for biomimetic approaches to hard-soft interfaces.

Content

1. Introduction	1
1.1. Hard-soft interfaces	1
1.2. Biomimicry	2
1.3. Outstanding examples of biological hard-soft interfaces	3
1.3.1. Entheses	3
1.3.2. Cartilage	5
1.4. The extracellular matrix	5
1.4.1. Tendon extracellular matrix	6
1.4.2. Collagens	6
1.4.2.1. Fibril-forming collagens	9
1.4.2.2. Fibril-associated collagens with interrupted triple helices	9
1.4.2.3. Network-forming collagens	9
1.4.2.4. Collagen cross-links	9
1.4.2.5. Diversity of fibril structure in cartilage and tendon	11
1.4.3. Proteoglycans	11
1.5. Tissue regeneration and tissue engineering	12
1.6. Motivation	13
2. Materials and Methods	15
2.1. Enthesis sample preparation for imaging and elemental analysis	15
2.2. Confocal microscopy	15
2.2.1. Immunofluorescence labeling	16
2.2.2. Cell labeling	16
2.2.3. Calcium labeling	16
2.2.4. Confocal imaging	17
2.3. Widefield transmitted light microscopy	17
2.4. Electron microscopy	17
2.5. Energy dispersive X-ray spectroscopy	18
2.6. Computed tomography	18
2.6.1. Micro-computed tomography	18
2.6.2. High-resolution micro-computed tomography	19
2.7. Proteome analysis	19
2.7.1. Sample preparation	19
2.7.2. LC-MS/MS	21
2.7.3. Peptide and protein identification and quantification	21
2.8. Transcriptome analysis	22
2.8.1. RNA extraction	22
2.8.2. RNA quality check	23
2.8.3. Next generation sequencing	24
2.8.4. Bioinformatics	24
2.9. Functional classification	25
2.9.1. Functional classification using PANTHER gene ontology	25
2.9.2. Functional classification with DAVID bioinformatics resources 6.8	25
2.9.3. Network prediction using STRING	25
2.10. Interface tissue engineering: cartilage regeneration	26
2.10.1. Sample preparation	26
2.10.2. Histochemistry	26
2.10.2.1. Hematoxylin and Eosin	26

2.10.2.2. Safranin O.....	27
2.10.3. Immunofluorescence	27
2.10.4. Imaging	28
2.11. Interface tissue engineering: enthesis decellularization.....	28
3. Geometrical transition of fibers at the enthesis	29
3.1. Fiber splaying	29
3.2. Fiber crimping.....	31
3.3. Discussion	31
4. Compositional transition at the enthesis	35
4.1. Compositional transition of fibers	35
4.2. Matrix composition at the enthesis.....	36
4.2.1. X-ray absorption at the interface.....	36
4.2.2. Proteome composition of the enthesis.....	37
4.2.2.1. Proteins in the interface region	41
4.2.2.2. Proteins in tendon.....	44
4.2.3. Calcium distribution at the enthesis	46
4.3. Fat distribution	49
4.4. Interface schematic.....	50
4.5. Discussion	52
5. Cell differentiation at the enthesis.....	57
5.1. Morphological characteristics.....	57
5.2. Transcriptomics	59
5.2.1. Transcriptome comparison of enthesis and tendon	62
5.2.2. Transcriptome comparison of enthesis and cartilage.....	68
5.2.3. Transcriptome comparison of cartilage and tendon	72
5.2.4. Biomarkers of the interface region.....	74
5.3. Discussion	77
6. Regeneration of hard-soft interfaces.....	83
6.1. Cartilage regeneration in vivo using fibrin scaffolds	83
6.2. Enthsis regeneration using decellularized scaffolds	85
6.3. Discussion	87
7. Outlook.....	91
8. References	93
9. Appendix	101
9.1. Identified transcription factors and growth factors	101
9.1.1. Enthsis	101
9.1.2. Tendon.....	105
9.1.3. Cartilage.....	108
9.2. Biomarker differences between proteome and transcriptome.....	110
9.3. Buffers and Solutions.....	112

9.3.1. Phosphate Buffered Saline (PBS, 10x).....	112
9.3.2. Phosphate Buffered Saline – Tween® 20.....	112
9.3.3. Decalcification Solution	112
9.4. Antibody list	113

Abbreviations

Abbreviations

μCT	micro-computed tomography
3D	three-dimensional
a.u.	arbitrary units
ADAMTS	a disintegrin and metalloproteinase with thrombospondin motifs
ADP	adenosine diphosphate
BCA	bicinchoninic acid
CCD	charge-coupled device
DAPI	4',6-diamidino-2-phenylindole
DMSO	dimethyl sulfoxide
DNA	deoxyribonucleic acid
DTT	dithiothreitol
ECM	extracellular matrix
EDS	energy-dispersive X-ray spectroscopy
EDTA	ethylendiamintetraessigsäure
FACIT	fibril-associated collagen with interrupted triple helices
FDR	false discovery rate
FPKM	fragments per kilobase of transcript per million mapped reads
GAG	glycosaminoglycan
GO	gene ontology
HE	hematoxylin and eosin stain
HEPES	4-(2-hydroxyethyl)-1-piperazineethanesulfonic acid
IgG	immunoglobulin G
IgM	immunoglobulin M
LC-MS/MS	liquid chromatography tandem mass spectrometry
MSC	mesenchymal stem cells
NA	numerical aperture
PBS	phosphate buffered saline
pH	potential of hydrogen
QC	quality check/quality checked
RNA	ribonucleic acid
Rpm	revolutions per minute
RT	room temperature
SDS	sodium dodecyl sulfate
SLRP	small leucine-rich proteoglycan
STRING	search tool for the retrieval of interacting genes/proteins
TEAB	tetraethylammonium bromide

1. Introduction

1.1. Hard-soft interfaces

Engineering junctions between dissimilar materials such as functionally graded materials is very challenging due to the complexity of these material systems^{3,5}. When load is applied, a soft material undergoes more deformation (strain) than a more rigid material. At an interface between a hard and a soft material, a sudden jump occurs between the levels of strain within the tissues, namely high strain in the soft tissue and low strain in the hard tissue. The occurring non-uniform deformation between the two materials causes local interfacial stress singularities that may lead to crack propagation and failure⁶. Theoretically, the difference in strain levels of the two tissues results in a divergence of the stresses. Simulations of hard-soft interfaces with smooth, direct, or compliant attachment show the effect of the attachment type on the mechanical response (Figure 1). The three different types of interface regions referred to are firstly an interface region with gradual transition of elastic moduli between the hard and soft regions (smooth), secondly an interface region with direct hard-soft attachment that occurs abruptly (direct), and thirdly an interface region with lower stiffness than the hard and soft materials (compliant).

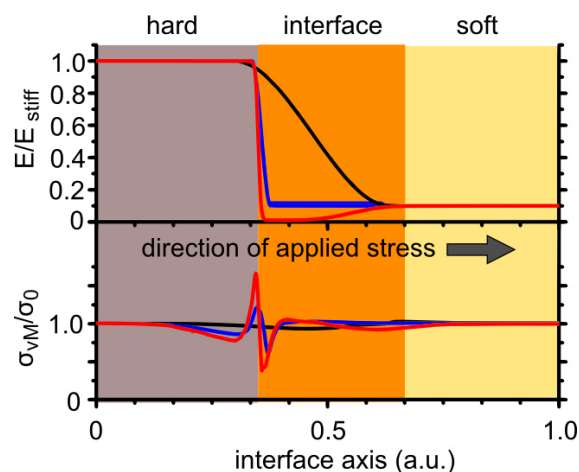


Figure 1: The mechanical response of a hard-soft interface was simulated using a continuum model. The upper plot shows elastic moduli of three different attachment types, a smooth attachment (black), a direct attachment (blue), and a compliant attachment (red). The lower plot shows von Mises stress for the corresponding interfaces under equal stress σ_0 . Interface axis is shown in arbitrary units. Courtesy of Leone Rossetti.

Since interfaces between mechanically dissimilar materials are prone to stress concentrations, the failure risk is increased⁶. The interfacial material property mismatch raises challenges with regard to stiffness, strength, and fracture behavior of the interface². Junctions between dissimilar materials can be realized by either changing material properties stepwise from one material to the other or by gradual variation of the properties such as in functionally graded materials². To successfully design sophisticated materials such as functionally graded materials, a comprehensive approach is needed which incorporates their micro-mechanical behavior as well as structure⁵. Various biological systems show graded interfaces which offer potential for biomimetic approaches to designing functionally graded materials^{5,7,8}.

1.2. Biomimicry

Biomimicry refers to biologically inspired design of materials by mimicking technically or scientifically interesting features that are found in nature, such as the lotus effect⁹. It involves deep understanding of outstanding biological functions, structures, or principles and transferring these to diverse commercial applications⁹. Biomimicry and bioinspiration are multidisciplinary approaches and promising tools to design innovative materials and systems¹⁰. Many materials found in nature have evolutionary evolved sophisticated features, such as highly hierarchical organization, resistance to environmental stresses, and adaptability¹⁰. Understanding these building principles and reproducing them to build bioinspired high-performing materials will greatly foster material science¹⁰. However, biomimetic approaches require interdisciplinary elucidation of the basic building principles to fully understand the chemical, biological, and physical properties¹⁰.

One outstanding feature of materials from nature is their efficient organization in which function and structure are optimized at different length scales¹⁰, such as fibrillary collagen that is highly aligned from nanoscale molecules to microscale fibers. It is not only the composition, but also the structure and function that determine tissue complexity. For example, the protein collagen type I holds different structural organization in different tissues to perform different functions¹⁰. It assembles to form rigid tissue in bone, elastic tissue in tendon, and transparent tissue in cornea¹⁰.

Strategic biomimicry has evolved in various fields, such as in the field of musculoskeletal regeneration, where seamless integration of bone with soft tissues such as tendon or cartilage are essential to restore tissue function¹¹. Functional assembly of these tissue-tissue

junctions depend on integration via interface regions that show spatial changes in cell phenotype, matrix composition, organization, and mechanical properties¹¹. As one understands the underlying structural and functional features, one can begin to use them for medical or technical applications⁹. However, current approaches have many limitations and the key structures that are needed to mimic the native structure-function relationship have yet to be identified¹¹. Thus, deeper understanding of the tissues is needed to successfully apply biomimetic approaches¹².

1.3. Outstanding examples of biological hard-soft interfaces

A wide variety of interfaces between mechanically dissimilar materials is found in nature². Particularly, the musculoskeletal system is rich in material junctions that are highly interesting with regard to biomimicry of hard-soft interfaces. These musculoskeletal material interfaces transfer load between a hard tissue – bone – and a soft tissue – for example tendon – through a complex material interface with distinct properties in composition, tissue architecture, and biomechanics. Two of these musculoskeletal material interfaces, entheses and cartilage, are described in the following paragraphs 1.3.1 and 1.3.2, respectively.

1.3.1. Entheses

Entheses are the attachment sites of tendon or ligament to bone¹³. They are highly specialized tissues that allow force transmission between two mechanically dissimilar materials. The rope-like, flexible tendon has a tensile modulus of 200 MPa¹⁴ and bears high tensile loads¹⁵, whereas the rigid, stiff bone has a tensile modulus of 20 GPa¹⁴ and resists high compressive loads¹⁵. To cope with the stress concentrations that occur at this bimaterial junction, the enthesis features a transitional tissue with graded biomolecular properties¹⁴. Tendon entheses have been histologically categorized into two types: fibrous entheses and fibrocartilaginous entheses¹⁶.

Fibrous entheses occur over large areas and typically have perforating mineralized collagen fibers⁴, often called “Sharpey’s fibers”. Sharpey’s fibers have been considered to occur in fibrous entheses, but not fibrocartilaginous entheses¹⁶. However, their nature and localized occurrence is still under debate¹⁶.

Fibrocartilaginous entheses are clinically more relevant and include insertion sites such as of the rotator cuff, anterior cruciate ligament and of the Achilles tendon¹⁵. Traditionally, fibrocartilaginous entheses have been described as to consist of four zones – tendon (I), uncalcified fibrocartilage (II), calcified fibrocartilage (III), and bone (IV)^{16,19}. Figure 2 depicts a histological image of an enthesis. The first zone consists of hierarchically organized, aligned collagen type I fibers. Additionally, non-collagenous extracellular matrix proteins have been suggested to play an important role in withstanding compressive and tensile stresses that arise during tendon load²⁰. The second zone consists of fibrocartilaginous proteins, such as collagens type II and III and proteoglycan aggrecan. The cells in fibrocartilage regions show a rounder morphology than cells in the tendon¹⁶. Zone III consists of fibrocartilage which is stiffened with mineral deposits. Zone II and III are proposed to be avascular zones that are separated from each other by a tidemark¹⁶. The tendon fibers continue across the tidemark which is the calcification front¹⁶. The fourth zone, bone, consists mainly of mineralized type I collagen¹⁶. It has been suggested that the fibrocartilaginous zone functions to balance the different elastic moduli of tendon and bone¹⁶. Interdigitation of bone and tendon may result in greater toughness of the interface²¹.

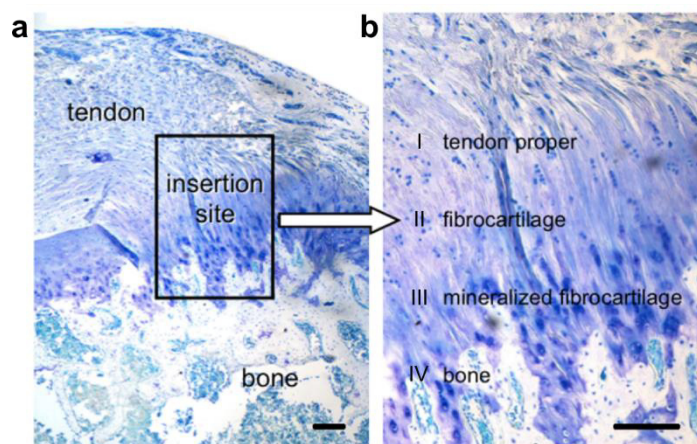


Figure 2: The tendon-bone insertion is characterized by a fibrocartilaginous transition site. a, Supraspinatus tendon-bone insertion stained with toluidine blue. b, Zoom of insertion site. Scale bars correspond to 200 μm . Figure adapted, with permission, from¹⁷. Images were originally published in¹⁸.

Recently, the four tissue regions have been proposed to be structurally continuous⁴. Extracellular matrix composition as well as collagen fiber orientation showed gradation across the enthesis rather than abrupt interfaces between four zones⁴. Mineral content increased across the insertion site from tendon to bone and aligned collagen fiber organization decreased^{15,22}. The fibrocartilaginous area was shown to be less stiff than tendon (~ 0.2 GPa) and bone (~ 20 GPa), but the structural features responsible for this compliant region are still not fully understood²². It has been reported that reduced collagen fiber alignment across the tendon-bone interface may lead to reduced stiffness. Furthermore, local variations in collagen fiber angle may affect load transfer from tendon to bone²³.

1.3.2. Cartilage

Cartilage is a resilient elastic tissue that is classified into three types; articular cartilage, hyaline cartilage, and fibrocartilage. Articular cartilage covers the surfaces of joints and provides a lubricated surface for joint movement²⁴. Articular cartilage is subjected to high mechanical demands since it has to transmit high forces within joints while ensuring low frictional wear²⁵.

Cartilage is avascular and depends on the perfusion of synovial fluids²⁶. It is maintained by the diffusion of nutrients through cartilage and across the joint surface²⁴. It has very low regenerative capacity²⁴. Cartilage is composed of a dense extracellular matrix that is rich in collagen, proteoglycans, and elastin²⁴. Cartilage is composed of four zones; the superficial zone, the middle zone, the deep zone, and the calcified zone²⁴. The superficial zone consists of tightly packed fibers of collagen types II and IX, which are parallel aligned to the cartilage surface²⁴. The middle zone is composed of high amounts of proteoglycans and thicker collagen fibrils that show an oblique organization²⁴. The deep zone comprises the thickest collagen fibrils and these are arranged perpendicular to the joint surface²⁴. The highest proteoglycan content is found in the deep zone²⁴. Aggrecan is the most abundant proteoglycan in cartilage and provides osmotic properties that enable compression resistance²⁴. The calcified cartilage zone is separated from the deep zone by a tidemark²⁴.

Chondrocytes derive from mesenchymal stem cells and they vary in morphology depending on the zone localization within cartilage²⁴. The cartilage cells, called chondrocytes, depict a flattened morphology in the superficial zone and a rounder shape in the middle zone²⁴. In the deep zone, the chondrocytes are arranged as columns that are perpendicular oriented to the joint surface²⁴. Their metabolic activity is low which results in the low regenerative capacity of cartilage^{24,26}. Trauma-related osteochondral defects may lead to chondrocyte necrosis and proteoglycan loss resulting in impairment of the cartilage which could potentially be regenerated using tissue engineering strategies²⁷.

1.4. The extracellular matrix

The extracellular matrix (ECM) has diverse tissue-specific functions and compositions. The cell microenvironments provided by the ECM regulate development and function of cells. Further, the ECM provides growth factors, hydration, and pH to ensure tissue maintenance²⁸. The diverse functions of the ECM in various tissues are achieved by its complex chemical compositions as well as structural tissue-specific organizations²⁸. ECMs can undergo remodeling to adapt to environmental stresses such as applied force²⁸. Tendon is a

rope-like tissue with sophisticated hierarchical architecture of its ECM. In the following paragraphs, some of the key components of the extracellular matrix will be introduced with a focus on tendon.

1.4.1. Tendon extracellular matrix

Tendons consist of fibrous, dense connective tissue and transmit forces from muscles to bone^{29,30}. The extracellular matrices of different tissues are uniquely composed and structurally organized²⁸. The distinct features of the ECM allow for the accomplishment of tissue-specific roles including force transmission and structural support²⁸.

The cells within tendon, tenocytes, are specialized fibroblasts that are mostly arranged in longitudinal rows between the fibers³⁰. Tenocyte markers include transcription factor scleraxis, tenomodulin, and tenascin-C. However, these markers are not specific for tendon, but also occur in other tissues³⁰. There is evidence that tendon cells respond to mechanical stimuli and that tendon adapts to use with regard to fiber diameter^{30,31}. Furthermore, tendons have relatively limited vascularization compared to muscle³¹. The vessels within tendons are small and run parallel to the fiber direction³⁰. Interestingly, tendons that wrap around bony pulleys show diminished vascularization in these regions³⁰.

The tendon ECM is primarily composed of collagen type I, elastin and proteoglycans³². Tendon has a distinct hierarchical structural organization (Figure 3) that facilitates the transmission of tensile forces and provides a scaffold for cell attachment^{28,32,33}. Briefly, collagen molecules are a triple helix consisting of three polypeptide α chains. The collagen molecules assemble into staggered microfibrils which bundle into fibers. Fibers group into fiber bundles, also called subfascicles, and the subfascicles assemble into fascicles^{28,30}. Endotenon, loose connective tissue, is present between fascicles and tertiary fiber bundles, which enables them to slide past each other³⁰. Sliding is not limited to higher hierarchical levels but also occurs between fibers³⁴. Fascicles bundle into tertiary fiber bundles and finally tendon, which is surrounded by a sheet of connective tissue that is called epitenon^{28,30}.

1.4.2. Collagens

Fibrous collagens are ubiquitous in all mammals and build the structural basis of connective tissues including bone and tendon³⁵. There are 27 unique collagen types^{36,37}, which belong to different collagen subfamilies, such as fibrillar collagens, network-forming collagens, and fibril-associated collagens with interrupted triple helices (FACIT)³⁸. The supramolecular organization of different collagens varies, but all collagens are trimers comprising one, two, or three distinct gene products of alpha chains³⁸. Table 1 displays a selection of collagen types

and the related features. Collagens mostly assemble into supramolecular structures either by themselves or involving other components of the extracellular matrix such as other collagen types³⁷.

Table 1: List of various collagen types adapted from^{36,39}.

Collagen Type	Subfamily	Chain composition	Tissue distribution (selection)
I	fibrillar	homotrimer or heterotrimer	widespread, e.g. bone, skin, tendon, cornea
II	fibrillar	homotrimer	cartilage, vitreous, enthesis
III	fibrillar	homotrimer	skin, intestine, uterus, vessel, enthesis
IV	network	heterotrimer	basement membrane
V	fibrillar	heterotrimer	widespread, e.g. bone, skin, cornea, placenta
VI	network	heterotrimer	widespread, e.g. bone, skin, cornea, cartilage, vessel
IX	FACIT	heterotrimer	cartilage, vitreous, cornea
X	network	homotrimer	hypertrophic cartilage
XI	fibrillar	heterotrimer	cartilage, intervertebral disc
XII	FACIT	homotrimer	skin, tendon, cartilage
XIV	FACIT	homotrimer	widespread, e.g. bone, skin, eye, tendon, cartilage

Interestingly, collagen type I shows very different patterns of tissue-specific organization, which may be explained by the fact that collagen-containing tissue suprastructures have complex macromolecular compositions which often not only involve other collagen types, but also non-collagenous components³⁸. These components play also a role in tissue architecture and function³⁸. One of these is small leucine-rich proteoglycan decorin. Decorin binds to collagen type I and is an important regulator of collagen fibrillogenesis, possibly by inhibiting lateral association of collagen molecules by its binding³⁵.

Collagen comprises three polypeptide chains, also called alpha chains (α), which form a triple helix⁴⁰. These α propeptides are left-handed peptide helices and consist of glycine- and proline-rich tandem repeats³⁷. Propeptides get hydroxylated at lysine as well as proline residues by lysyl hydroxylase and prolyl hydroxylase, respectively, for later cross-linking of the propeptides^{28,37}. Subsequently, hydroxylysines get glycosylated. Three post-translationally modified propeptides twist into a right-handed triple helix to form procollagen³⁷. Procol-

lagen is secreted into the extracellular space and then converted into tropocollagen molecules by enzymatical cleavage of the propeptides' C- and N-terminal ends³⁷. Subsequently, lysyl oxidase converts tropocollagen lysines and hydroxylysines into aldehyde groups that enable covalent cross-linking between tropocollagen molecules to form larger collagen aggregates³⁷. Tropocollagen molecules are 300 nm long and 1.5 nm wide³⁸. Tropocollagen molecules assemble to form collagen microfibrils (Figure 3), which arrange to form collagen fibers⁴¹⁻⁴⁴. In the fibrillar collagens, the molecules are staggered in D-periods (67 nm)^{44,45} that have an overlap region with five collagen molecules and a gap region with four collagen molecules in cross-section^{35,46}.

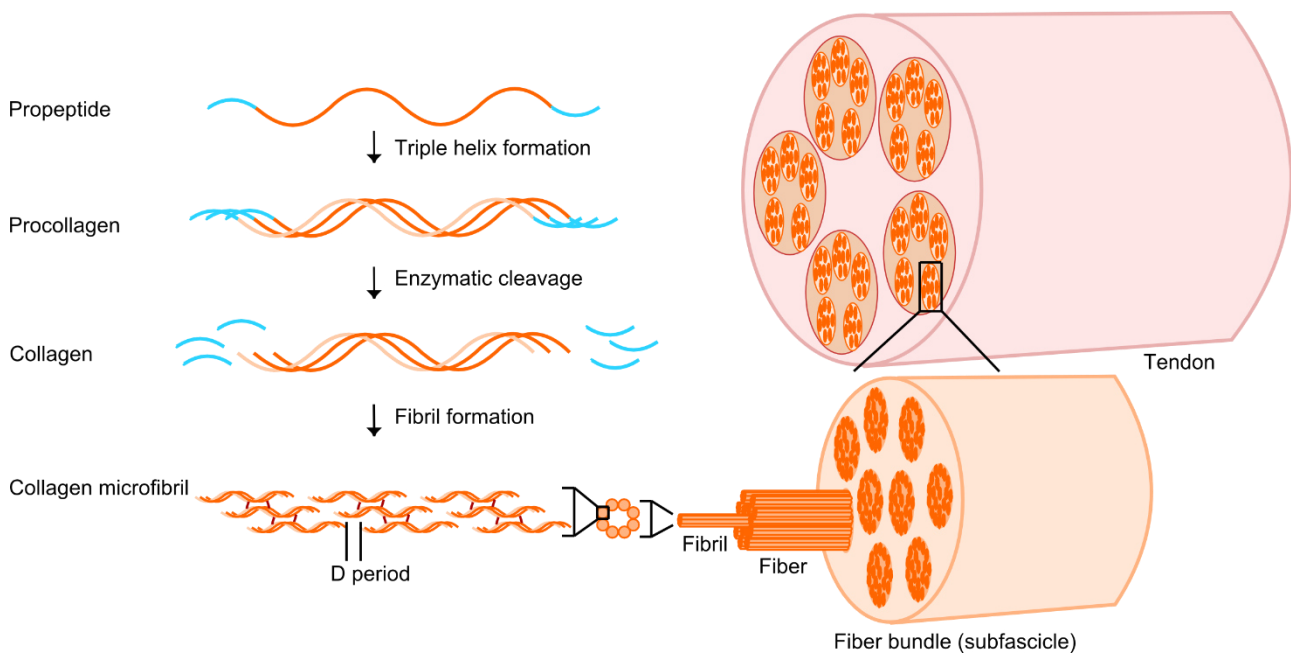


Figure 3: Fibrillar collagen assembly in tendon. Three propeptide chains assemble to form triple helical procollagen. Procollagen is secreted into the extracellular space where C- and N-terminal ends of procollagen are enzymatically cleaved. Collagen is staggered into banded microfibrils. The microfibrils are matured by intermolecular and intramolecular cross-linking of the collagen by lysyl oxidase to form fibrils. Fibrils are bundled to fibers and stabilized via interactions with other components of the extracellular matrix, such as fibril associated collagens with interrupted triple helices and small leucine-rich proteoglycans. Fibers are grouped into fiber bundles (subfascicles) which in turn are bundled into fascicles. The fascicles are assembled into tertiary fiber bundles that are bundled to form tendon. Adapted from^{28,38}.

1.4.2.1. Fibril-forming collagens

Fibril-forming collagens, such as type I, II, and III have a large triple helical domain and assemble into banded fibrils by staggering (Figure 4)³⁸. Collagen type II fibrils are much thinner than collagen type I fibrils, 35 nm compared to 100-200 nm, respectively⁴⁷. Collagen type I and collagen type II fibrils are similar in the 67 nm D-periodic fibril packing structure, but the molecular packing with regard to gap and overlap differs⁴⁷. Collagen type II fibrils exhibit more cross-linking binding sites than collagen type I fibrils⁴⁷. The different telopeptide conformations of collagen type I and II fibers suggests specific cross-linking binding patterns⁴⁷. The greater cross-linking potential of collagen type II may further result in greater capacity of forming network-like tissue structures⁴⁷.

1.4.2.2. Fibril-associated collagens with interrupted triple helices

FACITs, fibril-associated collagens with interrupted triple helices, are structurally diverse collagens that are found at the surface of collagen fibrils (Figure 4)⁴⁰. This subfamily includes collagen types IX, XII, and XIV. It has been proposed that selective expression of FACITs and their incorporation into collagen fibrils may be a mechanism to modify surface properties of collagen fibrils and their resulting biomechanical features³⁸. Some FACITs, for example collagen type IX, show incorporation of triple helical domains other than the FACIT domains into the collagen fibrils. This possibly occurs by antiparallel alignment with the fibrillar collagens³⁸. By becoming part of the fibril body, these FACITs are integral parts of molecular organization of the fibrils³⁸ (Figure 4).

1.4.2.3. Network-forming collagens

Network-forming collagens are important in the basal membrane and involve collagens, such as collagen type IV, VI, VIII and X. The suprastructures are diverse, for example arrangement as beaded fibrils, broad banded fibrils, or hexagonal lattices³⁸.

1.4.2.4. Collagen cross-links

Collagen's tensile strength and the stability of fibrils depend on covalent intermolecular cross-links between the collagen molecules^{47,48}. Covalent bonds between collagen molecules are formed from lysyl and hydroxylysyl sidechain aldehydes produced by lysyl oxidase⁴⁸. Different collagen type molecules cross-link heterotypically to assemble multi-component fibrils⁴⁸. The chemistry of cross-link variations seems to be more tissue-specific than collagen-type specific⁴⁸. Molecular packing constraints of collagen molecules by cross-linking play a role in structural organization of collagen fibers as well as the chemistry of the

links themselves⁴⁸. Collagen molecules have different cross-linking sites. For example, collagen type IX serves as template within composite fibrils and has seven known cross-linking sites for collagen types I, II or III. Of these cross-linking sites, two are located each in the $\alpha 1$ and $\alpha 2$ chains and three in the $\alpha 3$ chain⁴⁸. Further, three different lysyl hydroxylases exist in human that regulate collagen cross-linking. Lysyl hydroxylase 3 is proposed to have additional enzymatic cross-linking activity by acting as collagen galactosyl transferase and glucosyl transferase⁴⁹. Glycosylation of hydroxylysines changes the cross-linking pattern and is thus another regulatory step⁴⁸. Collagen type II molecules exhibit more cross-linking residues than collagen type I molecules possibly resulting in more stable network-like tissue organization⁴⁷.

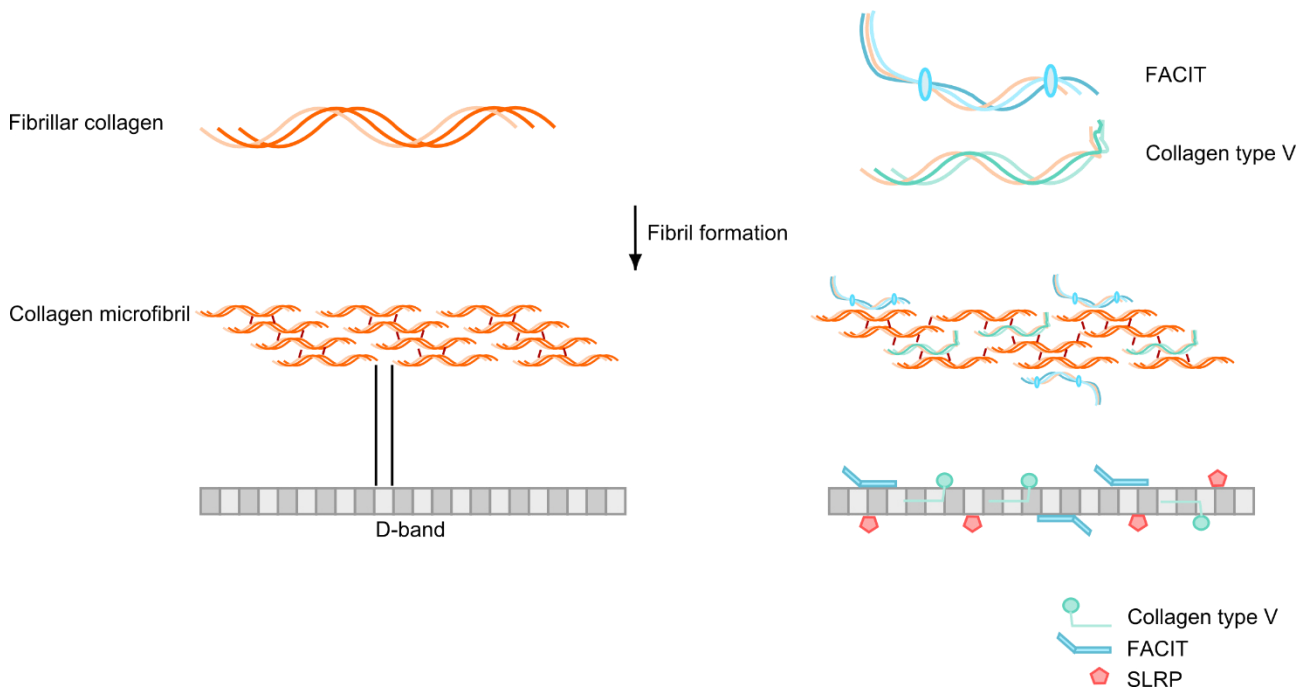


Figure 4: Collagen fibrils assemble from heterotypic components. Collagen fibrils are mostly heterotypically composed from fibrillar collagens such as collagen types I and II as well as other collagenous components such as collagen type V and IX. The triple helix of collagen type V is incorporated within the fibrils while the amino terminal region protrudes from the gap region and is present on the fibril surface. Fibril associated collagens with interrupted triple helices (FACIT) have non-collagenous regions that lead to kinks in the structure. FACITs and small leucine-rich proteoglycans (SLRP) stick to the surface of the fibrils and stabilize higher order structures. Adapted from^{28,38}.

1.4.2.5. Diversity of fibril structure in cartilage and tendon

Cartilage fibrils are the main tensile component and bear the swelling pressure that is generated by osmotic binding of water to negatively charged proteoglycans within the extracellular matrix³⁸. Their main component is collagen type II that usually occurs as macromolecular composite with other components such as collagen type IX and XI³⁸. Two types of fibrils have been described for cartilage. Firstly, thin fibrils with a diameter of 20 nm that are enriched in the territorial matrix that surrounds and separates chondrocytes³⁸. These fibrils are mostly oriented parallel to the chondrocyte surface. Secondly, wider fibrils with a range of diameters in the interterritorial matrix that are mostly parallel aligned to the long axis of the respective bone³⁸.

Tendon fibrils are oriented uniaxially and have very different diameters³⁸. They consist of mainly collagen type I and lower amounts of other components such as collagen types III and V³⁸. The fibril structure depends on the predominant collagen types as well as the incorporated biomolecules.

1.4.3. Proteoglycans

Proteoglycans are a heterogeneous group of macromolecules and are ubiquitous in the extracellular matrix⁵⁰. Proteoglycans are glycoproteins consisting of a large core protein with attached negatively charged glycosaminoglycan (GAG) chains²⁸. The GAGs, such as keratin sulfate, heparin sulfate, chondroitin sulfate, dermatan sulfate, and hyaluronan, are long, linear chains of disaccharide repeats and their negative charges lead to water binding within the tissue²⁸. Water binding by negatively charged GAGs provides a swelling pressure within the tissue that serves to reversibly absorb loading forces⁵⁰. Proteoglycans provide distinct biochemical and hydrodynamic features by enabling hydration and compressive resistance²⁸.

Small leucine-rich proteoglycans (SLRP) are a family of proteoglycans that have a conserved leucine-rich repeat motif^{28,51}. SLRPs consist of a small core protein to which 1-2 chondroitin or dermatan sulfate GAGs or several keratin sulfate GAGs are attached²⁰. SLRP can function as structural constituent of the ECM as well as signaling molecule by interacting with several different receptors⁵¹. SLRPs, such as decorin and biglycan, bind to collagen and play a role in regulating collagen fibril assembly (Figure 4)^{28,51}. They also interact with other ECM components, such as fibronectin or growth factors²⁰.

Large modular proteoglycans, also called lecticans or hyalectans, are a proteoglycan family that exhibits large protein cores as well as high amounts of attached chondroitin sulfate and

keratin sulphate chains²⁸. Hyalectans such as aggrecan and versican provide tissues with high resistance to compressive forces²⁰.

Interestingly, mechanical load influences proteoglycan expression in load-bearing tissues. Tensile load has been shown to induce decorin expression whereas compressive load induces expression of large proteoglycan aggrecan^{20,52}. Compressed tissues such as cartilage and enthesis have higher concentrations of GAGs than tendon, namely cartilage up to 55 × more GAGs and enthesis 17.5 - 20 × more GAGs than tendon²⁰.

1.5. Tissue regeneration and tissue engineering

Wound healing is the process in which tissue regenerates after injury. It is divided into several phases: hemostasis (blood clotting), inflammation, proliferation, and tissue remodeling. The first phase happens within minutes after injury and is characterized by blood platelets aggregating at the injured site to form a hemostatic plug⁵³. Fibrin gets activated and enables clot formation to prevent blood loss⁵³. Platelets release chemoattractants that induce cell migration to the injury site and promote inflammation⁵³. In the second phase, damaged cells as well as pathogens are phagocytosed by macrophages as part of the inflammatory response⁵³. In the proliferative phase, fibroblasts migrate into the wound site and deposit granulation tissue⁵³, which is rich in collagen type III and fibronectin. The granulation tissue is remodeled during the remodeling phase by replacement of collagen type III with stronger collagen type I, realignment of collagen fibrils along tensile axes, as well as apoptosis of unneeded cells.

The regenerative capacity of tendon and cartilage is limited. After surgical repair of injured tendon, the tissue mostly remains as disorganized scar tissue in which the tendon fibrils lack their parallel alignment¹⁴. Further, the molecular composition of tendon scar tissue is altered. Collagen type III levels are elevated after tendon injury and may have a role in tendon healing¹⁴. The mechanical properties of repaired tendons are impaired compared to uninjured tendon, presumably caused by the lack of physiological tissue structure and composition¹⁴. Connective tissue adapts to prolonged mechanical load with increased synthesis and turnover of matrix proteins, such as collagen⁵⁴.

There is much interest in regeneration of tissue interfaces that have low regenerative capacity such as cartilage²⁶ or tendon/ligament entheses¹⁵. Tissue engineering is a promising approach to tackle the challenge of repairing musculoskeletal tissues with low regenerative capacity¹⁵. However, tissue engineering is sophisticated due to the complex structure, microfunction, and composition of natural tissue extracellular matrices and several strategies

are conceivable. Firstly, biomimetic approaches that recapitulate the intricate structural and compositional features of the native tissue using a specially designed scaffold¹⁵. This could be an artificial biomaterial scaffold with graded properties seeded with autologous cells such as mesenchymal stem cells isolated from the bone marrow¹⁵. These bioengineered constructs could be composed of three-dimensional pore architectures, gels, or composite scaffolds and the ultimate goal would be to deliver cells and provide mechanical support to the respective regenerating tissue⁵⁵. Secondly, biological scaffolds composed of extracellular matrix from decellularized donor tissues are promising, since the regulatory cues for cell behavior may remain within the tissue⁵⁶. Approaches to use decellularized extracellular matrix from donor tissue for tissue repair have already been applied to heart valves⁵⁷, liver⁵⁸, and kidney^{59,60}. The key concept is to remove native cells (decellularization) from the extracellular matrix of a donor tissue using chemicals and physical treatment to produce a three-dimensional scaffold that preserves the native tissue structure. Subsequently, the scaffold is seeded with patient-derived cells (recellularization) from the patient who will receive the bioengineered tissue⁵⁹. Decellularized donor tissue scaffolds that are reseeded with autologous patient cells have potential for translation into the clinics⁵⁶.

To functionally regenerate hard-soft tissue interfaces using tissue engineering strategies, thorough understanding of the physiological structure and function of these interfaces is inevitable. Biomimetic approaches that utilize this knowledge are very promising for application to interface tissue regeneration.

1.6. Motivation

Biomimicry is an emerging field that aims in learning and imitating nature to solve complex challenges. Designing resilient interfaces between hard and soft materials is a common engineering challenge that may be solved by biomimicry. This thesis aims to understand how nature achieves highly functional junctions between hard and soft materials to pave the way for biomimetic strategies to design durable and resilient hard-soft interfaces. The focus was laid on the Achilles tendon enthesis, an outstanding biological hard-soft interface, to understand the biological solution to the attachment of hard and soft materials. By using a broad spectrum of advanced characterization methods, this thesis had three objectives: firstly, analysis of the structural arrangement of fibers at the tendon-bone interface; secondly, investigating the molecular composition of the distinct extracellular matrix of the enthesis; thirdly, characterizing the cells and their differentiation markers within the enthesis. Additionally, two applications with regard to tissue engineering of hard-soft interfaces were investigated. Firstly, regeneration of cartilage, which has evolved to endure high compressive

loads, using fibrin scaffolds. Secondly, decellularization of the Achilles tendon enthesis, which has biologically evolved to endure high tensile loads, as tissue engineering scaffolds. The new in-depth understanding of the Achilles tendon enthesis can be transferred to biomimetic approaches for the design of hard-soft interfaces, such as scaffold design for tissue engineering of tendon-bone interfaces.

2. Materials and Methods

Extracts of the materials and methods section were similarly published in our paper in *Nature Materials*¹.

2.1. Enthesis sample preparation for imaging and elemental analysis

Achilles tendon-bone insertion (enthesis) samples were dissected from porcine legs (n = 70) obtained from a local abattoir. Pigs (*Sus scrofa*) were 6 months old at slaughter. Skin and fat tissue was carefully removed and entheses samples were retrieved in the dimensions of ~ 4 cm Achilles tendon attached to ~ 1.5 cm of the calcaneus. Samples were frozen at - 20 °C in Dulbecco's Modified Eagle Medium (Sigma-Aldrich) or phosphate buffered saline (PBS, 9.3.1) and cut into sagittal 2 mm slices using a diamond coated band saw (Exakt 300CL). The obtained 2 mm thick sagittal entheses slices will be referred to as entheses slices.

For micromechanical analyses¹, entheses slices were visually inspected to ensure fully intact fibers ranging from the bone to the position where they would be clamped. These samples were stored in individual falcon tubes filled with PBS and frozen.

For confocal imaging and scanning electron microscopy, entheses slices were fixed in 4 % paraformaldehyde for 48 h and washed with water. Afterwards, the samples were partially decalcified using a custom-made decalcification solution (0.27 M citric acid / 0.1 M EDTA / PBS; as described in 9.3.3). Samples were incubated in decalcification solution for 4 to 6 weeks with continuous agitation. Needle puncture was used to assess whether the decalcification was sufficient for subsequent cryocut sectioning. Subsequently, decalcified entheses slices were cryocut sectioned into 7 µm or 200 µm thick sections for confocal imaging (2.2) and electron microscopy (2.4), respectively, using Cryo-Star HM 560V (ThermoScientific).

2.2. Confocal microscopy

Partially decalcified entheses slices (2.1) were cut into 7 µm thick cryocut sections and air-dried overnight. Cryocut sections were then stored at - 80 °C until use. Cryocut sections were thawed and air dried for 15 min. Subsequently, the sections were fixed in a mixture of 1:1 (vol/vol) acetone:methanol for 15 min and afterwards air dried for 15 min. Samples were rehydrated with phosphate buffered saline (PBS, pH 7.4) for 10 min. Immunofluorescence staining, staining for cells, and labeling of residual calcium were performed as described in 2.2.1, 2.2.2, 2.2.3, respectively.

2.2.1. Immunofluorescence labeling

Rehydrated samples were blocked with Dako ready-to-use Protein Block (Dako) for 30 min at room temperature (RT) in a humid chamber. Primary antibodies (both 1:1000 diluted in Dako Antibody Diluent diluted) to target collagen type I (Abcam ab90395) as well as collagen type II (Abcam ab34712) were applied. For double stainings, two primary antibodies were simultaneously applied by diluting them in the same volume of Dako Antibody Diluent. PBS was applied instead of primary antibody as negative control. Unspecific antibodies were applied as isotype controls; normal rabbit IgG (Peprotech), mouse IgM isotype (eBioscience), mouse IgG1k isotype (eBioscience). Subsequently, samples were incubated at 4 °C overnight in a humid chamber. Then, samples were rinsed in PBS-Tween® 20 (0.01 % Tween®) and incubated with secondary antibodies (1:200 diluted in PBS) Atto 647n anti-rabbit IgG (Sigma 40839), Alexa Fluor® 594 anti-mouse IgG (Dianova 115-587-003), or Alexa Fluor® 488 anti-mouse IgG (Dianova 115-545-062) at RT for 30 min. All primary and secondary antibodies are listed in Table 14. Additional labeling of cells or calcium residuals was performed as described in chapters 2.2.2 and 2.2.3, respectively. Subsequently, samples were washed with PBS-Tween® 3 x 5 min and PBS for 5 min. 2-3 drops of Fluorescence Mounting Medium (Dako) was applied to each cryocut section. Sample slides were covered with high precision microscope cover glasses (Marienfeld).

2.2.2. Cell labeling

Rehydrated unstained samples or priorly immunofluorescently labeled samples were stained for cells using SYTO® 13 (ThermoFisher Scientific) or Yo-Pro®-1 (ThermoFisher Scientific). SYTO® 13 or Yo-Pro®-1 were 1:1000 diluted in PBS and 70 µl dilution was applied per cryocut section. For larger samples, such as *enthesis slices*, volume was upscaled per sense of proportion. Samples were incubated for 20 min at RT in the dark. Subsequently, samples were washed with PBS-Tween® 3 x 5 min, washed in PBS for 5 min, and covered using Fluorescence Mounting Medium (Dako) and high precision microscope cover glasses (Marienfeld).

2.2.3. Calcium labeling

Rehydrated unstained cryocut sections or priorly immunofluorescently labeled samples were stained with 5(6)-FAM-RIS bisphosphonate (BioVinc) that binds to bone hydroxyapatite. Residual hydroxyapatite was labeled by incubation of the cryocut sections with 0.1 µM 5(6)-FAM-RIS bisphosphonate (diluted in PBS) for 20 min. Subsequently, samples were

washed with PBS-Tween® 3 x 5 min. Samples were then washed in PBS for 5 min and covered using Fluorescence Mounting Medium (Dako) in combination with high precision microscope cover glasses (Marienfeld).

2.2.4. Confocal imaging

Imaging was performed using an inverted laser-scanning confocal microscope (Leica TCS SP5) with a 63 x oil objective, NA = 1:4 (Leica HCX PL APO). Sample areas with up to the order of 80 mm² were imaged by acquiring tiles of sub-images. Stacks of images were acquired with 5-10 slices in z covering a thickness of 7-20 µm. Stacks were z-projected and the sub-images stitched by the Leica software. For all images the fluorescence signals of the fluorophores were detected as well as the reflection signal from the excitation laser. Images were analyzed using ImageJ⁶¹.

2.3. Widefield transmitted light microscopy

Enthesis cryocut sections (7 µm) were prepared as described in 2.1. Connective tissue was visualized using a Masson-Goldner's trichrome staining kit (CARL ROTH). Sections were stained for cells using a hematoxylin-eosin staining kit (CARL ROTH). Adipose tissue was stained using Sudan III (Merck) following the protocol of Romeis⁶². Images were acquired with a Zeiss AxioObserver Z1 and the Zeiss AxioVision software. MosaiX tile scan images were taken with a 5 x and 10 x Zeiss objective.

2.4. Electron microscopy

Partially decalcified entheses samples were cut into 200 µm cryocut sections (2.1) using cryostat Cryo-Star HM 560V (Thermo Scientific) and fixed overnight in 2.5 % (vol/vol) glutaraldehyde diluted in 0.1 M HEPES (pH 7.2). The sections were then treated with an ascending alcohol series; 2 x 15 min 50 % ethanol, 2 x 15 min 70 % ethanol, 2 x 15 min 80 % ethanol, 2 x 15 min 99 % ethanol. Samples were stored in 99 % ethanol until usage. Critical point drying was performed using Bal-TEC CPD 030 critical point dryer. Samples were transferred into the machine and covered with absolute ethanol. Ethanol was cooled to 8 °C and subsequently carefully exchanged to liquid carbon dioxide. When ethanol was completely replaced by carbon dioxide, heating to 31 °C at 75 bar was performed for critical point drying. Gaseous carbon dioxide was removed. Samples were then attached to a sample holder and gold-sputtered for 40 s at 40 mA using a BAL-TEC SCD 005 sputter coater. Imaging was then performed using a JEOL JSM-6060LV scanning electron microscope operated at 5 kV.

2.5. Energy dispersive X-ray spectroscopy

2 mm enthesis slices (2.1) were thawed at room temperature and fixed overnight in 2.5 % (vol/vol) glutaraldehyde diluted in 0.1 M HEPES (pH 7.2). An ethanol series was performed with 2 x 15 min each of 50 %, 70 %, 80 %, and 99 % ethanol. Samples were critical point dried using Bal-TEC CPD 030 critical point dryer as described in 2.4. Subsequently, samples were coat sputtered with BAL-TEC SCD 005 sputter coater. Scanning electron microscope JEOL JSM-6060LV was used for imaging and coupled to a Bruker AXS Mikroanalysis X Flash Detector 3001 for analyzing elemental distribution across the tendon-bone interface via energy dispersive X-ray spectroscopy (EDS). EDS mappings were performed at 30 kV for selected elements (Ca, P, C, O, S, N). Quantax 200 software Esprit 1.7 was used for mapping. Intensities over distance across the interface were analyzed using ImageJ⁶¹.

2.6. Computed tomography

Computed tomography was performed to investigate the structural arrangement of fibers at the Achilles tendon-bone interface. Computed tomography measurements were performed in collaboration with Jonathan Schock from the Technical University of Munich Chair of Biomedical Physics. Whole entheses were investigated using micro-computed tomography with a GE phoenix v|tome|x to obtain a resolution of ~ 30 μm (2.6.1) and smaller regions of interest were investigated using high-resolution micro-computed tomography with a Zeiss Xradia VersaXRM 500 to obtain a resolution of ~ 2 μm (2.6.2).

2.6.1. Micro-computed tomography

Porcine Achilles tendon bone interfaces were carefully dissected from pig legs that were obtained from a local abattoir. Entheses were prepared to preserve the full extent of tendon-bone interface and to have a dimension of 2 cm of attached bone and 4 cm of attached tendon. Samples were fixed in 4 % PFA for 48 h under agitation and then washed with tap water for 48 h under agitation. Soft tissue contrast was observed to be very low, so that no structural features could be observed. Therefore, samples were treated with Imeron[®] 300 contrast agent (Bracco) to enhance soft tissue contrast. Samples were placed in to falcon tubes filled with Imeron[®] 300 and vacuum was applied with an exsiccator vacuum pump (Vacuubrand) for 24 h at 1000 mbar to enhance tissue penetration. Samples were then washed in PBS 3 x 5 min and transferred into new 50 ml falcon tubes for data acquisition.

Data acquisition was performed using phoenix v|tome|x (GE) in dual acquisition mode. High energy mode x-ray micro-computed tomography was acquired at 160 kV, 180 μA (exposure

1000 ms, AV 3, Binning 1 x 1, Skip 1, Sensitivity 1000) in transmission mode with a voxel size $(32.67 \mu\text{m})^3$ and 1001 projections. Low energy scans were performed at 40 kV, 610 mA (exposure 5000 ms, AV 3). High energy and low energy data sets were normalized and subtracted to obtain dual energy data sets with the software GE phoenix datos|x 2.0. For rendering, Avizo Fire (Version 8:10, FEI Visualization) was used, imageJ⁶¹ was used for image analysis.

2.6.2. High-resolution micro-computed tomography

Achilles tendon enthesis samples were carefully dissected and cut into cubes with ~ 5 mm per edge using a diamond coated band saw (Exakt 300CL). Enthsis cubes were fixed in 4 % paraformaldehyde for 48 h under agitation and then washed in water for 5 h under agitation. Samples were transferred into contrast agent Imeron[®] 300. Vacuum (1000 mbar for 1 min) was applied to enhance tissue penetration. Subsequently, samples were incubated in Imeron[®] 300 overnight under agitation. Samples were washed in 70 % ethanol and stored in 100 % ethanol for measurement.

High-resolution micro-computed tomography was performed using a Zeiss Xradia VersaXRM 500 with an optical magnification of 4 and a 760 μm SiO₂ filter. 1601 projections were measured with an exposure of 30 s at 80 kV and 6 W. The sample-source distance was 40 mm and the sample detector distance 30 mm resulting in an effective voxel size of $(1.94 \mu\text{m})^3$. The CT acquisitions were reconstructed with the XMReconstructor (Version 10.7.3245) provided with the scanner, using dynamic ring artifact correction, automatic center shift correction and a reconstruction binning of 1. For rendering, Avizo Fire (Version 8.10, FEI Visualization) was used, imageJ⁶¹ was used for image analysis.

2.7. Proteome analysis

The highly complex matrix compositions of Achilles tendon and Achilles tendon enthesis were analyzed and compared in a proteome study. The proteome analysis was performed in collaboration with Elena Kunold from the Technical University of Munich Chair of Proteomics and Bioanalytics.

2.7.1. Sample preparation

Pig legs from ~ 6 months old pigs were obtained from a local abattoir (n = 12). Achilles tendon and interface region were excised and shock frozen in liquid nitrogen. Each tissue sample was entirely cut into 2 μm thick cryocut sections using Cryo-Star HM 560V (Thermo Scientific) to enhance tissue homogenization and protein extraction. Tissue cryocut sections

of each tissue sample were thoroughly mixed. To increase the number of biological replicates, pools of enthesis and tendon samples were produced by thoroughly mixing enthesis or tendon samples from three biological replicates each. In total, enthesis and tendon samples from three individual biological replicates were analyzed as well as three enthesis and tendon pools containing each three biological replicates. In total, enthesis and tendon samples from twelve pigs were measured.

Samples of tissue cryocut sections were collected in low bind Eppendorf tubes and lyophilized for 2 h at 1 mbar. Lyophilized cryocut sections of each sample were thoroughly mixed to ensure averaged sample composition and 30 mg of each tissue sample were ground with Precellys Ceramic Kit 2.8 mm in Peqlab Precellys 24 (6 × 5500 rpm × 20 s). Lysis was performed using 4 M guanidinium chloride in Ceramic Kit SK38 (6 × 5500 rpm × 20 s) and cooling on ice. After lysis, samples were centrifuged for 1 h at 17000 × g at 4 °C. Supernatants were transferred into low bind Eppendorf tubes and then centrifuged at room temperature (RT) for 5 min. BCA assays were performed to estimate protein concentrations of the sample supernatants. 85 µg protein per sample were reduced with 5 mM dithiothreitol (DTT) for 30 min at 56 °C. Samples were then alkylated with 14 mM iodoacetamide for 30 min at RT and 500 rpm centrifugation in the dark. Alkylation was quenched with 5 mM DTT at RT for 15 min and 500 rpm centrifugation. Samples were predigested at 1:100 enzyme:protein ratio with Lys-C for 2 h at 25 °C. Then, samples were 1:4 diluted with 50 mM TEAB. Trypsin digestion was performed at 1:100 enzyme:protein ratio and 25 °C overnight. Digestion was quenched by addition of formic acid to a pH of 3. Subsequently, samples were centrifuged for 3 min at RT and 16200 × g. For dimethyl labeling⁶³, supernatants were transferred to 50 mg SepPak C18 Cartridges. SepPak C18 columns (Waters) were equilibrated using 2 × 1 ml acetonitrile, 1 ml elution buffer (80 % acetonitrile, 0.5 % formic acid in ddH₂O) and 3 ml aqueous 0.5 % formic acid solution. Samples were then loaded on to columns and washed with 5 ml aqueous 0.5 % formic acid solution. Labeling was performed with 5 × 1 ml of the respective dimethyl labelling solution (light, intermediate or heavy). Light labeling solution was 30 ml NaBH₃CN, 0.2 % CH₂O, 10 mM NaH₂PO₄, 35 mM Na₂HPO₄, pH 7.5, intermediate labeling solution consisted of 30 mM NaBH₃CN, 0.2 % CD₂O, 10 mM NaH₂PO₄, 35 mM Na₂HPO₄, pH 7.5 and heavy labeling solution consisted of 30 mM NaBHD₃CN, 0.2 % ¹³CD₂O, 10 mM NaH₄PO₄, 35 mM Na₂HPO₄, pH 7.5. Labeled peptides were eluted with 3 × 250 µl elution buffer (80 % acetonitrile, 0.5 % formic acid in ddH₂O), mixed according to the label switches and dried using vacuum centrifugation.

2.7.2. LC-MS/MS

Peptides were analyzed using liquid chromatography tandem mass spectrometry (LC-MS/MS). Labeled samples were dissolved in 0.5 % formic acid and filtered using centrifugal filters (modified Nylon, 0.45 μm , low protein binding, VWR International). Nanoflow LC-MS/MS analysis was performed with an UltiMate 3000 Nano HPLC system (Thermo Scientific) coupled to an Orbitrap Fusion (Thermo Scientific). Samples were loaded on a trap column (Acclaim C18 PepMap100 75 μM ID \times 2 cm) and washed with 0.1 % formic acid (5 $\mu\text{l min}^{-1}$ flow rate) for 10 min. Subsequently, peptides were transferred to an analytical column (Acclaim C18 PepMap RSLC, 75 μM ID \times 15 cm) and separated using a 125 min gradient from 3 % to 40 % (120 min from 3 % to 25 % and 5 min to 40 %) acetonitrile in 0.1 % formic acid and 5 % DMSO at a constant flow rate of 200 nl min^{-1} . Sample peptides were ionized at 1.9 kV using a nanospray source and a capillary temperature of 275 $^{\circ}\text{C}$. Orbitrap Fusion was operated using a cycle time of 3 s in a top speed data dependent mode. Full scan acquisition (scan range of 300–1700 m/z) was performed in the orbitrap at a resolution of 120,000 (at $m/z = 200$). Automatic gain control was an ion target value of $4e5$. Monoisotopic precursor selection as well as dynamic exclusion of 60 s were enabled. Internal calibration was performed using the ion signal of fluoranthene cations (EASY-ETD/IC source). Intense precursors with intensities $\geq 5e3$ and charge states of 2 - 7 were selected for fragmentation. Isolation was performed in the quadrupole using a window of 1.6 m/z . Ions were collected to a target of $1e2$. Maximum injection time was 250 ms with “inject ions for all available parallelizable time” enabled (“Universal” method). Fragments were generated with higher-energy collisional dissociation and detected at a rapid scan rate in the ion trap.

2.7.3. Peptide and protein identification and quantification

Raw data was analyzed with MaxQuant software (version 1.5.1.2) and Andromeda as search engine. The search included carbamidomethylation of cysteines as a fixed modification as well as variable modifications oxidation of methionines and acetylation of protein N-termini. Trypsin was specified as the proteolytic enzyme with N-terminal cleavage to proline. Two missed cleavages were allowed. Precursor mass tolerance was set to 4.5 ppm, fragment mass tolerance to 0.5 Da. Searches were performed using the Uniprot database for *Sus scrofa* (taxon identifier: 9823, 20/02/2015) and second peptide identification option was enabled. False discovery rate determination was performed using a decoy database. Thresholds were set to 1 % both at peptide-spectrum match and protein levels. “ $I = L$ ”, “requantification” and “match between runs” options were enabled. Analysis of the resulting

proteingroups.txt - table was performed with Perseus 1.5.1.6. A total of six biological replicates (with dimethyl label switches) which included pooled tissue samples from 12 pigs were used for statistical analysis. Putative contaminants, reverse hits as well as proteins that were identified by site only, were removed. Rows were filtered to contain at least four out of six valid values per group. Normalized ratios were transformed using $\log_2(x)$ as well as normalized using z-score. The average values of technical replicates were calculated and a two sided one sample t-test with Benjamini-Hochberg false discovery rate (FDR) correction was used for calculating p-values. Proteins enriched ≥ 2 -fold were categorized by gene ontology (GO) analysis using the PANTHER classification system⁶⁴. Biological processes complete PANTHER over-representation tests (release 2015 – 04 – 30) with GO ontology database (released 2015 – 08 – 06) and *Homo sapiens* as reference list were used to analyze gene lists that showed statistically significant differences of at least twofold in the tissue proteomes.

2.8. Transcriptome analysis

To identify biomarkers of cells at the interface for tissue engineering approaches, a transcriptome study was performed. Gene expression patterns of cells present at the enthesis were characterized and compared with the gene expression profiles of cells present within the tendon. Since the proteome study identified cartilage markers within the extracellular matrix of the enthesis, the enthesis transcriptome was further compared to the transcriptome of cartilage cells.

2.8.1. RNA extraction

Pig legs of six months old pigs obtained from a local abattoir were dissected within 5 hours after slaughter. During the development phase of the protocol for extraction of high quality RNA from entheses, it became clear that it is absolutely crucial to extract the RNA from freshly slaughtered samples. Therefore, a special permit (“Ausnahmegenehmigung für die Verwendung von tierischen Nebenprodukten zu Lehr- und Forschungszwecken gemäß Art. 17 Abs. 1 VO (EG) Nr. 1069/2009“) was obtained by authority from the district veterinary office to receive samples directly after slaughter.

Enthesis tissue was excised directly from the interface region, Achilles tendon tissue was excised ~ 1.5 cm cranial of the interface and cartilage tissue was excised from cartilage of the tibial plateau. Care was taken to remove all fat tissue and paratenon before retrieving tendon biopsies. At the enthesis, tendon tissue was carefully removed as much as possible prior to taking enthesis biopsies. However, since the enthesis is not fully distinguishable

from the tendon without staining, tissue residuals possibly remain in enthesis samples. All enthesis tissue was excavated and pooled to reduce differences that may occur due to extraction from medial or lateral location. Tissue samples were transferred into cryotubes, covered with PBS, and shock frozen in liquid nitrogen.

Shock-frozen tissue samples were transferred into - 80 °C cold pre-cooled RNA/*later*®-ICE Frozen Tissue Transition Solution (ThermoFisher Scientific) to stabilize the RNA within the tissue. Samples with RNA/*later*®-ICE Frozen Tissue Transition Solution were incubated at - 20 °C for at least 16 h to ensure proper diffusion of the RNA stabilizing solution into the tissue. Afterwards, stabilized samples were entirely cut into 7 µm thick cryocut sections using a cryostat HM 560 (Thermo Scientific Microtom) at - 21 °C. Cryocut sections were then stored in RNA/*later*®-ICE Frozen Tissue Transition Solution until use. For RNA extraction, sample cryocut sections were taken out of the stabilizing solution and residual solution was quickly removed from the cryocut sections by dipping the sample onto a paper towel. For each extraction using a Qiagen RNeasy Fibrous Tissue Mini Kit, ~ 25 mg of cryocut sections per sample were suspended in 300 µl Buffer RLT containing β-mercaptoethanol according to the manufacturer's instructions. Samples with RLT buffer were transferred to 2 ml Eppendorf tubes containing one autoclaved stainless steel bead each (bead diameter 5 mm). Homogenization was performed with a TissueLyser LT at cycles of 2 x 2 min at 20 Hz, followed by 2 min at 30 Hz and subsequently 1 min at 40 Hz. If tissue was not sufficiently homogenized, samples underwent another homogenization cycle for 1 min at 40 Hz. Lysates were transferred into new microcentrifuge tubes and 590 µl RNase-free H₂O as well as 10 µl proteinase K solution were added and thoroughly mixed. Proteinase K digestion was incubated for 10 min at 55 °C. On-column DNase treatment was performed at 30 °C for 15 min and RNA extraction was performed according to manufacturer's instructions of the Qiagen RNeasy Fibrous Tissue Mini Kit. RNA was eluted twice in 30 µl RNase-free water and immediately frozen at - 80 °C.

2.8.2. RNA quality check

Integrity of extracted RNA was assessed during RNA extraction protocol development and for final RNA quality check prior to next generation sequencing. RNA integrity number (RIN) that quantifies RNA integrity was determined using an Agilent 2100 Bioanalyzer system (Agilent Technologies) and the RNA 6000 Nano Assay. Following the instructions of the Agilent RNA 6000 Nano kit, bioanalyzer electrodes were decontaminated before each measurement using RNase ZAP™ (Sigma-Aldrich). Agilent RNA nano Labchips® were primed with gel-dye mix that was produced following the protocol of the Agilent RNA 6000 Nano kit. RNA

samples and RNA ladder were heat-denatured for 2 min at 70 °C to minimize secondary structures. The chips were loaded following the manufacturer's instructions and subsequently vortexed at 2200 rpm using a vortex mixer MS3 (IKA). Loaded chips were transferred to the 2100 Bioanalyzer system and "Eukaryote Total RNA Nano Series" RNA assay was performed in combination with 2100 Expert Software (Agilent). RNA with RIN \geq 7 passed quality check for next generation sequencing. RNA extraction was performed on enthesis and tendon samples from nine pigs including 2-3 technical replicates with regard to RNA extraction. 3 pools each for enthesis samples and tendon samples and 2 pools for cartilage samples were produced by mixing RNA that passed quality check. Each pool consisted of RNA from three biological replicates and from 2-3 extractions per biological replicate. Overall, each of the 8 pools contained RNA from 5-9 different RNA extractions.

2.8.3. Next generation sequencing

Random primed cDNA libraries were produced and analyzed by GATC Biotech (ISO 17025 accredited). Poly(A)⁺ RNA was isolated from total RNA samples (2.8.2) and was fragmented. Fragmented mRNA was transcribed into random-primed cDNA library. cDNA synthesis was performed with random hexamer priming. Adaptors were ligated to cDNA strands and cDNA was amplified via polymerase chain reaction.

Single end cDNA sequencing was performed on a Genome Sequencer Illumina HiSeq next generation sequencing system in sequence mode HSHOV4 SR50. A total of 30 million single reads were performed with a read length of 1 x 50 base pairs.

2.8.4. Bioinformatics

The sequencing reads were aligned to the pig (*Sus scrofa*) reference genome Sscrofa10.2 (http://www.ensembl.org/Sus_scrofa/Info/Index) with annotations Sscrofa10.2.86 using Bowtie⁶⁵ generating genome alignments. TopHat identified potential exon-exon splice junctions of the initial alignment. Subsequently, Cufflinks identified and quantified the transcripts from the preprocessed RNA sequence alignment assembly. Cuffmerge merged the identified transcript fragments to full length transcripts. Then, full length transcripts were annotated based on the given genome annotations Sscrofa10.2.86. To determine differential mRNA expression levels, merged transcripts from enthesis, cartilage, and tendon samples were compared using Cuffdiff. Alternative splice variants as well as single nucleotide polymorphisms and insertion/deletion mutations were assessed based on existing gene models for eukaryotes.

2.9. Functional classification

Identified genes and proteins were classified using PANTHER gene ontology, DAVID bioinformatics resources 6.8., and networks were predicted with STRING database.

2.9.1. Functional classification using PANTHER gene ontology

Gene ontology (GO) analysis was performed using PANTHER Classification System^{64,66}. In the proteome study, PANTHER overrepresentation test for biological processes complete (released 2015-08-06) with GO ontology database (released 2015-08-06), Homo sapiens as reference list, and Bonferroni correction was performed for the lists of proteins enriched more than twofold in either enthesis or tendon. In the transcriptome study, PANTHER reactome pathways overrepresentation test (released 2016-07-15) with reactome version 58 (released 2016-12-07), Sus scrofa as reference list, and Bonferroni correction was used to categorize genes detected in the tissues for overrepresentation of reactome pathways. Overrepresentation of biological processes was investigated using PANTHER overrepresentation test (released 2016-07-15), PANTHER version 11.1 (released 2016-10-24) for slim biological process and GO ontology database (released 2016-12-28/2017-01-26) for biological process complete, Sus scrofa as reference list, and Bonferroni correction.

2.9.2. Functional classification with DAVID bioinformatics resources 6.8.

To identify candidates with transcription factor activity or growth factor activity, the Functional Annotation Tool of DAVID bioinformatics resources 6.8 (NIAID/NIH) was used⁶⁷. Lists of genes at least twofold enriched in one of the tissues were uploaded to screen ensemble gene IDs, official gene names and entrez gene IDs. Sus scrofa was used as background. For cartilage candidates with official gene names, Homo sapiens was used as background due to lack of annotation for Sus scrofa. Functional annotation tables were exported for GOTERM_MF_FAT. Functional annotation tables were manually screened to identify candidates with associated GO terms involving transcription factor activity or growth factor activity.

2.9.3. Network prediction using STRING

Interactions between growth factors and transcription factors identified with DAVID bioinformatics resources 6.8 Functional Annotation Tool were predicted using STRING Database^{68,69} version 10.0. Lists of proteins were entered via the “multiple proteins” function and investigated for protein-protein interaction using Sus scrofa as reference. Protein-protein

interaction networks were investigated using textmining, experiments, databases, co-expression, neighborhood, gene fusion, and co-occurrence as active interaction sources. Default setting medium confidence (0.400) was defined as minimum required interaction score. Networks were exported with confidence view settings in which line thickness indicates the strength of data support.

2.10. Interface tissue engineering: cartilage regeneration

The histological end-point investigation of cartilage regeneration was performed as visiting researcher at the Heike Daldrup-Link lab at Stanford University.

2.10.1. Sample preparation

Histology samples were acquired from knees of Göttinger minipigs. The minipigs had undergone surgery 12 weeks before, in which cartilage defects of the femoral groove had been filled with mesenchymal stem cells seeded fibrin scaffolds. The defect samples were excised from the pig knees, fixed in formalin for 48 h, and subsequently washed in deionized water for ~ 4 h. Samples were then decalcified for 4 - 6 weeks as described in 9.3.1 and subsequently cut in half. Half of the defect was embedded into paraffin and sectioned into 5 μm thick sections using a microtome (Microm HM 330) for histochemistry (2.10.2). The other half of the defect was sectioned into 7 μm thick cryocut sections using a cryotome (Leica CM3050) for immunofluorescence (2.10.3).

2.10.2. Histochemistry

2.10.2.1. Hematoxylin and Eosin

Hematoxylin and eosin (HE) stain is a principal stain in histology. Hematoxylin is a basic dye that stains cells in a purple color and eosin is an acidic dye that binds to positively charged proteins resulting in a pink/red color.

Sections were deparaffinized in a series of 2 \times xylene (Fisher Chemical), 100 % ethanol (Gold Shield), 95 % ethanol, 70 % ethanol, and distilled water for 5 min each. Sections were circled with an Elite Mini PAP pen (Diagnostic Biosystems). One drop hematoxylin (Sigma-Aldrich) per section was applied followed by incubation for 1 min. Samples were washed twice in distilled water for 3 min each. One drop of eosin (Sigma-Aldrich) was applied per section and incubated for 1 min. Subsequently, samples were washed twice in distilled water for 3 min each. Samples were dehydrated in increasing graded concentrations of ethanol (70 %, 95 %, 100 %) followed by xylene for 3 min each. Coverslips were mounted using Permount mounting media (Fisher Scientific).

2.10.2.2. Safranin O

Safranin O stains carboxylated polysaccharides and is used to detect cartilage, mucin, and mast cell granules.

Samples were deparaffinized in a series of 2 × xylene (Fisher Chemical) for 10 min, 2 min each 2 × 100 % ethanol (Gold Shield), 95 % ethanol, 70 % ethanol, and distilled water for 5 min. Subsequently, sections were circled with an Elite Mini PAP pen (Diagnostic Biosystems). One drop hematoxylin (Sigma-Aldrich) per section was applied and incubated for 3 min. Samples were washed in deionized water for 5 min and destained by dipping them 3 × quickly in acidic ethanol (125 µl concentrated HCl (EMD) in 50 ml 70 % ethanol). Samples were washed in deionized water 2 × for 1 min each and stained with 0.001 % fast green solution (Pfaltz & Bauer, 0.01 g fast green in 1000 ml deionized water) for 5 min. Samples were rinsed with 1 % acidic acid (0.5 ml glacial acetic acid in 49.5 ml deionized water) for 10-15 s and subsequently stained with 0.1 % safranin O (350 Harleco® Safranin O, EMD Millipore, 0.05 g Safranin O in 50 ml deionized water) for 5 min. Then, samples were dehydrated in increasing graded concentrations of ethanol (70 %, 95 %, 100 %) for 40 s each followed by 2 × xylene for 2 min each and covered using Permount mounting media (Fisher Scientific).

2.10.3. Immunofluorescence

Slides with cryocut sections were thawed and air dried for 15 min. Slides were transferred into a mixture of acetone/methanol (1:1) for fixation and incubated for 15 min. Afterwards, samples were air dried for 15 min, sections were circled using an Elite Mini PAP pen (Diagnostic Biosystems) and slides subsequently rehydrated in PBS for 10 min. LabVision™ Ultra V Block (ThermoFisher Scientific) was applied and incubated for 5 min. Primary antibodies for collagen type I (Abcam ab90395, mouse monoclonal), collagen type II (Abcam ab34712, rabbit polyclonal), and collagen type III (Abcam ab7778, rabbit polyclonal) were diluted in PBS and applied at dilutions of 1:1000, 1:500, and 1:100, respectively. For collagen type I/II and collagen type I/III double stainings, antibodies for different targets were applied simultaneously by diluting in the same volume of PBS. Isotype controls for rabbit (rabbit IgG isotype 02-6102, ThermoFisher Scientific) and mouse (Mouse Isotype, eBioscience) were applied at same concentrations as primary antibodies. PBS was applied instead of primary antibody as negative control. Samples were incubated with primary antibodies over night at 4 °C. Then, samples were washed 3 × 5 min in cuvettes with PBS-Tween® followed by application of secondary antibodies. Secondary antibodies were Alexa Fluor® 488 labeled anti-

mouse (ThermoFisher Scientific A1101) and Alexa Fluor® 647 labeled anti-rabbit (ThermoFisher Scientific A21245) which were applied 1:200 PBS-diluted and incubated for 30 min. All antibodies are listed in Table 14. Samples were washed 3 × 5 min PBS-Tween® followed by a dip into PBS. One drop of ProLong® Gold Antifade Mountant with DAPI (Molecular Probes Life Technologies) was applied per section and coverslips mounted. After an incubation of 24 h, samples were imaged.

2.10.4. Imaging

Tiled brightfield images were acquired with a 10× Zeiss Plan Apochromat objective (NA 0.45) on an AxioImager Widefield Fluorescence Microscope with a Zeiss AxioCam MRc color CCD camera. Tiled three-color multi-channel fluorescence images were acquired with a 10× Zeiss Plan Apochromat objective (NA 0.45) on an AxioImager Widefield Fluorescence Microscope with a Zeiss AxioCam HRm monochrome CCD camera. For fluorescence imaging, Zeiss Filter Set 50, Zeiss Filter Set 38 HE, and Zeiss Filter Set 49 were used for detecting the Alexa Fluor® 647-, Alexa Fluor® 488-, and DAPI-labeled regions, respectively. Brightfield and fluorescence images were collected with 10 % overlap and stitched with the Mosaic option of the AxioVision (v. 4.6.3) software. Images were analyzed using ImageJ⁶¹.

2.11. Interface tissue engineering: entheses decellularization

A protocol for entheses decellularization was established with Dr. Kai Xu, guest scientist from Huazhong University of Science and Technology (Wuhan, China). Chemical detergents as well as physical treatments were analyzed with regard to their efficiency to decellularize porcine Achilles tendon entheses. Samples of up to 2 mm thickness were decellularized to provide three-dimensional scaffolds with relevance for biomechanical function. The study was performed in a two-phase approach: first, the effect of various concentrations of sodium dodecyl sulfate (SDS) and *t*-octylphenoxypolyethoxy-ethanol (Triton X-100) were investigated with regard to their efficiency of removing cells from the tissue scaffolds. Second, the most efficient combination of SDS and Triton X-100 was then analyzed in combination with different physical decellularization methods to enhance decellularization efficiency. Physical methods included repeated freeze-thaw cycles, ultrasound treatment, perfusion of the scaffolds, and hydrostatic washing. Biomechanical testing was performed to analyze whether the decellularization process changed the biomechanical properties of the tissue scaffolds. Cell counting, DNA quantification, and histology as well as all other analyses were performed as described in Xu K & Kuntz L, et al. (2017)⁵⁶.

3. Geometrical transition of fibers at the enthesis

3.1. Fiber splaying

The structural arrangement of fibers at the interface was investigated using confocal reflection microscopy, scanning electron microscopy, and high-resolution micro-computed tomography as described in 2.2, 2.4, and 2.6.2, respectively.

For confocal imaging and electron microscopy, enthesis slices were chemically fixed with paraformaldehyde, partially decalcified, and cryocut sectioned into 7 μm and 200 μm thick sections, respectively, as described in 2.1. Confocal reflection and electron microscopy showed that tendon fibers continue towards the bone. A splaying of fibers from thicker tendon fibers to thinner fibers, referred to as interface fibers, was observed in confocal reflection (Figure 5). These interface fibers splay out symmetrically with an angle up to 15° as determined from confocal images.

To rule out any artifacts that may evolve from sample cryocut sectioning, the three-dimensional structure of near-physiological samples was measured using high-resolution micro-computed tomography. For high-resolution micro-computed tomography, entheses were cut into cubes of 3-5 mm per edge as described for enthesis slices (2.1). This non-destructive sample preparation prevents any potential sample distortions that possibly occur with serial sectioning approaches⁷⁰. High-resolution micro-computed tomography (2.6.2) allowed for a three-dimensional reconstruction of enthesis architecture with a resolution of up to 1.5 μm under preservation of near physiological conditions.

All structural analyses from these three imaging techniques showed that there is a transition in fiber geometry $\sim 500 \mu\text{m}$ before tendon attaches to the bone (Figure 5). At the interface region, tendon fibers unravel and splay into thinner interface fibers as observed in confocal imaging as well as micro-computed tomography. The structural transition in fiber diameter was quantitatively determined using high-resolution micro-computed tomography and confocal reflection data sets of 12 biological samples. The observed mean diameters of porcine Achilles tendon fibers and interface fibers are $(105 \pm 21) \mu\text{m}$ and $(13 \pm 4) \mu\text{m}$, respectively.

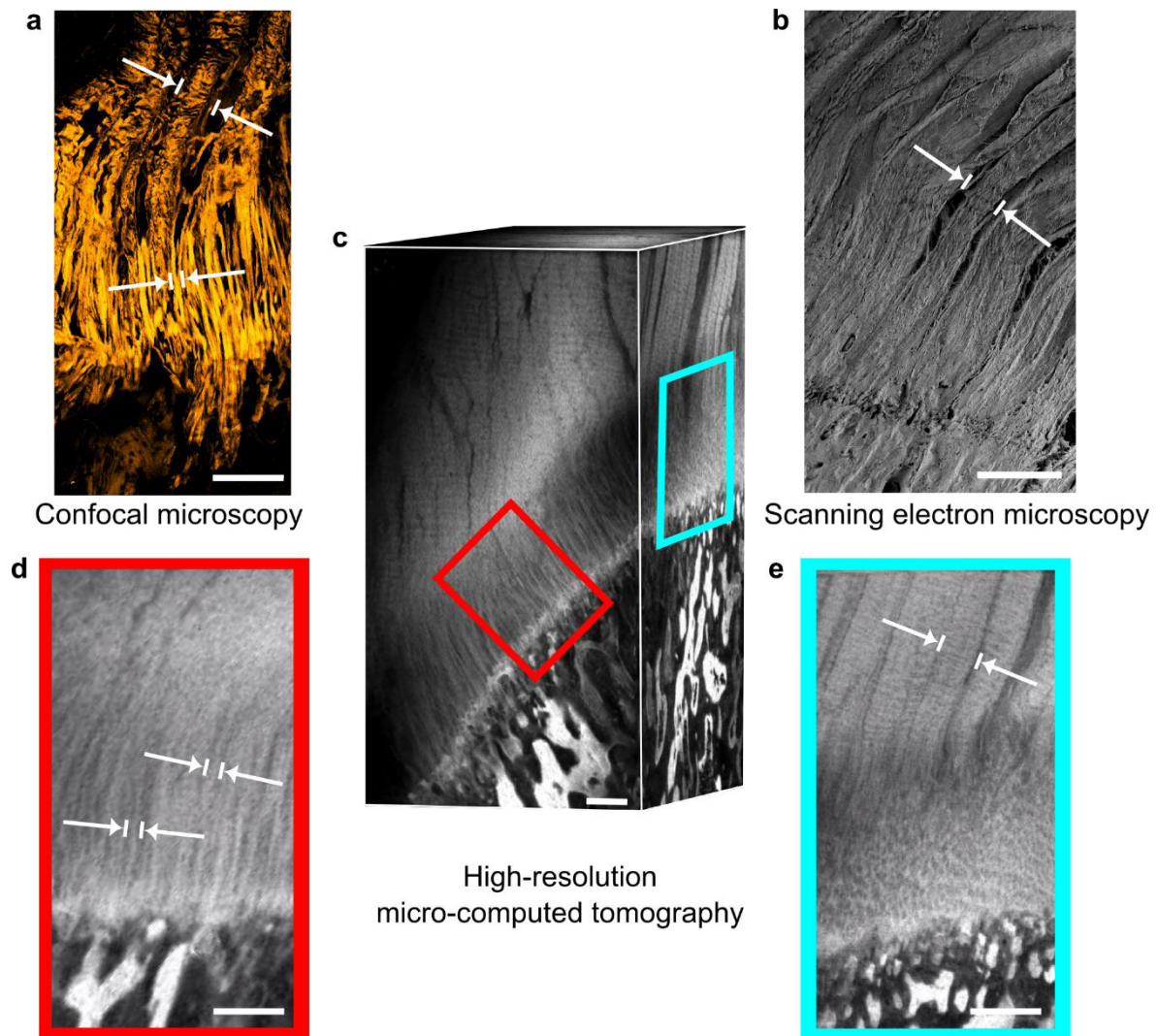


Figure 5: Geometrical transition of fibers before attaching to bone. High-resolution micro-computed tomography (μ CT) of enthesis cubes and confocal reflection imaging as well as scanning electron microscopy of porcine enthesis cryocut sections showed that fibers continue from tendon towards bone. Tendon fibers with a mean diameter of $(105 \pm 21) \mu\text{m}$ unravel into thinner interface fibers with a mean diameter of $(13 \pm 4) \mu\text{m} \sim 500 \mu\text{m}$ before attaching to bone. a, Tendon fibers and interface fibers imaged with confocal reflection microscopy. b, Tendon fibers observed using scanning electron microscopy. c, Rendered volume of μ CT acquisition showed both interface fibers and tendon fibers. d, Interface fibers observed using high-resolution μ CT. e, Tendon fibers observed with μ CT. White arrows indicate fiber width. Scale bars correspond to $250 \mu\text{m}$. Figure was similarly published in our paper in *Nature Materials*¹.

The interface fibers attach to the bone along an interdigitated area at which groups of fibers interlock with the bone thereby increasing the area of the attachment.

3.2. Fiber crimping

Fiber crimping is the wavelike arrangement of collagen fibers and is a characteristic phenomenon in tendon³². It is a heterogeneous, irregular feature of tendon and the crimp angle varies which may be explained by varying proteoglycans contributing to the crimp pattern by different cross-linking properties³². In high-resolution micro-computed tomography as well as confocal reflection microscopy, fiber crimping was observed for Achilles tendon fibers, but not for interface fibers (Figure 6). While interface fibers appear smooth (Figure 6a) in high-resolution micro-computed tomography, tendon fibers exhibit a wavelike pattern (Figure 6b). Confocal reflection microscopy concurs in showing wavelike arrangement of tendon fibers and smooth interface fibers (Figure 6c).

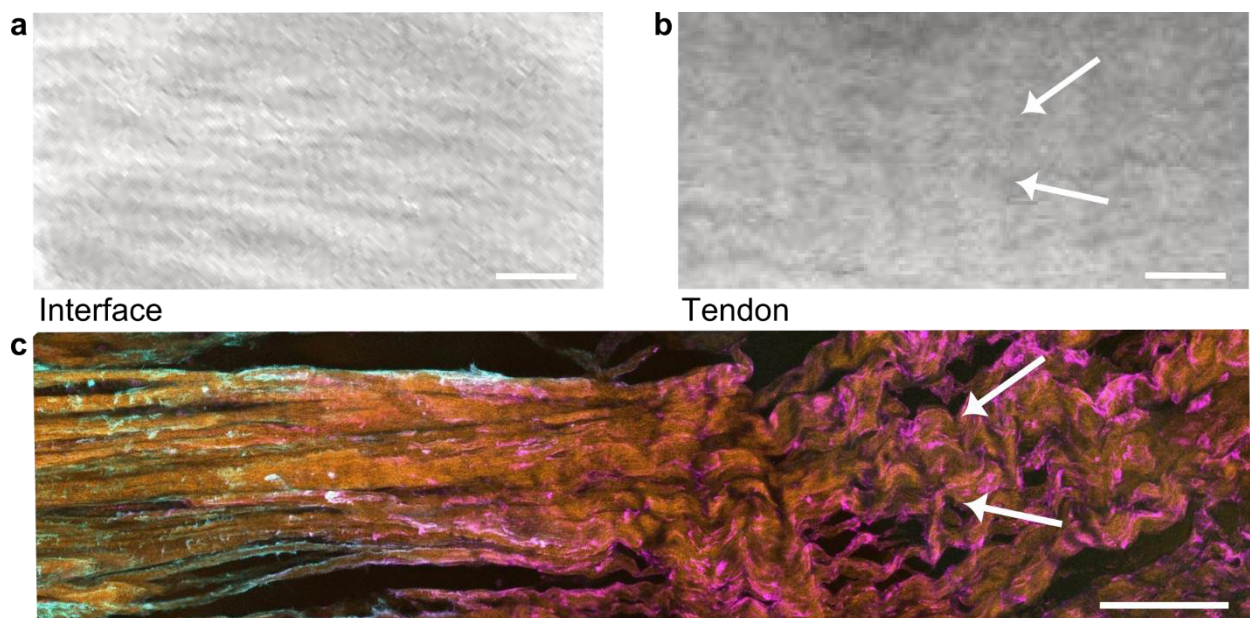


Figure 6: Fiber crimping was observed for tendon fibers, but not interface fibers. a, Interface region in high-resolution μ CT showed smooth interface fibers. b, Tendon fibers showed wavelike crimp pattern in high-resolution μ CT. c, Fiber crimping was observed using confocal reflection imaging in the region of tendon fibers (right, marked with arrows), but not in the interface region (left). Scale bars correspond to 100 μ m.

3.3. Discussion

Crimped, parallel aligned tendon fibers with a diameter of (105 ± 21) μ m undergo a geometrical transition towards smooth, splayed interface fibers with a much smaller diameter of (13 ± 4) μ m. The change in fiber geometry occurs ~ 500 μ m before the fibers attach to bone.

The observed geometrical transition of fibers has great implications for the mechanical function of the enthesis.

Splaying and subdivision of tendon fibers into interface fibers allows for a heterogeneous mechanical response contributing to the reduction of stress concentrations at the interface. Splayed fibers enable fiber recruitment processes in response to strains acting from different angles. Different pulling angles are expected to elicit different responses such as shear, buckling and in-plane rotation of individual fibers¹.

Micromechanical analysis of the tendon-bone insertion identified two typologies of mechanical responses using a custom-made micromechanical testing device coupled to a confocal microscope¹. The first typology of mechanical response was a sharp increase in displacement within the interface region that corresponded to a high local longitudinal strain. In the tendon an increase in displacement up to a factor of ten slower was observed, indicating that the interface region behaved as if it were more compliant than tendon and bone. This compliant attachment occurred on a similar length scale as the $\sim 500 \mu\text{m}$ spanning interface region where fiber splaying was observed (3.1).

The second typology of mechanical response was a smoother transition between tendon and bone in which the displacement did not show a sudden sharp increase in the interface region. Smaller displacement at the interface region in the second typology could indicate that some fibers are not subjected to the same load as others, possibly through fiber recruitment processes¹. Strains from two different angles were applied to the enthesis showing that areas that underwent displacement of the first typology under longitudinal pulling could exhibit displacement of the second typology when pulled at a 45° angle and vice versa. Therefore, the interface's local mechanical properties indeed depended on the angle of force application. This is an indication for a load sharing mechanism in which different groups of fibers are recruited for bearing load depending on the angle of load application¹. In turn, the heterogeneous mechanical response in the transverse direction via fiber recruitment processes allows for directional variability of load application to bone and thus locomotion.

Splaying of fibers does not only allow for angle-dependent redistribution of forces within different fibers¹, but also enforces stress dissipation via increasing the area of the attachment. Firstly the splaying of interface fibers and secondly the interdigitation with bone both increase the area over which forces are transduced at the attachment resulting in the reduction of stress localizations at the interface¹. The change in fiber diameter from thicker tendon fibers with a diameter of $(105 \pm 21) \mu\text{m}$ to smaller interface fibers with a diameter of

(13 ± 4) μm most likely also affects the force transmission and resulting mechanical behavior. In the present data it was not possible to three-dimensionally track individual fibers from tendon fibers to interface fibers. Therefore it has not yet been possible to determine whether the sum of cross sectional areas from all splayed interface fibers that are connected to one tendon fiber is greater than the tendon fiber cross sectional area or whether the total cross sectional area is conserved. Since stress equals to force per area, an increase in total cross sectional area would also contribute to a decrease in stress at the interface.

Conclusively, as reported in Rossetti & Kuntz et al.¹, splaying of tendon fibers into interface fibers is a key feature for the durability of the Achilles tendon enthesis by decreasing stress concentrations at the interface and thus contributing to the enthesis' unexpected resilience. Interestingly, similar splaying mechanisms are also used on larger length scales to redistribute stresses and enable different angles of force application, such as in the shoulder joint¹⁹. Besides splaying of fibers, crimping of fibers also affects the mechanical behavior of the tissue. It was shown in chapter 3.2 that tendon exhibits fiber crimps, periodic waved structural features, along the longitudinal axis of the enthesis. Fiber crimps have been suggested to play a role in the mechanical function of tendon¹⁴. Tendon presents a stress-strain curve that is characterized by three regions: the toe region, the heel region, and the elastic region. The flattening of fiber crimps has been correlated with the non-linear mechanical behavior observed in the toe region of the stress-strain curve¹⁴ (Figure 7).

It has been suggested that crimps may act as shock absorber during tendon tensing^{71,72}. Small strains straighten kinks in the collagen structure and higher strains lead to molecular gliding of the fibrils and finally to disrupting fibrils⁷³. Strain within collagen fibers is smaller than in the whole tendon⁷³. Therefore, the elongation of tendon is not only due to stretching of fibers⁷³ and the mechanical behavior of tendon cannot be explained by collagen fibers alone¹⁴. Rather, collagen fibers both stretch and slide relative to adjacent fibers when a tendon is submitted to load⁷⁴. Alternative mechanisms of load transfer that play a role, such as relative movement of entire fibers⁷³ via fiber sliding, may be mediated by stress transfer through the non-fibrillar matrix¹⁴. In particular, the mechanical response of tendon relies also on fibril-proteoglycan interactions as well as collagen cross-links¹⁴. Therefore, varying molecular composition such as presence of different proteoglycans within interface region and tendon may affect the observed structural difference in fiber crimping features.

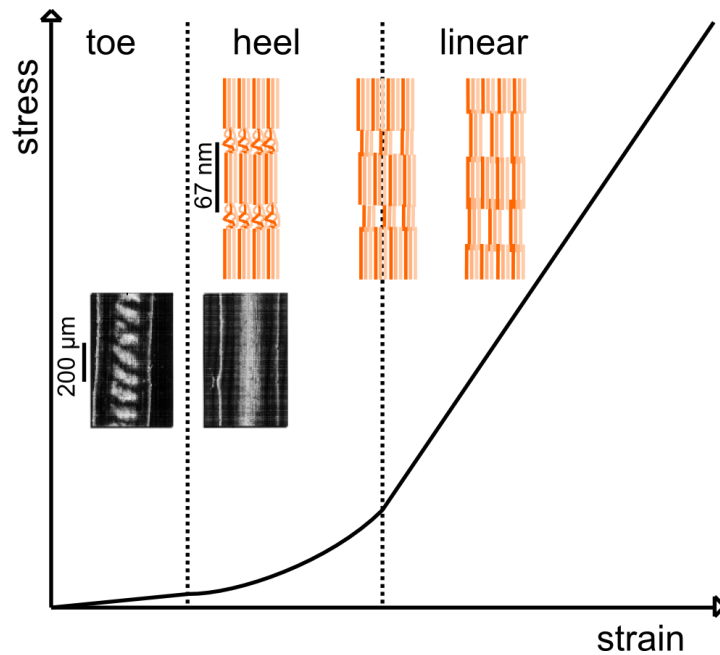


Figure 7: Stress-strain curve of tendon. Fiber crimps are straightened in the toe region where tendon is extended with low force. In the heel region, structural changes may occur at the molecular level, where molecular kinks in the gap regions of collagen fibers are straightened. In the linear region, fiber sliding processes are involved in the mechanical function of tendon. Graph is adapted from⁷³.

Due to the importance of the extracellular matrix in its whole complexity for the mechanical function of the tendon and thus the tendon-bone insertion, the extracellular matrices of tendon and interface region were investigated and are described in chapter 4. Tendon exhibits a variety of fiber dimensions and the challenge remains to understand how the composition of the extracellular matrix and the expressional processes of the residing cells result in the final structure of the fibers⁷⁵. Matrix composition and cell expression are elucidated within chapters 4.2.2 and 5.2, respectively.

4. Compositional transition at the enthesis

4.1. Compositional transition of fibers

The composition of fibers at the enthesis was investigated using immunofluorescence confocal microscopy. Enthesis cryocut sections were immunofluorescently labeled for collagen type I and collagen type II as described in 2.2.1. Confocal imaging of immunofluorescently labeled enthesis cryocut sections revealed region-dependent compositional differences at the enthesis. Collagen type I was highly abundant in tendon and bone (Figure 8a, magenta). At the interface region between tendon and bone, collagen type I levels were low. Reciprocally, very high levels of collagen type II were observed in the interface region, but very low collagen type II levels in tendon and bone (Figure 8a, cyan). The region of high collagen type II content coincided with the region of fiber splaying described in chapter 3.1.

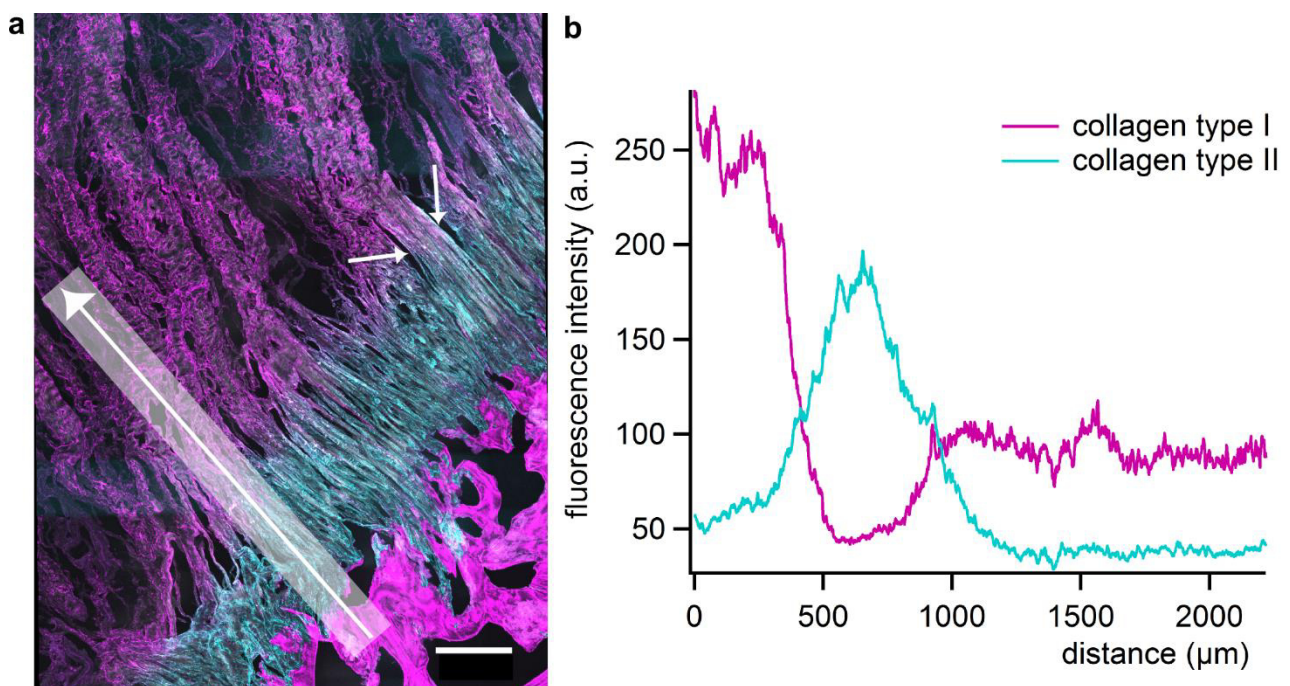


Figure 8: Compositional transition of tendon fibers before attaching to bone. Fiber composition changes from collagen type I to collagen type II before inserting to bone. a, Confocal image of porcine cryocut section immunofluorescently labeled for collagen type I (magenta) and collagen type II (cyan). Confocal reflection is depicted gray. Fiber composition changes from collagen type I to collagen type II $\sim 500 \mu\text{m}$ before inserting to bone. The transition in fiber composition coincides with the geometrical transition of fiber splaying (short arrows in a). Scale bar corresponds to $300 \mu\text{m}$. b, Fluorescence intensities plotted over distance across the tendon-bone insertion (long arrow in a). The regions of high collagen type I content and the region of high collagen type II content are complementary.

The plot of fluorescence intensity over distance across the insertion shows the distributions of collagen type I and collagen type II levels (Figure 8b). A region with very low collagen type I level was detected and it was observed that this region overlapped with a region of high collagen type II level. Vice versa, the regions of high collagen type I level showed very low collagen type II level. Thus, there is a compositional transition of fibers at the attachment site. Simultaneous detection of confocal reflection showed that the region of compositional transition coincided with the region of geometrical transition, where tendon fibers splayed into interface fibers (Figure 8a, small arrows) as described in chapter 3.

4.2. Matrix composition at the enthesis

4.2.1. X-ray absorption at the interface

When micro-computed tomography measurements were performed on Achilles tendon-bone interface samples, it was observed that a dark stripe occurred at the interface between tendon and bone. The dark stripe between tendon and bone indicated less X-ray absorption at the interface than in tendon or bone. Plotting X-ray absorption gray values over distance across the enthesis (yellow arrow in Figure 9a) revealed that the interface region indeed showed less X-ray absorption than tendon and bone (Figure 9b). The area with lower absorbance spanned $\sim 500 \mu\text{m}$ across the tendon-bone insertion and coincided with the area of fiber transition described in chapters 3 and 4.1.

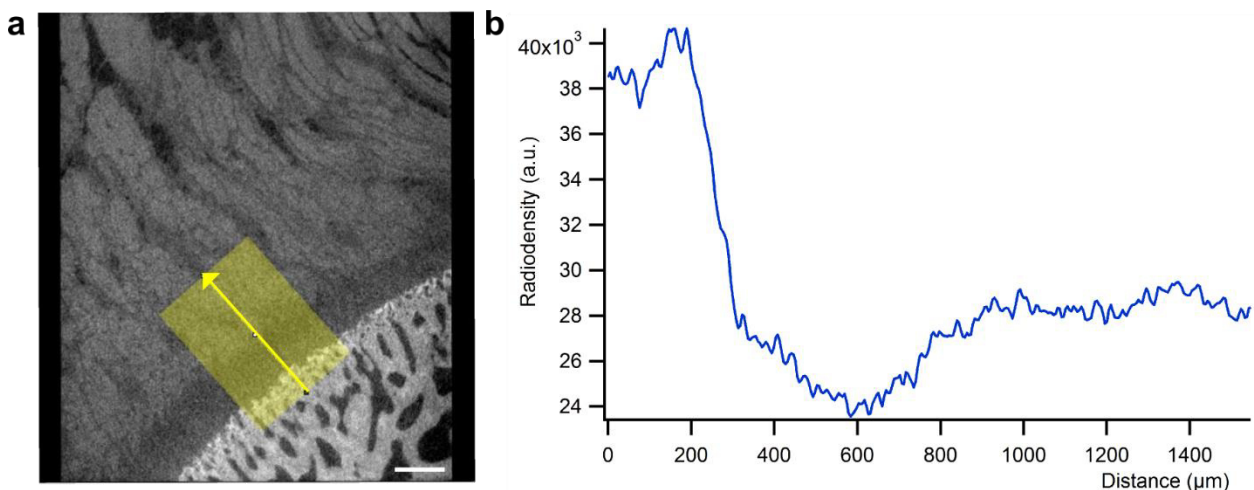


Figure 9: Interface region showed less X-ray absorption than tendon or bone. a, Slice from three-dimensional rendered image stack of tendon-bone insertion measured using micro-computed tomography. The interface region showed lower absorbance than tendon or bone indicated by the dark stripe observed between tendon and bone. Tendon appeared to interdigitate with bone within the interface region. b, Intensity was plotted over distance across the interface (yellow arrow in a). An area of $\sim 500 \mu\text{m}$ at the interface showed lower intensity than tendon or bone.

The observed difference in absorption of the interface region compared to tendon and bone may derive from several causes. Measured gray values of X-ray absorption are influenced by several parameters. Firstly, they depend on the linear attenuation coefficient which describes the fraction of a beam of X-rays that is absorbed per unit thickness of a tissue⁷⁶. The linear attenuation coefficient depends on the tissue density as well as on the atomic number z of the atoms present within the tissue. For example, fat tissue has low atomic numbers and density resulting in very low absorbance. The interface tissue shows different absorbance than tendon, possibly resulting from a different linear attenuation coefficient.

Since the dominant elements of soft tissue (C, H, O, and N) did not give much contrast⁷⁶, contrast agent Imeron® was used to increase the contrast of low-absorbing features. Imeron® contains the watersoluble and iodinated contrast agent iomeprol ($C_{17}H_{22}I_3N_3O_8$) and has a molecular weight of 777.1 g/mol. Due to application of the contrast agent Imeron®, secondly, the measured gray values also depended on the uptake of contrast agent into the tissue. Thus, the observed difference in absorbance may also be influenced by differential uptake of contrast agent.

Matrix structure and charge densities play a crucial role in diffusivity of biomolecules through the matrix. A correlation of solute diffusivity with matrix density and mechanical properties of compressed cartilage has been described⁷⁷. Studies on solute transport in cartilage indicate significant variation in diffusivity with regard to matrix structure^{78,77}, glycosaminoglycan content⁷⁸ and fixed charge densities⁷⁹. Therefore, a differential uptake of contrast agent Imeron® into the interface region compared to tendon may have firstly resulted from the presence of glycosaminoglycan negative charges within the interface region which may prevent uptake of contrast agent. Secondly, differences in matrix density of tendon and interface region may have contributed to the observed low absorbance at the interface region.

Conclusively, different X-ray absorption properties were detected for tendon and interface region using micro-computed tomography. Different X-ray absorption properties indicate that the chemical composition differs between interface region and tendon. This may be either due to different tissue density or due to less uptake of contrast agent Imeron® into the interface region.

4.2.2. Proteome composition of the enthesis

The proteome refers to the entire set of proteins expressed within a tissue. The complex molecular compositions of interface region proteome and tendon proteome were compared in a quantitative proteome analysis. The proteomes of tendon and interface region were compared to elucidate the differences in the extracellular matrices of the two tissues. The

proteomes were characterized using liquid chromatography tandem mass spectrometry (Figure 10). Briefly, porcine legs obtained from a local abattoir were dissected, tissue samples of interface region and tendon were excised and immediately shock-frozen in liquid nitrogen. Shock-frozen tissue samples of interface region and tendon were cryocut sectioned to enhance subsequent protein extraction. Cryocut sections were then lyophilized, proteins were extracted, dimethyl labeled and liquid tandem mass spectrometry (LC-MS/MS) was performed as described in 2.7.

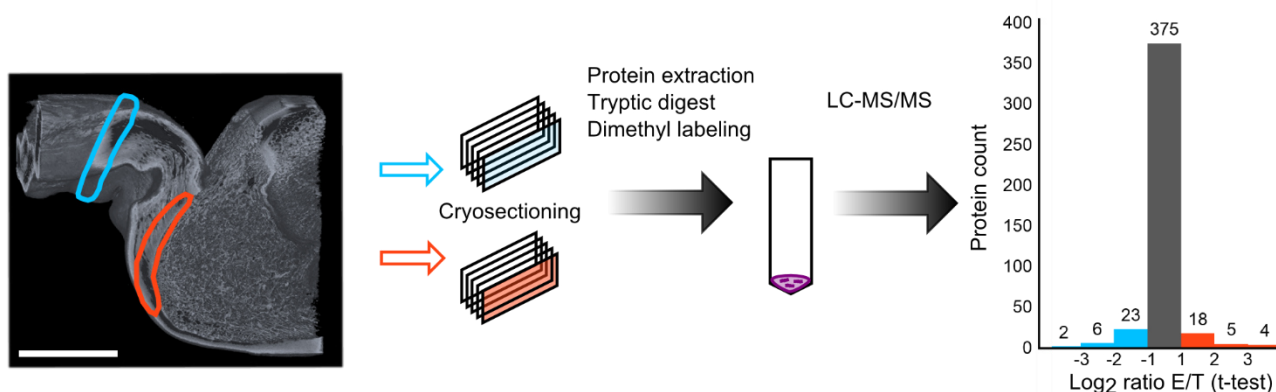


Figure 10: Experimental design of proteome study. Tendon (blue) and interface region (orange) samples were retrieved, shock-frozen, and cryocut sectioned. Proteins were extracted, trypsin digested and dimethyl labeled. Labeled peptides were mixed and measured using liquid chromatography tandem mass spectrometry. Protein counts grouped according to \log_2 protein ratios are shown in the histogram. In total, ≥ 400 proteins were detected, 31 proteins were enriched in tendon (T) and 27 in enthesis (E). Scale bar corresponds to 1000 μm .

Dimethyl labeling prior to tandem mass spectrometry allowed for direct comparison of protein levels in interface region and tendon for each biological sample. Twelve biological samples were analyzed and 433 proteins were detected in tendon and interface region. Of all measured proteins, 31 showed at least twofold elevated levels in tendon and 27 in the interface region. 375 of all detected proteins did not show a significant difference in expression level between interface region and tendon. The other 48 proteins showed statistically significant differences in expression with at least twofold enrichment in either tendon or interface region (Benjamini Hochberg FDR 0.05, t-test $p < 0.013$). Of these, 22 proteins were statistically significant enriched in the interface region tissue and 26 proteins in the tendon tissue as described in 4.2.2.1 and 4.2.2.2, respectively.

It has to be noted that the proteome difference may be underestimated since a sample preparation precision limitation leads to tendon residues in interface samples. Interface region and tendon are not distinguishable by eye and have to be labeled to be identified. Since fresh tissue has to be used for the proteome analysis, a labeling prior to dissection is not eligible. The interface region spans only $\sim 500 \mu\text{m}$ and the borders of the interface region have to be visually approximated. Therefore, it is very likely that tendon residuals remain within the interface region samples. For future proteome studies of tendon or ligament entheses, a laser cutting technique might be evaluated to retrieve interface region samples that do not contain residual tendon. However, a laser cutting technique for sample preparation has to be considered with care, since new challenges arise such as possible burn artifacts within samples and limitations with regard to the localization of the sampling. It has to be ensured that the sampling takes place within the interface region and that the sample covers a “tissue mean” and not just a single localized tissue extract.

Differences in expression between tendon and interface were quantitatively determined (Figure 11). Statistical significance of protein level differences as a function of average protein ratios are shown in the volcano plot (Figure 11a). Orange and blue dots represent proteins that are significantly enriched in the enthesis (E) or tendon (T), respectively. All proteins that were at least twofold enriched ($\log_2 \text{ratio} > |1|$) and passed the Student's t-test with regard to a Benjamini-Hochberg false discovery rate of 0.05, were considered to be statistically significant enriched. All 22 proteins statistically significant enriched in enthesis and all 26 proteins statistically significant enriched in tendon are listed in Figure 11b.

The lists of proteins enriched in either enthesis or tendon were further analyzed with regard to the respective protein functions and with regard to gene ontology. Results of the functional classification of proteins enriched in interface region or tendon are described in the following paragraphs 4.2.2.1 and 4.2.2.2, respectively.

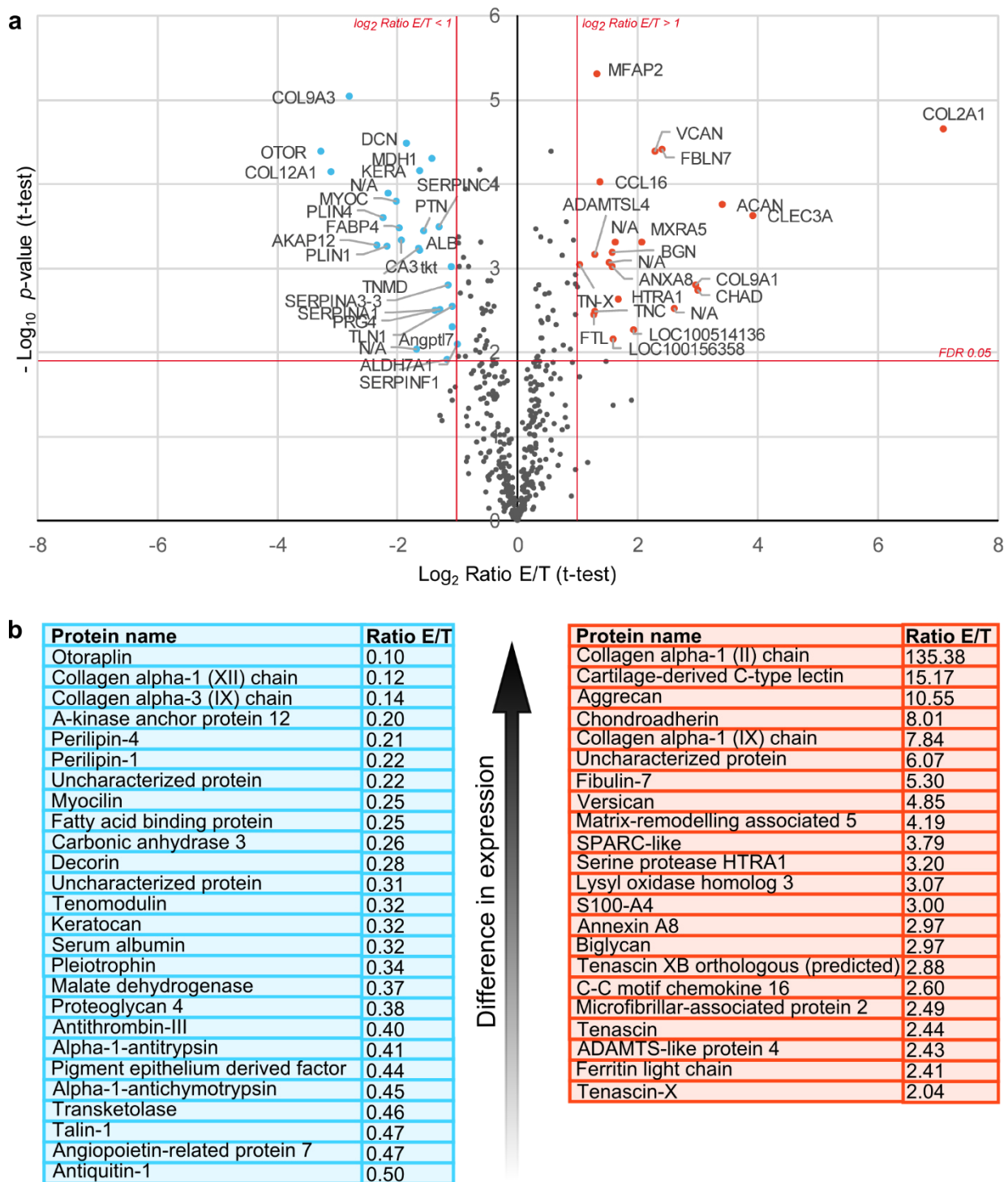


Figure 11: Quantitative proteome analysis of differences in expression between tendon (blue) and interface region (orange). a, Volcano plot of p-values (statistical significance of differences) as function of protein ratios from all biological replicates. Blue and orange dots represent proteins which are significantly enriched in tendon and interface region, respectively (Benjamini-Hochberg FDR 0.05, truncation at $-\log_{10} p\text{-value} > 1.9$). b, Tables list proteins that were statistically significant at least twofold enriched in tendon (blue) or interface (orange), respectively.

4.2.2.1. Proteins in the interface region

Matrix composition of entheses is directly related to the mechanical demands it encounters such as local compressive stress⁸⁰. Some cartilage-related molecules have been histologically described to be localized within the interface region^{16,80}. Here, we characterized the full complexity of the interface region by studying its proteome using tandem mass spectrometry.

22 proteins were identified to be statistically significant at least twofold enriched compared to tendon (Figure 11). All statistically significant enriched proteins with their respective functions are listed in Table 2. Genome annotation of *Sus scrofa* is still much less detailed than genome annotation of *Homo sapiens*, therefore some protein functions have not yet been annotated and had to be predicted using their sequence homology to human.

Table 2: Functions of all annotated proteins that were at least twofold enriched in the interface region.

Gene	Protein	Function	Log ₂ fold enrichment
COL2A1	collagen type II, alpha-1	fibrillar collagen	7.08
CLEC3A	cartilage derived c-type lectin	cell adhesion	3.92
ACAN	aggrecan	hyalectan proteoglycan, cartilage-specific proteoglycan core protein, withstands compression	3.40
CHAD	chondroadherin	small leucine-rich protein, interacts with collagen type II, may regulate chondrocyte growth and proliferation	3.00
COL9A1	collagen type IX, alpha-1	cross-links to surface of type II collagen fibrils	2.97
N/A (I3LPA7)	uncharacterized		2.60
FBLN7	fibulin-7	cell adhesion molecule	2.41
VCAN	versican	hyalectan proteoglycan	2.28
MXRA5	matrix-remodelling associated 5	adhesion protein	2.07
LOC100514136	SPARC-like	osteonectin, promotes mineral crystal formation	1.92
HTRA1	serine protease HTRA1	serine protease, targets ECM proteins such as fibronectin	1.68
N/A	lysyl oxidase homolog 3	cross-links collagen fibrils	1.62
LOC100156358	S100-A4	Ca ²⁺ -binding protein, may inhibit assembly of myosin filaments	1.58
ANXA8	annexin A8	bone-matrix induced protein	1.57

BGN	biglycan	small leucine-rich repeat proteoglycan, may play a role in mineralization of bone	1.57
N/A	tenascin XB orthologous (predicted)	collagen fibril organization	1.53
CCL16	c-c motif chemokine 16	cytokine, CC chemokine family	1.38
MFAP2	microfibrillar-associated protein 2	extracellular matrix organization, elastin-associated microfibrils	1.32
TNC	tenascin	glycoprotein	1.28
ADAMTSL4	ADAMTS-like protein 4	accelerates elastin microfibril formation	1.28
FTL	ferritin light chain	involved in iron storage	1.27
TN-X	tenascin-X	glycoprotein	1.03

Collagens are a vast family of biomolecules and play a very important role in tissue architecture and function³⁸. In the interface region, several collagens were detected to be enriched. Firstly, fibril-forming collagen type II (alpha-1) showed very high enrichment compared to tendon. This is consistent with confocal microscopy in which a collagen type II rich interface region was also observed (Figure 8). More specifically, the enthesis proteome contained 135 times more collagen type II than the tendon proteome. Secondly, enrichment of collagen type IX (alpha-1) was measured. Collagen type IX does not belong to the fibril-forming collagens as collagen type II, but belongs to the fibril-associated collagens with interrupted triple helices (FACIT). FACITs are incorporated into the body of heterogeneous collagen fibers and are thus integral for the molecular organization of the fibers³⁸.

Several proteoglycans were detected, which are a family of macromolecules that contain negatively charged glycosaminoglycan side chains²⁸. In the interface region, high levels of aggrecan (~ 10-fold enrichment) and high levels of versican (~ 5-fold enrichment) were detected. These two proteins belong to the proteoglycans (1.4.3), particularly to the family of hyalactans, which are large chondroitin sulfate proteoglycans. Hyalactan proteoglycans provide a swelling pressure within the tissue⁵⁰ and are known to occur primarily in compressed tissue regions. Proteins of a different family of proteoglycans were also enriched, namely chondroadherin and biglycan. Chondroadherin and biglycan belong to the family of small leucine-rich repeat proteoglycans (SLRP) which function as structural constituent of the extracellular matrix⁵¹.

The interface region proteome contained high levels of multiple proteins that are known to occur in cartilage. These were, for example, collagen type II, cartilage-derived c-type lectin, aggrecan, and chondroadherin (Figure 11). Interestingly, the interface region also showed

high levels of proteins that are involved in fibril formation, fibrillar organization and crosslinking. These are lysyl oxidase homolog 3, which is involved in collagen cross-linking, tenascin XB orthologous, which is predicted to be involved in collagen fibril organization, microfibrillar associated protein 2, which is involved in elastin-associated microfibril organization, and ADAMTS-like protein 4, which accelerates microfibril formation.

A PANTHER gene ontology analysis of the list of genes that was enriched in the interface region was performed with regard to overrepresentation of biological processes. Gene ontology analysis showed that many cartilage-related biological processes were overrepresented. Overrepresented biological processes included cartilage condensation, glycosaminoglycan metabolism, proteoglycan metabolism, mucopolysaccharide metabolism, and extracellular matrix organization as well as skeletal development (Figure 12).

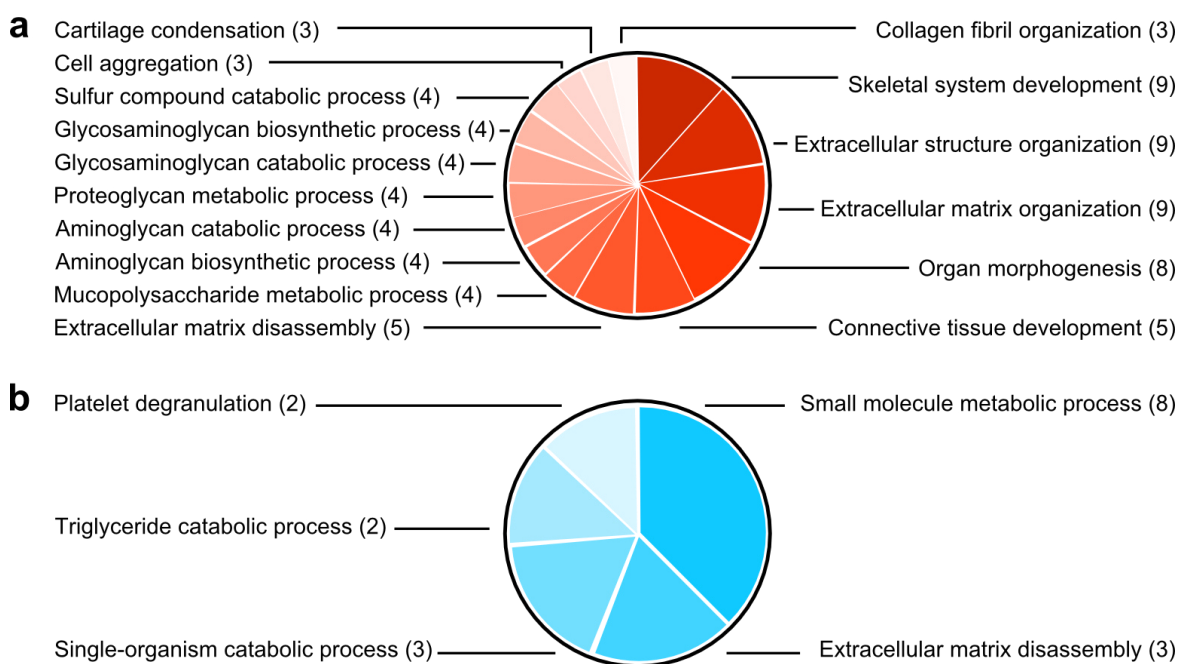


Figure 12: PANTHER gene ontology analysis of enriched proteins in enthesis and tendon for overrepresented biological processes complete. Gene ontology analysis of gene lists corresponding to proteins that were enriched in a, interface region and b, tendon identified multiple statistically overrepresented biological processes.

4.2.2.2. Proteins in tendon

Previous studies of tendon/ligament proteomes identified a total of 252 proteins in superficial digital flexor tendon⁸¹, 178 proteins in anterior cruciate ligament⁸² and 166 in patellar tendon⁸². Here we present highly resolved proteome data of Achilles tendon identifying more than 400 proteins within the Achilles tendon. It is likely that the number of proteins present in different tendon/ligament tissues is within a similar range. Presumably, differences in protein number range between different studies arise from a difference in resolution power of the techniques used to obtain the proteomic data sets. Here we used a combination of advanced sample preparation with cryocut sectioning prior to protein extraction and evaluation of different extraction protocols as well as high-end mass spectrometry to characterize the tendon proteome and were able to detect more than 400 proteins in the Achilles tendon proteome.

Tendon proteome and enthesis proteome were compared. The tendon proteome contained 26 proteins that were statistically significant at least twofold enriched compared to the enthesis proteome. The 26 proteins enriched in tendon and the respective functions of the proteins that were annotated are listed in Table 3. Gene ontology revealed overrepresentation of biological processes such as triglyceride metabolism and platelet degranulation (Figure 12b). Interestingly, several proteins involved in fat metabolism or transport were enriched in the tendon such as perilipin-1, perilipin-4, fatty acid binding protein, and serum albumin. Furthermore, several proteins involved in blood regulation or angiogenesis were enriched such as pleiotrophin, antithrombin III, alpha-1-antitrypsin, pigment epithelium derived factor, and angiopoietin-related protein 7. Several proteins known to be localized in the eye and to be involved in corneal transparency were also enriched in the tendon such as myocilin and keratocan. It is astonishing, how nature achieves such diverse biological functions of different tissues using similar building blocks.

Comparing tendon proteome to enthesis proteome, two enriched collagen types were identified; type IX collagen (alpha-3) and type XII collagen (alpha-1). These two collagens belong to the sub-family of fibril-associated collagens with interrupted triple helices. Type IX collagen and type XII collagen can be also regarded as “part-time proteoglycans” because they sometimes carry glycosaminoglycan side chains^{51,75}. Collagen type XII expression has been shown to be upregulated by mechanical stress^{51,75}.

There were also two types of proteoglycans enriched in the tendon proteome; proteoglycans decorin and keratocan. These two proteoglycans belong to the family of small leucine-rich proteoglycans, decorin is a class I SLRP and keratocan a class II SLRP. The name decorin

derives from its ability to “decorate” collagen fibrils; it binds to collagen type I fibrils and plays an important role in matrix assembly by regulating lateral association of collagen molecules into proper fibrils⁵¹. Keratocan is involved in corneal transparency, but is also expressed in other organs such as skin, tendon, and cartilage⁵¹. Interestingly, another proteoglycan was enriched in the tendon, namely proteoglycan 4 which is also called lubricin. Lubricin is a lubricant biomolecule and may play a role in tendon fiber sliding processes³⁰.

Table 3: Functions of all annotated proteins that were at least twofold enriched in tendon.

Gene	Protein	Function	Log ₂ fold enrichment
OTOR	otoraplin	melanoma-inhibiting activity, suggested to play a role in cartilage development	-3.28
COL12A1	collagen type XII, alpha-1	FACIT collagen, often associated with collagen type I fibrils	-3.11
COL9A3	collagen type IX, alpha-3	extracellular matrix structural constituent conferring tensile strength	-2.80
AKAP12	A-kinase anchor protein 12	binds to protein kinase A, scaffold protein in signal transduction	-2.35
PLIN4	perilipin-4	coats lipid droplets in adipocytes	-2.24
PLIN1	perilipin-1	cAMP-dependent protein kinase substrate in adipocytes	-2.17
N/A	uncharacterized		-2.16
MYOC	myocilin	cytoskeletal function, expressed in eye humor	-2.02
FABP4	fatty acid binding protein	involved in fat accretion	-1.98
CA3	carbonic anhydrase 3	metalloenzyme, catalyzes hydration of carbon dioxide	-1.94
DCN	decorin	small leucine-rich proteoglycan, binds to collagen type I fibrils	-1.85
N/A	uncharacterized		-1.68
TNMD	tenomodulin	suggested tendon marker	-1.64
KERA	keratocan	proteoglycan, involved in corneal transparency	-1.63
ALB	serum albumin	cell-growth inhibiting protein, carrier protein for fatty acids	-1.63
PTN	pleiotrophin	heparin-binding growth factor	-1.57
MDH1	malate dehydrogenase	oxidation of malate	-1.44
PRG4	proteoglycan 4	lubricin, lubricating molecule	-1.38
SERPINC1	antithrombin-III	serine peptidase inhibitor, regulates blood coagulation	-1.31
SERPINA1	alpha-1-antitrypsin	serine protease inhibitor, suggested to regulate blood coagulation	-1.30

SERPINF1	pigment epithelium derived factor	regulation of angiogenesis, adipogenesis, and bone formation	-1.17
SERPINA3-3	alpha-1 antichymotrypsin	serine protease inhibitor, inhibits elastase and trypsin	-1.15
TKT	transketolase	connects pentose phosphate pathway and glycolysis	-1.11
TLN1	talin-1	predicted to be involved in connection of cytoskeleton and membrane	-1.09
ANGPTL7	angiopoietin-related protein 7	involved in regulation of angiogenesis	-1.09
ALDH7A1	antiquitin	oxidation of aldehydes	-1.01

4.2.3. Calcium distribution at the enthesis

Traditionally, a distinct calcification front, referred to as tidemark, has been considered to be the boundary between the “hard” and “soft” part of the enthesis. More recently, a mineral gradient has been suggested to connect the mineralized tissue with the soft tissue using Raman spectroscopy⁸³. This gradation in mineral content is believed to play an important role in stress dissipation at the insertion site⁸⁴. To clarify the nature of the calcification front, here the mineral distribution across the Achilles tendon-bone interface was analyzed using energy dispersive X-ray, confocal microscopy, and high-resolution micro-computed tomography.

Firstly, calcium distribution at the interface region was analyzed using energy dispersive X-ray spectroscopy (EDS) of enthesis slices (Figure 13a). Large areas of enthesis slices were mapped using EDS and distributions of calcium, phosphate, and other elements were analyzed (chapter 2.5). Counts per unit were plotted over distance across the bone border. A linear calcium/phosphate gradient spanning ~ 100 μm across the interface was observed.

Secondly, confocal microscopy was performed using enthesis cryocut sections stained for residual calcium (Figure 13b). Bisphosphonate binds to hydroxyapatite of bone, therefore a FAM-RIS labeled bisphosphonate was used to stain residual hydroxyapatite. Since cryocut sectioning can only be performed on partially decalcified samples, hydroxyapatite content was altered from the “physiological” enthesis. It was assumed that the decalcification procedure worked uniformly and this technique was used to back-up the data acquired from energy dispersive X-ray involving un-decalcified samples. Indeed, confocal imaging of partially decalcified enthesis cryocut sections also indicated a linear calcium gradient across the tendon-bone interface.

However, both energy dispersive X-ray and confocal imaging rely on quasi two-dimensional analysis of calcium distribution. This could lead to artifacts due to overlapping of signal from

tissue layers below the measured data point. Therefore, three-dimensional imaging was performed using high-resolution micro-computed tomography of near-physiological enthesis cubes that were prepared as described in 2.6.2 but not stained with the contrast agent Imeron® (Figure 13c). In the reconstructed data a bone border was observed with small bony cones appearing to interdigitate with the soft tissue. A calcium gradient was not resolved. This could be either due to the calcium gradient not being resolvable with the given data acquisition technique or a calcium gradient not being present. Since existing literature is still ambiguous with regard to the nature of the calcium distribution across the interface, it is highly recommended to further elucidate this by a systematic study of all parameters that are chosen for the μ CT data acquisition. Parameters that could be adjusted include the voltage, the size of the sample, the size of the region of interest, the distance of source and detector from the sample, a dual acquisition mode using two different energies, and the filters, amongst others. Systematic evaluation of different measurement settings could shift the threshold towards an area, in which the putative gradient would be measurable.

The present literature is still ambiguous whether there is a mineral gradient as predicted by models⁸⁵ and observed using Raman spectroscopy^{22,83,84} or a distinct tidemark as observed in histological studies^{13,16,80}. The presented data indicate the presence of a linear mineral gradient in the two-dimensional acquired data, yet the three-dimensional distribution of mineral across the interface remains to be elucidated before clear conclusions can be drawn. An extensive study assessing all decisive parameters for mineral detection thresholds in micro-computed tomography of the enthesis in combination with different sample preparation techniques would be advisable to finally disclose the three-dimensional calcium distribution at the interface.

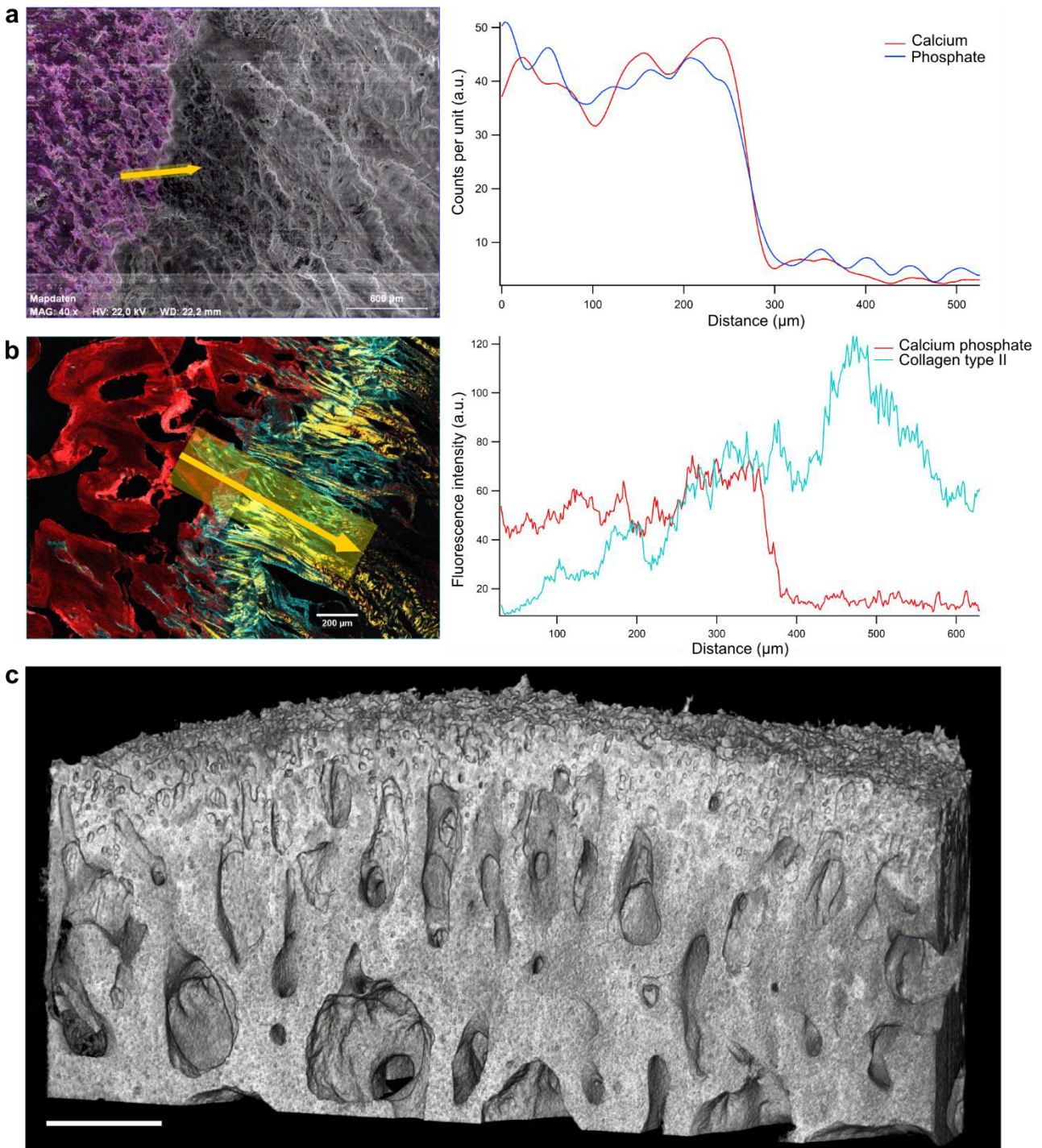


Figure 13: Calcium distribution at the interface. a, Elemental distribution of calcium and phosphate investigated using energy dispersive X-ray spectroscopy (EDS). EDS counts per unit in arbitrary units (a.u.) were plotted over distance along the yellow arrow shown in the elemental map. b, Confocal image of an enthesis stained for bone mineral (red) and collagen type II (cyan). Reflection is depicted yellow. The plot of fluorescence intensity over distance along the yellow arrow endorses a linear calcium gradient. c, Bone volume observed in X-ray computed tomography (CT). A linear gradient was not resolvable with the given CT acquisition parameters. Scale bar corresponds to 500 μm.

4.3. Fat distribution

Proteins related to metabolism of adipose tissue were detected in the tendon proteome. Therefore, a histological investigation of fat distribution was performed. Porcine enthesis cryocut sections were stained using Masson-Goldner's trichrome stain and sudan III to investigate the connective tissue and the distribution of adipose tissue within the Achilles tendon-bone interface, respectively. Masson-Goldner's trichrome staining revealed a different staining pattern at the interface region compared to tendon and bone (Figure 14a). Typically, the Masson-Goldner's stain colors cytoplasm and muscle fibers in red and connective tissue in green. The Masson-Goldner's staining is not specific enough to draw explicit conclusions with regard to composition of the matrix, but it became clear that the stain uptake of interface region and tendon differ since the interface region took up primarily green stain whereas the tendon region took up both green and red stain.

Sudan III was used to stain adipose tissue resulting in an orange coloring of adipose depots. Staining of Achilles tendon-bone interface cryocut sections showed that adipose depots appeared to be distributed within bone and tendon, but much less in the porcine interface (Figure 14b). The fat within tendon could be ectopic fat or dispersed fat from the fat pads adjacent to the enthesis. It has been described that fatty endotenon is a feature of tendons that flare out considerably at their enthesis, most likely fulfilling the function of filling space between bundles of collagen fibers⁸⁰.

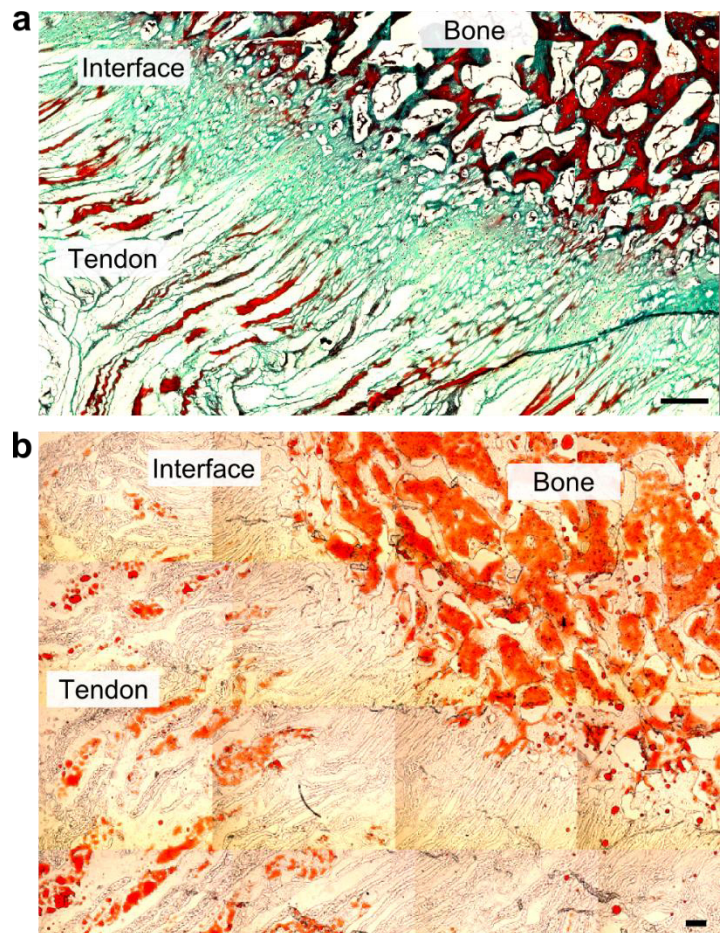


Figure 14: Histological investigation of the enthesis. a, Masson's trichrome stain of the enthesis. The interface bound less red stain than tendon and bone. Image with courtesy of Dr. Kai Xu, visiting researcher from China. b, Sudan III stain of the enthesis showed less presence of fatty tissue within the interface region. Image with courtesy of Katharina Kuempel, student assistant. Scale bars corresponds to 300 μm .

4.4. Interface schematic

In the previous paragraphs it was shown that tendon fibers undergo a transition in both geometry and composition before attaching to bone. Collagen type I-rich tendon fibers with a diameter of $(105 \pm 21) \mu\text{m}$ splay and subdivide into collagen type II-rich interface fibers with a diameter of $(13 \pm 4) \mu\text{m} \sim 500 \mu\text{m}$ before the bone (Figure 15a). The composition of the matrices of tendon and interface region are distinct; different types of small leucine-rich proteoglycans as well as fibril associated collagens with interrupted triple helices are enriched in the two tissues. The interface region is also characterized by high levels of hyaluronan proteoglycans aggrecan and versican. A linear calcium gradient was indicated to be located at the tendon-bone interface spanning $\sim 100 \mu\text{m}$. Adipose depots were detected within the interfibrillar spaces of the tendon. The structural and compositional key facts about the Achilles tendon-bone interface identified in this thesis were visually summarized in the following schematic (Figure 15b).

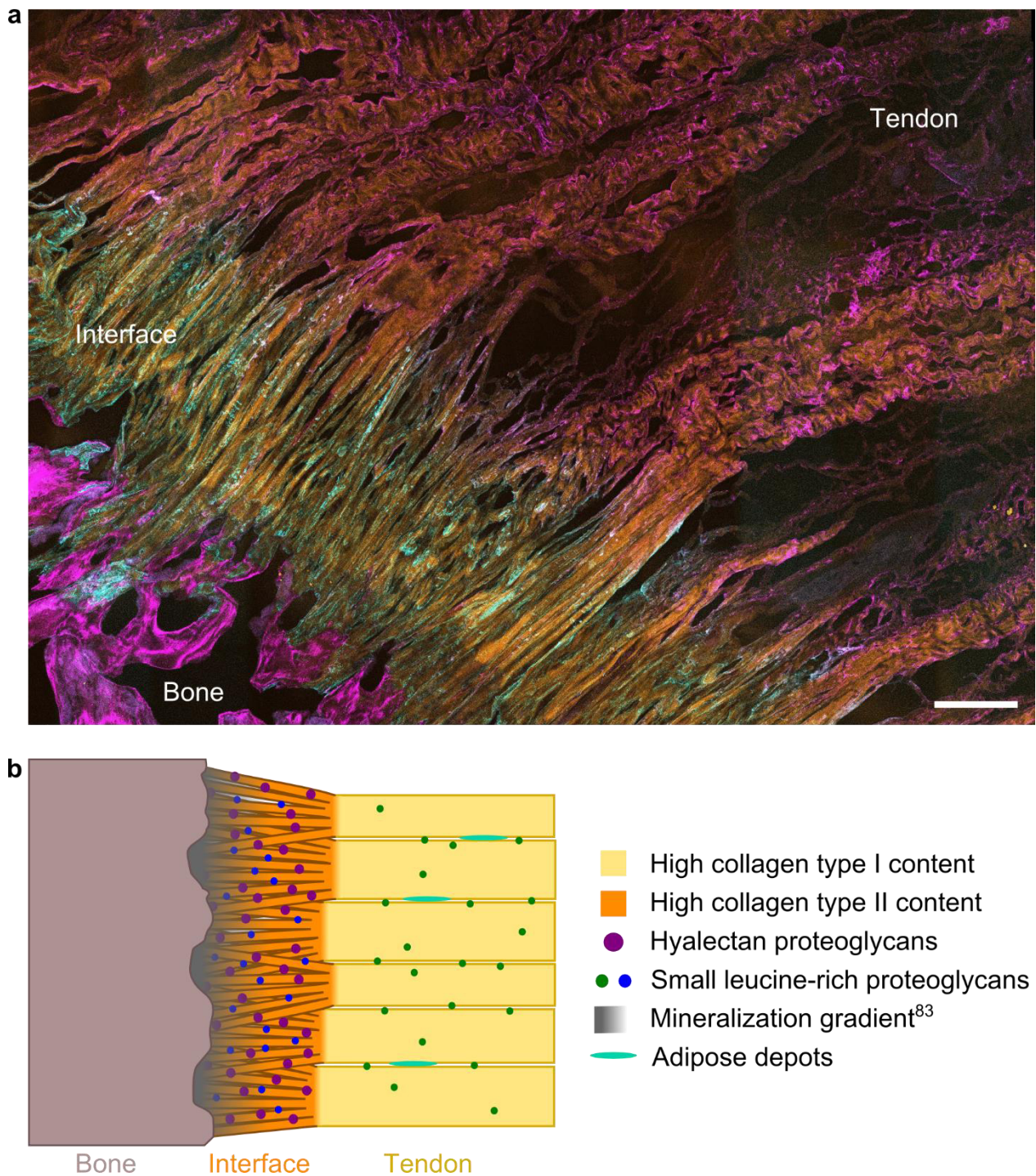


Figure 15: The porcine Achilles tendon-bone interface. a, Confocal image of enthesis cryocut section shows the interface region with geometrical and compositional transition. Cryocut section was stained for collagen type I (magenta) and collagen type II (cyan), reflection is depicted in yellow. Scale bar corresponds to 200 μm . b, Schematic of Achilles tendon enthesis. Collagen type I-rich tendon fibers undergo a transition in both geometry as well as composition $\sim 500 \mu\text{m}$ before attaching to bone. Collagen type II-rich splayed interface fibers are supported by a distinct extracellular matrix with enriched hyalectan proteoglycans aggrecan and versican. Different small leucine-rich proteoglycans are enriched in the interface region and tendon. Adipose depots are dispersed between tendon fibers. Schematic is adapted from Rossetti & Kuntz et al.¹.

4.5. Discussion

Extracellular matrices have diverse functions in different tissues which is achieved by their complex chemical compositions²⁸. The biomolecular composition of the Achilles tendon enthesis forms the molecular basis of its distinct structural and functional features¹. In this chapter, the compositional features of the extracellular matrix of tendon and interface region were investigated. Fibers were observed to undergo a compositional change from high collagen type I abundance in tendon to high collagen type II abundance in the interface region. The matrices of interface region and tendon showed different chemical properties by varying X-ray absorbance and/or uptake of contrast agent. The proteomes of interface region and tendon were characterized and 433 proteins were detected in total. Of these, 48 proteins showed statistically significant (FDR 0.05, $p < 0.013$) enrichment of at least twofold in one of the tissues. The lists of enriched proteins were analyzed for overrepresented biological processes detecting cartilage-related biological processes in the interface region. Furthermore, calcium distribution and fat distribution at the interface region were investigated. Investigation of fat distribution showed lower abundance of adipose depots at the interface region than in tendon and bone.

Collagenous components play an important role in the structural characteristics of an extracellular matrix. Enrichment of collagen type II in the interface region extracellular matrix was detected in both immunofluorescence confocal microscopy (Figure 8) of enthesis cryocut sections as well as the mass spectrometric proteome study (Figure 11). Immunofluorescence imaging of enthesis cryocut sections revealed that fibers not only underwent a compositional transition from high abundance of collagen type I in tendon to high abundance of collagen type II in the interface region (Figure 8), but also that this compositional transition coincided with the geometrical transition described in chapter 3.1. Interestingly, collagen type II, which was highly abundant in the interface region with splayed fibers, is also the main component of cartilage, which has a more network-like structure than the highly aligned tendon fibers²⁶. This indicates that the different properties of collagen type II and collagen type I may influence the structural transition observed.

In the proteome study, liquid chromatography tandem mass spectrometry was performed to reveal the full complexity of the tendon and interface matrices. Proteins present in the two tissues were directly compared for each biological sample. A total of 433 proteins in tendon and interface region was detected. 48 of these proteins showed a statistically significant difference in expression between interface region and tendon. The amount of proteins with statistically significant difference in expression was possibly underestimated, since there

was a technical limitation of sample preparation precision resulting in tendon residuals in the interface region samples. Besides collagen type II, a differential expression of various collagens was detected in the proteomes of tendon and interface region. Different FACIT collagens were detected in interface region and tendon. FACIT collagen type IX alpha-1 was enriched in the interface region and FACIT collagens type IX alpha-3 and type XII alpha-1 were enriched in the tendon. FACIT collagens are structurally very diverse collagens⁴⁰. FACIT collagens contain non-collagenous regions that lead to kinks in the macromolecular fiber structure²⁸ resulting in great importance of FACIT collagens for fiber structure. Therefore, expression of different FACIT collagens in tendon and interface region may play a role in the different fiber geometries described in chapter 3.

The proteome study further showed enrichment of several proteins that are involved in fibril formation, organization and crosslinking; microfibrillar-associated protein 2, lysyl oxidase homolog 3, tenascin XB orthologous, and ADAMTS-like protein 4. For example, lysyl oxidase mediates extracellular matrix cross-linking and promotes matrix stiffening in osteoarthritic cartilage⁸⁶. Tensile strength and fiber stability rely on the cross-links between collagen molecules⁴⁸. Collagen type II molecules have more cross-linking residues than collagen type I which may result in a more stable network-like tissue structure⁴⁷. ADAMTS-like protein 4 accelerates microfibril formation⁸⁷ and may thus be involved in the transition in fiber diameter observed in 3.1. Since these proteins all modulate fiber structure, it is very likely that these proteins are involved in facilitating the transition of fiber geometry described in chapter 3. Considering that a unique protein component such as collagen type I can perform different functions in different tissues while exhibiting different morphologies shows the importance of the associated cross-linking proteins or molecules; for example, collagen type I can form rigid and shock-resistant tissue in bone when associated with hydroxyapatite, it can behave like an elastomer with low rigidity in tendon, or exhibit optical properties like transparency in the cornea¹⁰. Conclusively, the observed presence of fibril organizational and cross-linking proteins plays an important role in both the mechanical function as well as the structural organization of the tissue.

Tissues adapt to the external demands they encounter. For example, tendon function depends on the structure of tendon and tendons get remodeled according to applied load with respect to their biochemistry and structure^{20,88,89}. The principle of “form follows function” relates to concept of mechanical load influencing the structure of a tissue⁸⁰. With increasing exercise, collagen cross-links, fiber diameter as well as fiber packing density change, and the proteoglycan content alters^{20,90}. The biological processes skeletal system development,

connective tissue development, and organ morphogenesis were detected as overrepresented in the gene ontology analysis of proteins enriched in the interface. This may indicate that adaptational mechanisms occur at the interface region in response to applied mechanical load which result in the observed difference in composition between interface region and tendon.

Several proteins related to fat metabolism were identified in the tendon proteome such as the perilipin proteins and fatty acid binding protein (Table 3). Histological investigation of enthesis using widefield transmitted light microscopy of histologically stained cryocut sections also indicated the presence of interspersed adipose depots within the tendon region of the enthesis. Endotenon adipose depots have been described to lie within the interfibrillar matrix that separates adjacent tendon fibers and are a feature of tendons that flare out at their attachment site⁸⁰. Interspersed fat at entheses is suggested to function in space-filling and proprioception⁸⁰. A retromalleolar (preAchilles) fat pad has been described which protrudes into the retrocalcaneal bursa⁸⁰. The fat pads are suggested to enable free movement between tendon and bone by reducing friction between tendon and bone and acting as variable space filler⁸⁰. Additionally, it may also have a role in proprioceptive monitoring of angle changes⁹¹. The adipose tissue depots contain blood vessels^{80,91}, which may explain for the detection of angiogenesis-related proteins in the tendon proteome.

Differential enrichment of various proteoglycans was detected in the proteomes of tendon and interface region. Proteoglycans are negatively charged due to their attached glycosaminoglycan chains and are predominantly localized in the interstices between collagen fibers⁵⁰. In the interface region aggrecan and versican were enriched, which are members of the large chondroitin sulfate proteoglycans, also called hyalactans. Hyalactan proteoglycans are reported to occur predominantly in compressed tissue regions²⁰. These highly negatively charged hyalactan proteoglycans lead to an osmotic pressure within the interface tissue that counteracts compressive stresses that arise when the tissue is under tension^{50,92}. Interestingly, mechanical load was shown to result in altered proteoglycan expression, in which tensile load induced decorin expression whereas compressive load induced hyalactan aggrecan expression^{20,52}. Enrichment of hyalactans in the interface region shields the interface region from compressive stresses and thus contributes to the resilience of the enthesis. Further, the heterogeneous micromechanical behavior¹ may also be influenced by interactions of aggrecan with collagen since they reduce collagen network stiffness and apparent viscosity by facilitating fiber sliding²⁰.

Additionally, members of the small leucine-rich proteoglycans (SLRP) were differentially enriched in tendon and interface region. SLRPs are small proteoglycans that contain a conserved leucine-rich repeat motif and that function as structural constituent of the ECM as well as signaling molecule⁵¹. SLRPs chondroadherin and biglycan were enriched in the interface region, while SLRPs keratocan and decorin were enriched in the tendon. Chondroadherin is usually present in cartilage and is involved in integrin-linkage of chondrocytes to the surrounding ECM⁵¹. Decorin is considered a key regulator of ECM assembly since it limits collagen fibril formation²⁰. The enriched SLRPs belong to different classes of proteoglycans, namely class I with regard to decorin and biglycan, and classes II and IV with regard to keratocan and chondroadherin, respectively⁵¹. Even the class I SLRPs decorin and biglycan differ; their predominant glycosaminoglycan side chains are dermatan sulfate and chondroitin sulfate, respectively⁵¹. SLRPs regulate fiber formation as well as fibril width and interact with FACIT collagens that stick to the surface of collagen fibers to stabilize higher order structure^{28,20}. Expression of different SLRPs in the two tissues may thus be one of the molecular causes for the observed change in fiber geometry described in chapter 3.

Beyond that, SLRPs can function not only as structural constituents, but also as signaling molecules such as in tissue remodeling processes⁵¹. Furthermore, SLRPs have been shown to play an important role in modulating fiber sliding^{74,93}. Fiber sliding results in the characteristic viscoelastic properties of tendon⁹³ that were presented in Figure 7. Conclusively, enrichment of different SLRPs in the two tissues may crucially influence enthesis characteristics; firstly affecting fiber geometry by modulating fiber structure as described in the previous paragraph and secondly affecting mechanical behavior by modulating fiber sliding properties. Interestingly, tendon shows enrichment of proteoglycan 4 (lubricin) which functions as boundary lubricant⁹⁴. Proteoglycan 4 expression in tendon may be involved in the extensive fiber sliding processes that are crucial for the mechanical function of the tendon.

Proteoglycans, especially the large hyalectan aggrecan mentioned above, contain very long glycosaminoglycan side chains that attract water due to their negative charge⁵¹. Because of the high amount of water that binds to the glycosaminoglycan side chains, the biomolecules present within the tissue engage a large volume with relatively low density of proteins per volume possibly resulting in altered tissue density. Solute transport in cartilage is dependent on glycosaminoglycan content⁷⁸, fixed charge densities⁷⁹, and matrix structure^{78,77}. Tissue density as well as the transport process of contrast agent through the tissue may result in the observed difference in μ CT signal. This is especially interesting with regard to the results

of enthesis decellularization described in Xu & Kuntz et al.⁵⁶ showing that the interface region of entheses decellularizes less efficiently than the adjacent tendon and bone regions. This difference in decellularization efficiency may derive from different tissue densities of interface region and tendon as well as possibly less diffusion of the decellularization reagents through the interface region tissue as described in chapter 6.2.

The data presented in this chapter gave insight into the compositional transition at the interface and the intricate interplay of the observed compositional transition with the structural transition described in chapter 3 as well as the influence on mechanical behavior¹.

5. Cell differentiation at the enthesis

Cells respond to the physicochemical cues from their microenvironment⁹⁵. Since cells in the interface region reside within a different microenvironment than cells in the tendon (Figure 16), it is highly interesting to further classify these cells with regard to future biomimetic tissue engineering strategies. In the following paragraphs, cell differentiation of interface region cells was compared to tendon cells as well as cartilage cells and biomarkers for interface cells were identified.

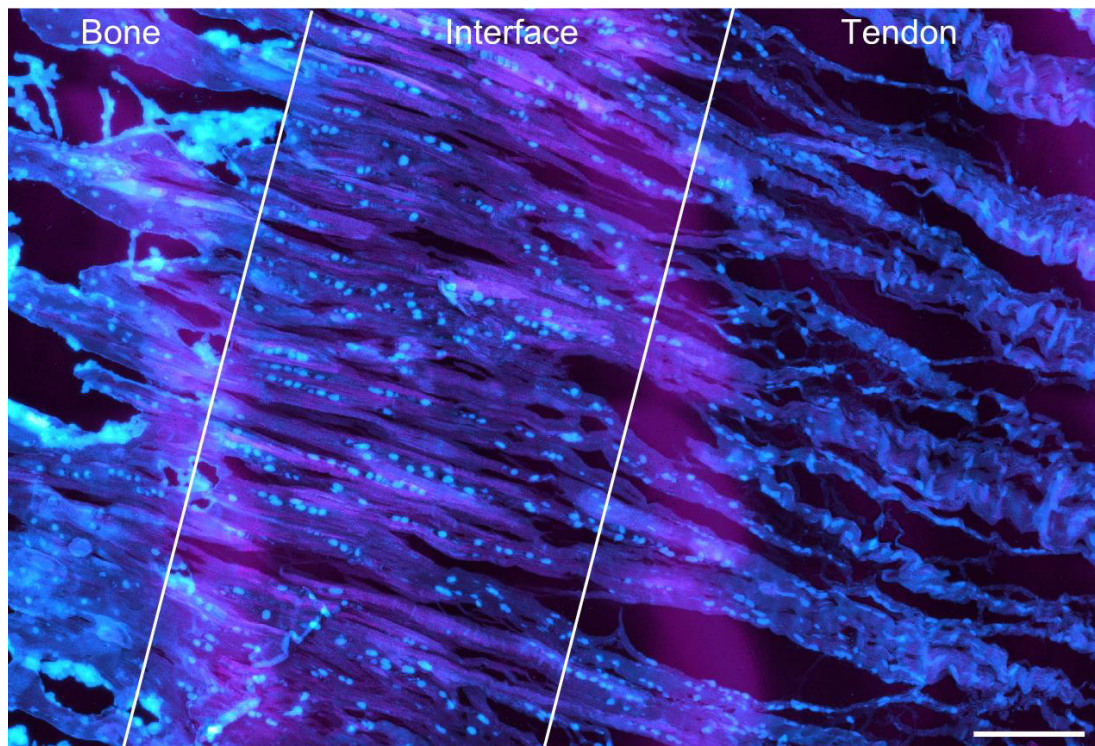


Figure 16: Microenvironments of cells within tendon and interface region differ. The microenvironments of cells within interface region differ geometrically as well as compositionally as discussed in chapters 3 and 4. Enthesis cryocut section was stained for cells using SYTO® 13. Cells are depicted cyan, confocal reflection is depicted magenta. Scale bar corresponds to 150 μm .

5.1. Morphological characteristics

Morphological differences of cells residing within the Achilles tendon and the interface region of the attachment were observed in confocal microscopy of enthesis cryocut sections

stained with fluorescent cell dyes Yo-Pro®-1 or SYTO® 13. Cells residing within the tendon were observed to be arranged in strings of cells that showed an elongated morphology and were aligned in the direction of tendon tension (Figure 17a,c). Cells at the interface were two-dimensionally observed to be round-shaped and to be often arranged pairwise (Figure 17b,c). The morphology of the cells at the interface resembled morphology of chondrocytes which are cartilage cells that are arranged in cartilage lacunae.

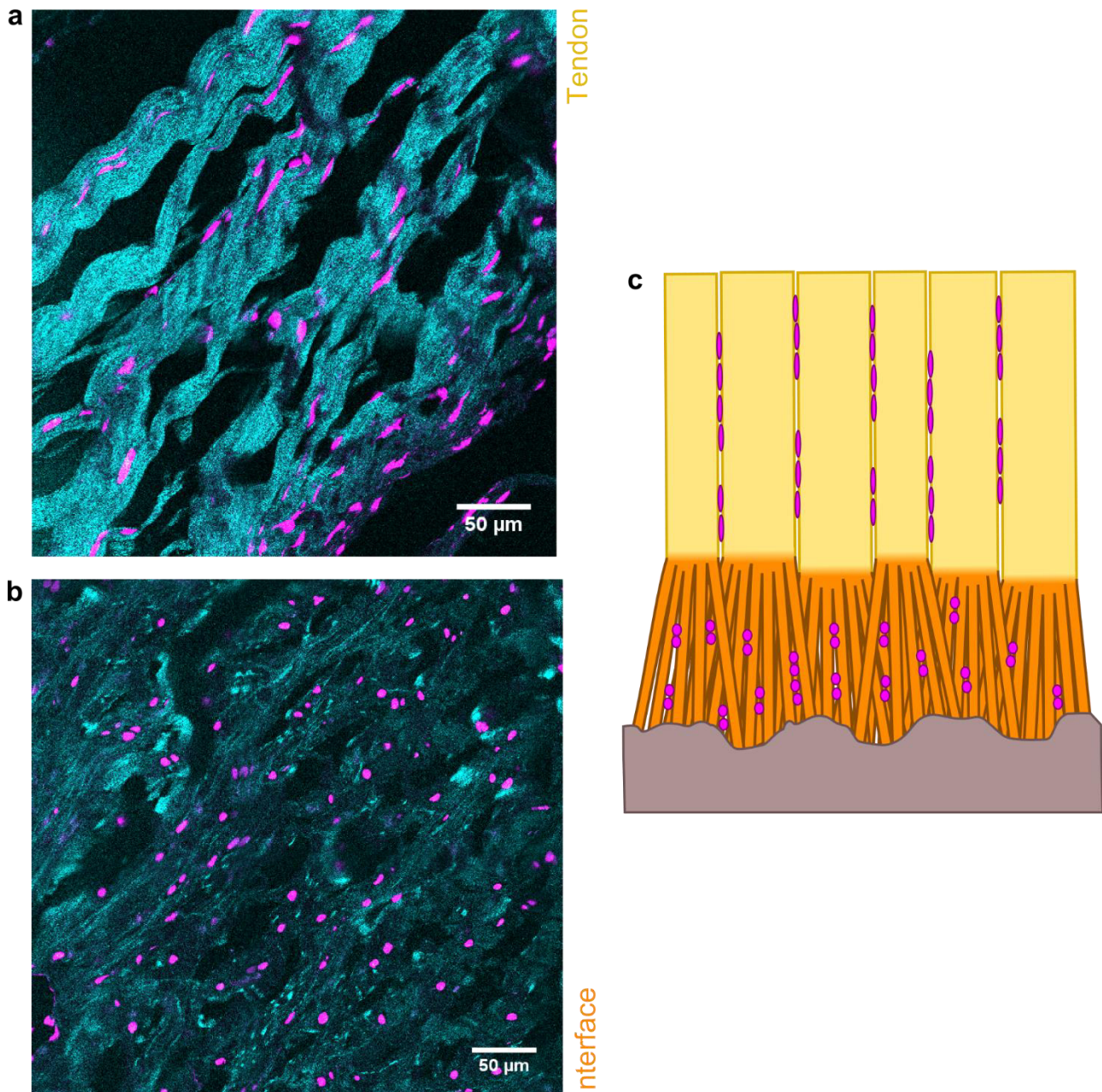


Figure 17: Morphological characteristics of enthesis cells. a, Cells residing within tendon were longitudinally arranged along the axis of tension in strings between tendon fibers. b, Cells within the interface were round shaped and were often arranged in pairs. c, Schematic of cell arrangement at the enthesis.

5.2. Transcriptomics

Due to observed morphological differences of cells residing within the interface region compared to tendon cells (5.1), cellular differentiation was investigated to identify biomarkers for interface cell differentiation that may result in the observed morphology. In the studies of enthesis matrix composition (4.2.2.1), many cartilage-related biomolecules were detected in the interface region. Therefore, interface region cells were also compared to cartilage cells from porcine knee cartilage. Samples were acquired from Achilles tendon enthesis interface region, Achilles tendon, and knee articular cartilage tissue, shock-frozen, cryocut sectioned, and mRNA was extracted as described in 2.8. Total mRNA samples were reverse transcribed into cDNA libraries for interface region, tendon, and cartilage. cDNA libraries were sequenced by GATC Biotech AG using an Illumina next generation sequencing platform (Figure 18).

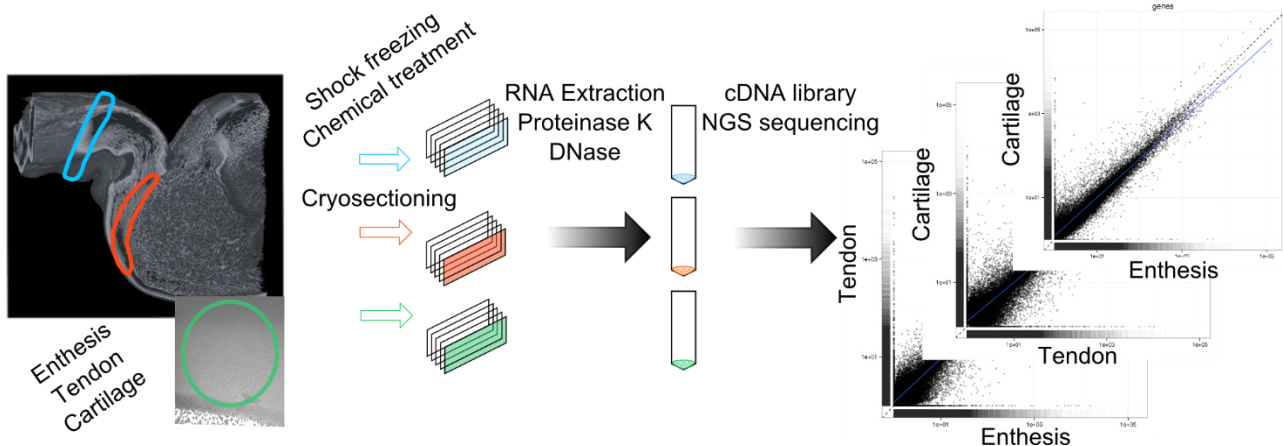


Figure 18: Experimental design of the transcriptomic study. Tendon (blue), interface region (orange), and cartilage (green) samples were excised, shock-frozen in liquid nitrogen, chemically treated to prevent RNA degradation and cryocut sectioned to enhance RNA extraction. High quality RNA was extracted using a refined protocol including proteinase K and DNase digests. cDNA libraries were produced and sequenced by GATC Biotech AG using next generation sequencing on an Illumina platform. Transcriptomes of enthesis, tendon, and cartilage were compared to each other.

The raw sequence data of all single end reads was quality checked (QC) and the QC passed sequencing reads were aligned to the pig reference genome Sscrofa10.2. The genome of Sscrofa10.2 (database version 87.102) had 21,630 annotated coding genes and 30,585

gene transcripts with 52,372 GENSCAN gene predictions. An average of 88.9 % of all QC passed reads were aligned to the reference genome *Sus scrofa*10.2 (Table 4).

Table 4: Summary of sequence alignment to the genome of pig (*Sus Scrofa*). Number of reads mapped to the porcine reference genome *Sus scrofa*10.2.

Sample	QC passed reads	Mapped reads	% mapped
Enthesis pool 1	95,101,732	84,440,834	88.79
Enthesis pool 2	95,101,732	84,440,834	88.79
Enthesis pool 3	30,955,077	27,599,523	89.16
Tendon pool 1	37,869,610	33,618,568	88.77
Tendon pool 2	53,789,951	48,086,845	89.40
Tendon pool 3	31,952,065	28,443,958	89.02
Cartilage pool 1	95,101,732	84,440,834	88.79
Cartilage pool 2	60,972,484	54,047,466	88.64

The software Cuffdiff tracked the mapped reads and determined values of fragment per kilobase per million mapped reads (FPKM) for each transcript in all samples indicating the level of expression.

In total, 34468 transcripts were detected in the three analyzed tissues which were tendon, enthesis, and cartilage (Table 5). Of these, 14128 were not functionally annotated meaning that the functions of the proteins that are encoded by the corresponding transcripts were not yet known. Values of FPKM = 0 were observed for 1217 transcripts in the enthesis, 989 transcripts in the tendon, and 382 transcripts in the cartilage indicating that they were either not expressed or below the detection limit with the given sequencing depth. In total, 33251 transcripts with FPKM > 0 were detected in the enthesis, 33479 transcripts with FPKM > 0 were detected in the tendon, and 34083 transcripts with FPKM > 0 were detected in cartilage.

Comparison of enthesis and tendon transcriptomes showed 3980 transcripts to be statistically significant differentially expressed in both tissues, of which ~ 46 % and ~ 54 % were enriched in enthesis and tendon, respectively (Table 5). Comparison of enthesis and cartilage transcriptomes identified 395 transcripts to be statistically significant differentially expressed in both tissues, of which ~ 2 % were enriched in enthesis and 98 % were enriched in cartilage. Comparison of the transcriptomes of cartilage and tendon detected 946 statistically significant differentially expressed transcriptomes in both tissues, of which ~ 29 % were enriched in tendon and ~ 71 % were enriched in cartilage (Table 5).

Table 5: Global differences in the transcriptomes of enthesis, tendon, and cartilage.

Number of transcripts	Enthesis vs. tendon	Enthesis vs. cartilage	Cartilage vs. tendon
Totally differentially regulated	3980	395	946
Upregulated in enthesis	1815 (45.6 %)	6 (1.5 %)	-
Upregulated in tendon	2165 (54.4 %)	-	274 (29.0 %)
Upregulated in cartilage	-	389 (98.5 %)	672 (71.0 %)
Not annotated (of total)	1600 (40.2 %)	207 (52.4 %)	387 (40.9 %)

Lists of all detected transcripts within the three tissues and their corresponding FPKM values were analyzed to identify all candidates with existing gene annotation and FPKM > 0. The identified lists of genes with gene annotation and FPKM > 0 of enthesis, tendon and cartilage were compared using GeneVenn⁹⁶. The venn diagram shows the number of tissue specific genes as well as the number of genes that overlapped between two of the tissues or all tissues (Figure 19). 13798 genes were expressed in all three tissues. Tendon exhibited 30 tissue specific genes whereas enthesis and cartilage had one tissue specific gene and 61 tissue specific genes, respectively. 39 genes were only expressed in tendon and cartilage,

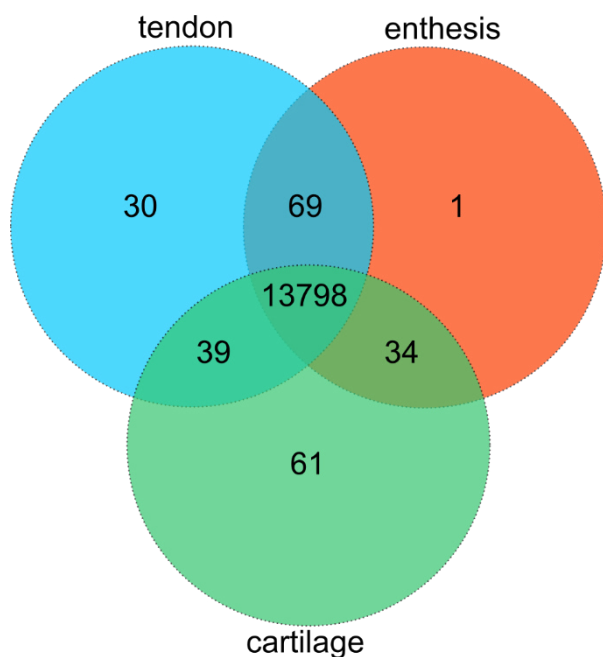


Figure 19: Venn diagram of genes detected in the three tissues showing the number of overlapping and differentially expressed genes.

Only genes that were annotated and had FPKM > 0 were considered, duplicates were not considered twice.

69 genes in tendon and enthesis, and 34 genes in enthesis and cartilage (Figure 19).

The sample preparation limitation described for the proteomic analysis (4.2.2) also applied to the transcriptome study. The differences of tendon and enthesis transcriptome are thus possibly larger than resolved here.

Of the 21640 porcine genes and 26487 known gene transcripts⁹⁷, 13976 genes were detected in the three tissues and successfully annotated. The identified lists of genes that were only expressed in one of the three tissues (Figure 19; 30 genes for tendon, 1 gene for enthesis, and 61 genes for cartilage) were analyzed using PANTHER gene ontology analysis for statistical overrepresentation of biological processes

and reactome pathways. The genes expressed in cartilage only showed overrepresentation of reactome pathways acyl chain remodeling of phosphatidylinositol and phosphatidylserine. No overrepresented reactome pathways were identified for the lists of genes only detected in tendon and enthesis. None of the lists of genes that were only expressed in tendon, enthesis, or cartilage showed overrepresented biological processes.

GO analysis of the list of genes that were detected in all three tissues showed overrepresentation of biological processes such as DNA repair, cell component biogenesis, vesicle-mediated transport and underrepresentation of biological processes such as blood circulation, natural killer cell activation, G-protein coupled receptor signaling, and sensory perception of smell. Further, reactome pathways RHO GTPase effectors, processing of capped intron-containing pre-mRNA, transcriptional regulation by TP53, M phase, membrane trafficking, asparagine n-linked glycosylation, and cellular response to stress were overrepresented.

The transcriptomes of enthesis and tendon (5.2.1), enthesis and cartilage (5.2.2), as well as cartilage and tendon (5.2.3) were compared (Figure 19) to identify similarities and differences in the expression patterns of the cells residing within enthesis, tendon, and cartilage and are further elucidated in the following paragraphs.

5.2.1. Transcriptome comparison of enthesis and tendon

Transcriptome comparison of enthesis cells and tendon cells showed differential gene expression levels in the two tissues (Figure 20). For the 34468 transcripts that were detected in total in the two tissues, 13971 corresponding annotated genes were identified that encode for the transcripts. The large gap in the numbers may derive from alternative splicing mechanisms meaning that several alternative spliced transcripts can be encoded by the same gene. Furthermore, since the *Sus scrofa* genome is not fully annotated, information can get lost due to the inability of allocating certain transcripts to genes. Numerous predicted protein-coding loci have still no functional annotation and there is even less information about the function of many non-protein-coding genes⁹⁸.

Of the 13971 identified genes, 13867 were expressed in both enthesis and tendon, 69 genes were detected only in tendon, and 35 genes only in enthesis. GO analysis of the 69 genes detected in tendon showed an overrepresentation of the reactome pathway NCAM1 interactions and the GO molecular function complete for extracellular matrix structural constituents. GO analysis of the 35 genes detected in enthesis did not identify any overrepresented processes or pathways.

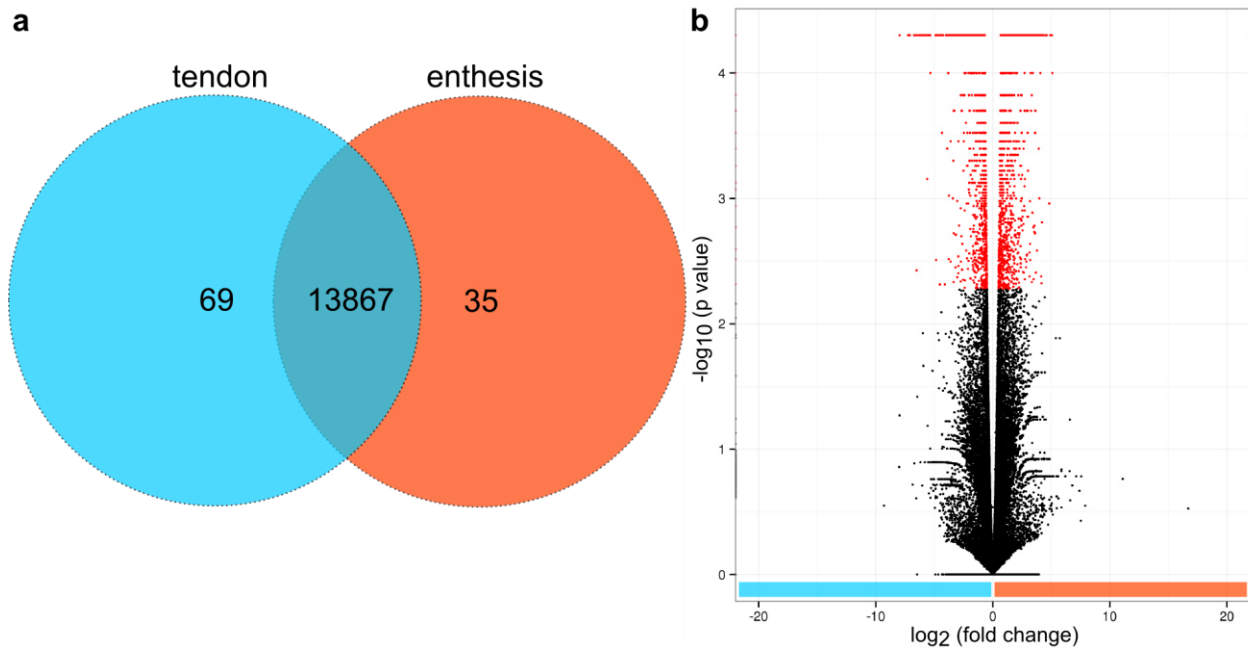


Figure 20: Differential expression of genes in enthesis and tendon. a, Venn diagram depicts the number of annotated genes that were only present in tendon (69) or enthesis (35) or present in both tissues (13867). b, Volcano plot of all differentially enriched transcripts detected in the transcriptomes of tendon and enthesis. Statistically significant enriched genes are marked red.

Of all 34468 detected transcripts, 3980 transcripts were identified that were differentially expressed in the two tissues, meaning that they occurred in both tissues, but were expressed in statistically significant different levels. 1600 transcripts of the 3980 transcripts that were either enriched in enthesis or tendon were not functionally annotated, so the function remained unknown (Table 5).

Enthesis tissue compared to tendon showed 1815 statistically significant enriched transcripts in total and 733 of these transcripts were statistically significant at least twofold enriched (Figure 20). 433 of all transcripts enriched in enthesis were not detected in tendon (FPKM = 0). Tendon tissue compared to enthesis tissue exhibited 2165 statistically significant enriched transcripts in total, of which 1648 were statistically significant at least twofold enriched. 635 of the tendon enriched transcripts were not detected in the enthesis (FPKM = 0).

PANTHER overrepresentation test gene ontology (GO) analysis of biological process complete showed multiple enriched biological processes in enthesis tissue compared to tendon. All genes that were at least twofold enriched were analyzed for overrepresentation of biological processes with *Sus scrofa* as reference list. Overrepresented biological processes

included proteoglycan biosynthesis, chondrocyte differentiation, collagen fibril organization, cartilage development, ADP metabolism, stem cell proliferation, morphogenesis of a branching structure, connective tissue development, ossification, ECM organization, angiogenesis, and skeletal development. A GO analysis was also performed for overrepresented reactome pathways and the identified pathways included Abl in Robo-Slit signaling, chondroitin sulfate biosynthesis, glycolysis, collagen biosynthesis, assembly of collagen fibrils, ECM proteoglycans, ECM organization, and integrin cell surface interactions.

GO analysis of the genes at least twofold enriched in tendon identified multiple overrepresented biological processes. The overrepresented biological processes included interferon-gamma production, immune response, leukocyte cell-cell adhesion, lymphocyte activation, cytokine production, fatty acid metabolism, cell migration, chemotaxis, positive regulation of locomotion, amongst many others. The overrepresented reactome pathways included rhodopsin-like receptors, G protein-coupled receptors signaling and immune system.

The top 10 genes with statistically significant highest and lowest \log_2 fold change and thus most distinct enrichment in enthesis and tendon, respectively, were identified and were listed in Table 6.

Table 6: Top 10 genes with highest and lowest \log_2 fold change in enthesis/tendon transcriptome comparison. Gene names and functions derive from GeneCards[®] and Ensembl⁹⁹.

Enriched in	Gene symbol	Gene name	Function	\log_2 fold change
Enthesis	-	ID: XLOC_025407	uncharacterized	8.0
	CLEC3A	c-type lectin domain family 3 member a	carbohydrate binding	7.2
	SCRG1	stimulator of chondrogenesis 1	can enhance differentiation potential of mesenchymal stem cells	7.1
	IBSP	integrin binding sialoprotein	binds to calcium and hydroxyapatite, mediates cell attachment	7.1
	EXTL1	exostosin like glycosyltransferase 1	glycosyltransferase, involved in chain elongation of heparan sulfate	6.7
	MMP13	matrix metalloproteinase 13	degradation of extracellular matrix such as in tissue remodeling	6.6
	C2orf82	chromosome 2 open reading frame 82	uncharacterized	6.5
	COL9A1	collagen type IX alpha-1 chain	collagen component of cartilage	6.4
	COL2A1	collagen type II alpha-1 chain	fibrillar collagen found in cartilage and the vitreous humor of the eye	6.3
	MELTF	melanotransferrin	iron binding function	6.2

Tendon	ADIG	adipogenin	adipocyte differentiation	-5.1
	RDH16	retinol dehydrogenase 16 (all-trans)	oxidoreductase	-5.1
	ENSSSCG00000030522	HCOP predicted: alcohol dehydrogenase	uncharacterized	-4.9
	LEP	leptin	regulation of energy balance, acts as a growth factor on certain tissues	-4.8
	ENSSSCG00000010992	SAQP7	uncharacterized	-4.6
	ADGRG3	adhesion G protein-coupled receptor G3	orphan receptor	-4.6
	TTC36	tetratricopeptide repeat domain 36	uncharacterized	-4.5
	ENSSSCG00000009699	-	uncharacterized	-4.4
	GALR1	galanin receptor 1	interaction with G-protein-coupled receptors	-4.2
	LGALS12	galectin 12	beta-galactoside-binding protein	-4.2

Transcription factors and growth factors play an important role in regulation of transcription and differentiation of cells. Generally, transcription factors are molecules that bind to DNA, either directly or indirectly, and regulate their transcription. Growth factors are molecules that interact with other molecules to influence cellular behavior such as proliferation and differentiation. Due to the importance of transcription factors and growth factors for the biological function of cells, the enriched gene lists were analyzed with regard to identification of expressed transcription factors and growth factors using DAVID bioinformatics resources 6.8. (2.9.2).

In the list of genes enriched in enthesis compared to tendon, 53 candidates with predicted transcription factor activity were identified as well as 23 candidates with predicted growth factor domains. All identified candidates with transcription factor or growth factor activity were listed in the appendix in Table 10. The protein-protein interaction network (Figure 21) of identified candidates was analyzed using the database Search Tool for the Retrieval of Interacting Genes/Proteins (STRING) of the European Molecular Biology Laboratory as described in 2.9.3. Interestingly, two transcription factors RUNX2 and SOX9, which are well-known in musculoskeletal tissues, were identified as nodes within the network. RUNX2 is a transcription factor that is essential to bone development and regulates the differentiation of chondrocytes and osteoblasts^{100,101}. SOX9 is a key regulator of chondrogenesis and has been suggested to mediate differentiation of tenocytes towards the chondrocyte lineage¹⁰².

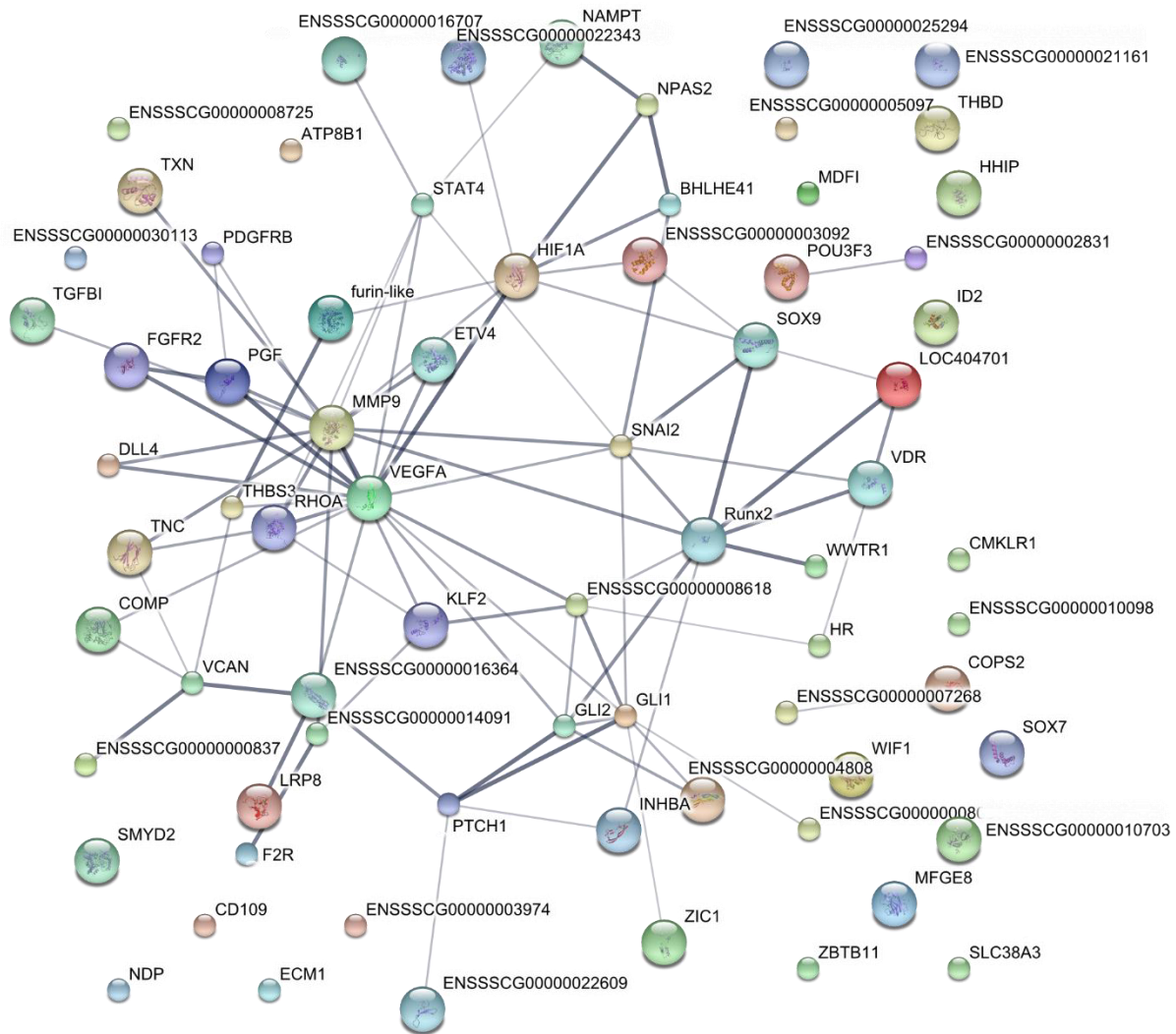


Figure 21: Protein-protein interaction network of transcription factors and growth factors enriched in enthesis. Protein-protein interactions were predicted using the database Search Tool for the Retrieval of Interacting Genes/Proteins (STRING). Line thickness indicates strength of data support for protein-protein interaction.

Additionally, the list of genes enriched in tendon was analyzed for candidates with growth factor or transcription factor activity. 32 candidates with transcription factor activity and 27 candidates with growth factor-like domains were identified within tendon. All identified candidates as well as the respective GO terms of tendon were listed in Table 11 in the appendix. The protein-protein interaction network of the identified candidates with transcription factor or growth factor activity was analyzed using STRING database. Several nodes were identified within the network (Figure 22) such as plasminogen activator (PLAU), CCAAT/enhancer-binding protein alpha (CEBPA), peroxisome proliferator-activated receptor gamma

5.2.2. Transcriptome comparison of enthesis and cartilage

The proteome study identified several cartilage-related molecules in the interface region. Therefore, interface region cells were not only compared to tendon cells but also to cartilage cells to identify differences and similarities of the expression patterns. Of all detected transcripts in enthesis and cartilage, 14002 were matched to annotated genes and analyzed using GeneVenn⁹⁶ (Figure 23a). Of all annotated genes, expression of 13832 genes was detected in both enthesis and cartilage, expression of 70 genes was detected only in enthesis and expression of 100 genes was detected only in cartilage.

PANTHER GO analysis detected that genes related to the GO term biological process of negative cell cycle regulation were overrepresented in the list of 70 genes that were only expressed in the enthesis. In the list of genes that were only detected in cartilage, an overrepresentation of reactome pathways was observed; hydrolysis of lysophosphatidylcholine and acyl chain remodeling of several phospholipids.

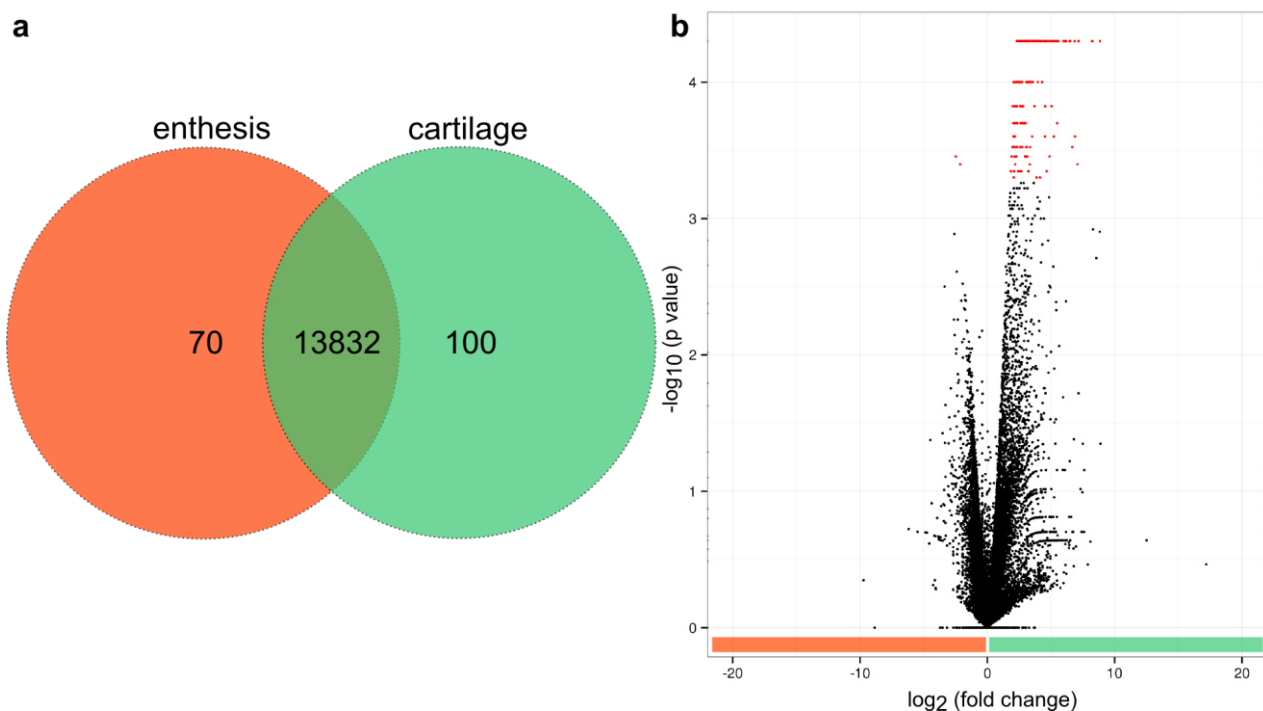


Figure 23: Differential expression of genes in enthesis and cartilage. a, Venn diagram depicts the number of annotated genes that were only present in enthesis (70) or cartilage (100) or present in both tissues (13832). b, Volcano plot of all differentially enriched genes detected in the transcriptomes of enthesis and cartilage. Statistically significant enriched genes were marked red.

Transcriptome comparison of enthesis and cartilage cells revealed a strong overlap between the two transcriptomes. Only 6 transcripts were enriched in enthesis cells compared to cartilage cells of which 4 transcripts were not functionally annotated (Figure 23). The same 4 transcripts that were not functionally annotated further had a value of FPKM = 0 in the cartilage tissue meaning that they were below the detection threshold. In total, 389 transcripts were enriched in cartilage compared to enthesis and were all at least twofold enriched. 203 of these transcripts were not functionally annotated. In total, 197 transcripts that were enriched in cartilage were not detected in the enthesis tissue (FPKM = 0). The top 10 genes with highest and lowest \log_2 fold change and thus enrichment in enthesis or cartilage, respectively, were listed in Table 7.

Table 7: Top 10 genes with highest and lowest \log_2 fold change in enthesis/cartilage transcriptome comparison. Gene names and functions derive from GeneCards® and Ensembl⁹⁹.

Increased in	Gene symbol	Gene name	Function	Log ₂ fold change
Enthesis	IGLC	immunoglobulin lambda constant	antigen binding	-2.5
	CXCL14	C-X-C motif chemokine ligand 14	cytokine	-2.1
	-	XLOC_012195	unknown	$-\infty$
	-	XLOC_041171	unknown	$-\infty$
	-	XLOC_041579	unknown	$-\infty$
	-	XLOC_041580	unknown	$-\infty$
Cartilage	CYTL1	cytokine like 1	cytokine-like protein	8.8
	ENSSSCG00000010546	unknown	unknown	8.2
	ENSSSCG00000000468	HCOP* predicted: WNT inhibitory factor 1	prevents Wnt signalling	7.2
	CPN1	carboxypeptidase N subunit 1	plasma metallo-protease	7.1
	CHAC1	chaC glutathione specific γ -glutamylcyclotransferase 1	pro-apoptotic component	6.9
	VWCE	von willebrand Factor C And EGF Domains	calcium ion binding	6.9
	ENSSSCG00000023305	HCOP* predicted: metallothionein	binding of heavy metals	6.7
	ENSSSCG00000030998	HCOP* predicted: WNT inhibitory factor 1 (WIF1)	prevents Wnt signalling	6.5

MATN3	matrilin 3	involved in formation of filamentous networks, homeostasis of cartilage/bone	6.5
DUSP2	dual specificity phosphatase 2	phosphatase, inactivates ERK1/2	6.2

* HCOP: HGNC Comparison of Orthology Predictions

The lists of genes that were at least twofold enriched were analyzed using PANTHER GO analysis for overrepresented biological processes and reactome pathways. No overrepresented processes nor reactome pathways were detected in the enthesis. In cartilage, multiple overrepresented biological processes were identified such as chondrocyte differentiation, cartilage development, angiogenesis, morphogenesis of branching epithelium, regulation of MAPK cascade, cell differentiation, developmental process, phosphate metabolism, tissue development, multicellular organismal development, regulation of cell proliferation. The analysis of GO reactome pathways detected acyl chain remodeling of phosphatidylinositol and phosphatidylserine as overrepresented.

The list of enriched genes in cartilage compared to enthesis was screened to identify candidates with transcription factor or growth factor activity. 11 candidates with transcription factor activity were identified as well as 13 candidates with growth factor activity and were listed in Table 12 in the appendix. Candidates with transcription factor or growth factor activity were classified for protein-protein interaction using STRING database (Figure 24). Bone morphogenetic protein 7 (BMP7), vascular endothelial growth factor A (VEGFA) and fibroblast growth factor 1 (AFGF) were identified as nodes within the protein network. BMP7 plays a role in skeletal development involving differentiation of mesenchymal cells towards osteoblasts and chondrocytes¹⁰³.

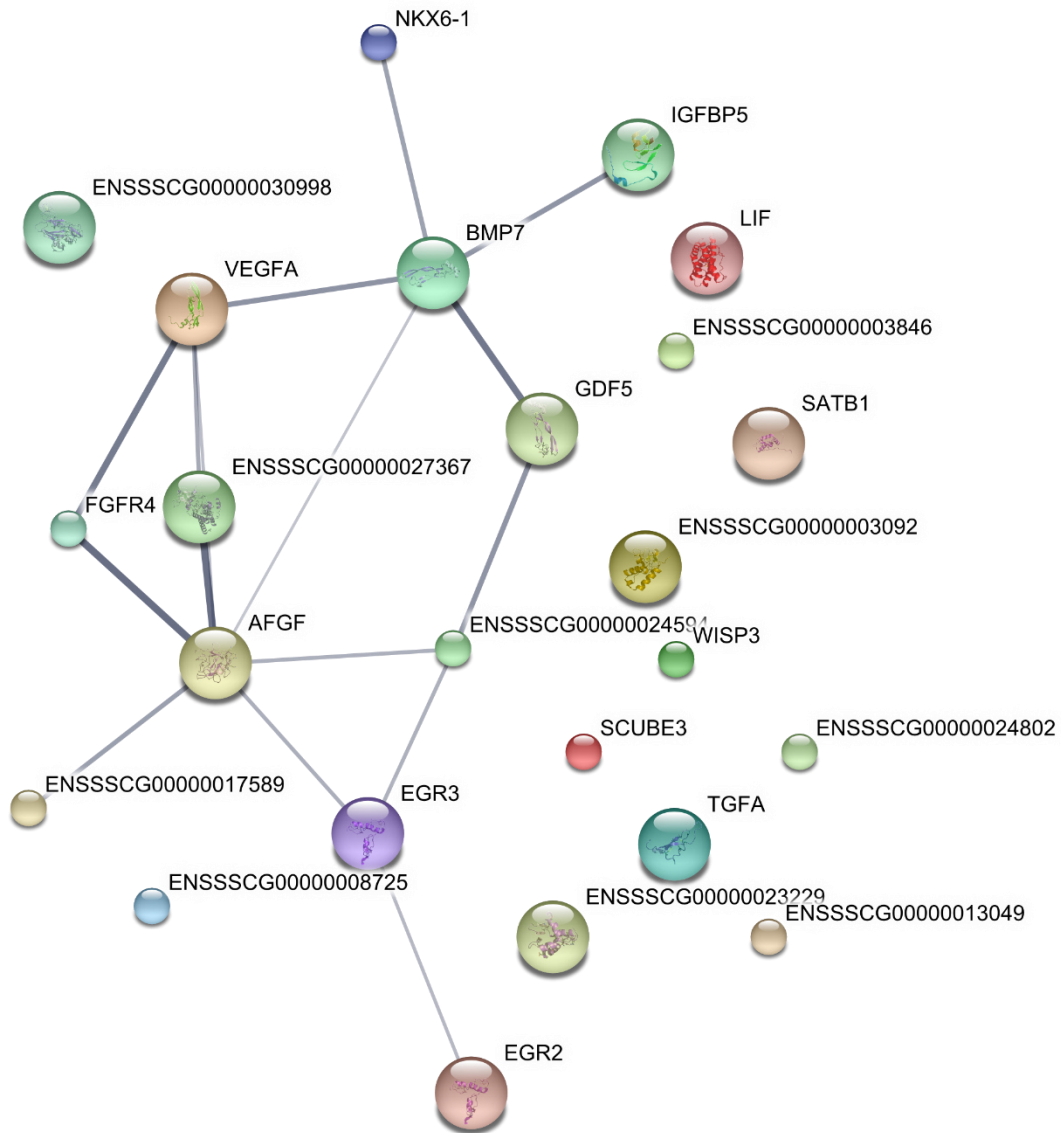


Figure 24: Protein-protein interaction network for transcription factors and growth factors enriched in cartilage. Protein-protein interactions were predicted using the database Search Tool for the Retrieval of Interacting Genes/Proteins (STRING). Line thickness indicated strength of data support for protein-protein interaction.

5.2.3. Transcriptome comparison of cartilage and tendon

For all transcripts detected in cartilage and tendon, 14031 corresponding annotated genes were matched. 13837 expressed and annotated genes were identified in both tendon and cartilage using GeneVenn (Figure 25a). 99 genes were only expressed in tendon. PANTHER GO analysis did not identify any overrepresented processes or pathways in the set of genes that was solely expressed in tendon using *Sus scrofa* as reference genome. 95 genes were only expressed in cartilage. GO reactome pathway acyl chain remodeling of phosphatidylinositol was overrepresented in the list of genes that were only expressed in cartilage.

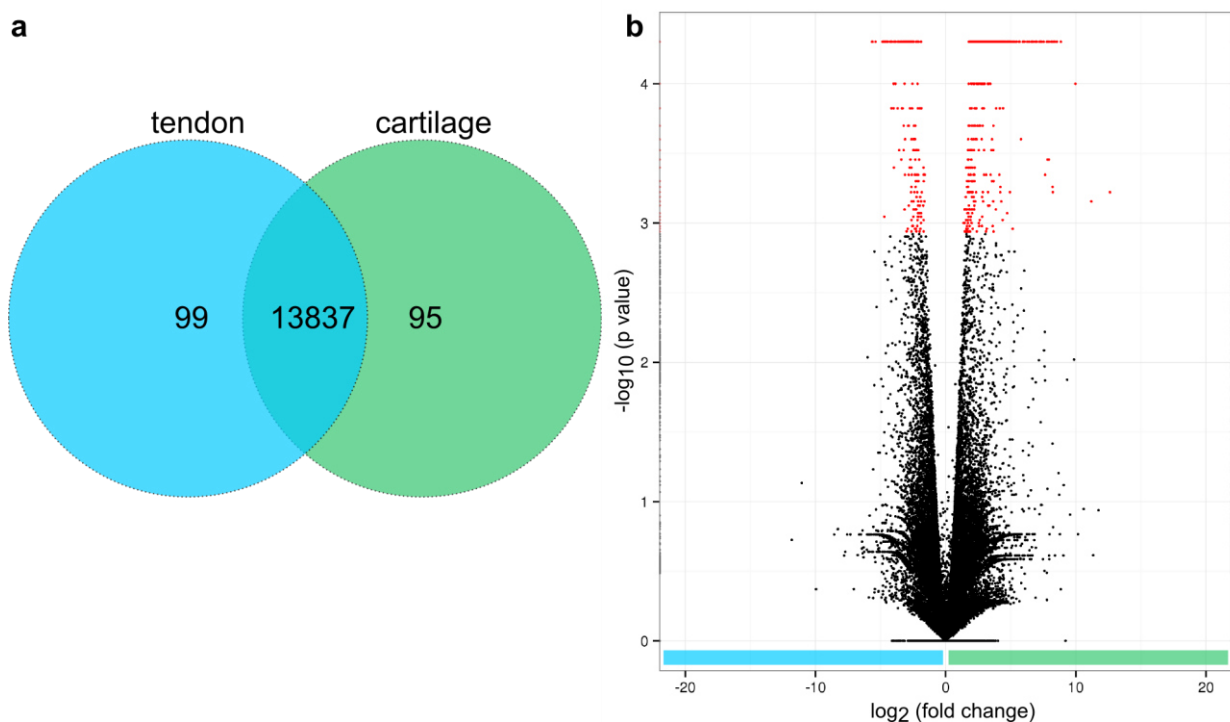


Figure 25: Differential expression of genes in tendon and cartilage. a, Venn diagram depicts the number of annotated genes that were only expressed in tendon (99) or cartilage (95) or expressed in both tissues (13837). b, Volcano plot of all differentially enriched transcripts detected in the transcriptomes of cartilage and tendon. Statistically significant enriched genes were marked red.

Comparison of cartilage and tendon transcriptomes identified 946 statistically significant differentially expressed transcripts (Figure 25b). Of these, 672 transcripts were at least twofold enriched in cartilage (~ 71 %) and 274 transcripts were at least twofold enriched in tendon

(~ 29 %). 282 transcripts that were detected in cartilage were not detected in tendon and 105 transcripts that were detected in tendon were not detected in cartilage (FPKM = 0). 387 of the all enriched transcripts were not annotated (~ 41 %). The top 10 genes with highest and lowest log₂ fold change were listed in Table 8.

Table 8: Top 10 genes with highest and lowest log₂ fold change in cartilage/tendon transcriptome comparison. Gene names and functions derive from GeneCards® and Ensembl⁹⁹.

Enriched in	Gene symbol	Gene name	Function	Log ₂ fold change
Cartilage	CYTL1	cytokine like 1	cytokine-like protein	12.6
	ENSSSCG00000030998	HCOP predicted: WNT inhibitory factor 1 (WIF1)	prevents Wnt signalling	11.2
	MATN3	matrilin 3	involved in formation of filamentous networks, involved in development and homeostasis of cartilage/bone	10.0
	MELTF	melanotransferrin	iron binding function	8.9
	COL9A2	collagen type IX alpha-2 chain	collagen component of cartilage, has an attached glycosaminoglycan chain unlike the other type IX alpha chains	8.6
	COL9A1	collagen type IX alpha-1 chain	collagen component of cartilage	8.4
	-	ID: XLOC_025408	unknown	8.3
	FOXA3	forkhead box A3	transcription factor	8.2
	-	ID: XLOC_025406	unknown	8.2
	CLEC3A	c-type lectin domain family 3 member A	carbohydrate binding	8.2
Tendon	MMRN1	multimerin 1	carrier protein for platelet factor V	-5.7
	CCL21	C-C motif chemokine ligand 21	CC cytokine	-5.6
	CADM2	cell adhesion molecule 2	cell adhesion molecule	-5.4
	CA3	carbonic anhydrase 3	reversible hydration of carbon dioxide	-4.9
	ENSSSCG00000001844	PLIN	lipid storage	-4.8
	PON3	paraoxonase 3	associates with high-density lipoprotein	-4.8
	APOL6	apolipoprotein L6	lipid binding	-4.7
	TUSC5	tumor suppressor candidate 5	may be involved in fat metabolism	-4.7
	TNMD	tenomodulin	angiogenesis inhibitor	-4.6
	FMO1	flavin containing monooxygenase 1	flavoenzyme	-4.6

GO analysis of enriched genes detected several overrepresented biological processes in cartilage compared to tendon. The overrepresented biological processes included proteoglycan biosynthesis, cartilage development, glycosaminoglycan biosynthesis, chondrocyte differentiation, morphogenesis of a branching structure, biomineral tissue development, endochondral bone morphogenesis, bone mineralization, hair cycle, molting cycle, odontogenesis, extracellular matrix organization, stem cell differentiation, amongst others. Further, overrepresented reactome pathways were identified in cartilage compared to tendon including hedgehog 'on' state, glycosaminoglycan metabolism, and extracellular matrix organization.

GO analysis of genes enriched in tendon compared to cartilage identified multiple overrepresented biological processes such as neutrophil/granulocyte chemotaxis, protein kinase B signaling, response to external stimulus, regulation of locomotion, cell migration, regulation of body fluid levels, lipid metabolism, and cell adhesion. GO analysis did not detect any overrepresented reactome pathways for the list of genes that were enriched in tendon compared to cartilage.

5.2.4. Biomarkers of the interface region

Biomarkers for differentiation of chondrocyte-like interface cells were identified by comparing the data sets of the proteome and transcriptome studies. All genes that were statistically significant enriched in both the proteome as well as transcriptome data sets were regarded as biomarkers. In total, 39 genes were identified to be enriched in either tendon or enthesis in both proteome and transcriptome. Figure 26 shows all 39 genes that were differentially expressed in both the proteomics and transcriptomics sets with their corresponding \log_2 ratios.

24 biomarkers were identified for the interface region (orange in Figure 26). The identified 24 genes showed enrichment in proteomics and transcriptomics data set of the interface region. For tendon, 13 biomarkers were identified that were enriched in both tendon transcriptome and proteome (blue in Figure 26). Interestingly, two candidates were identified that were enriched in the proteome of tendon, but in the transcriptome of the interface region. These two genes were COL14A1 and ECM1 and encode two proteins of the extracellular matrix: collagen type XIV alpha-1 chain and extracellular matrix protein 1, respectively.

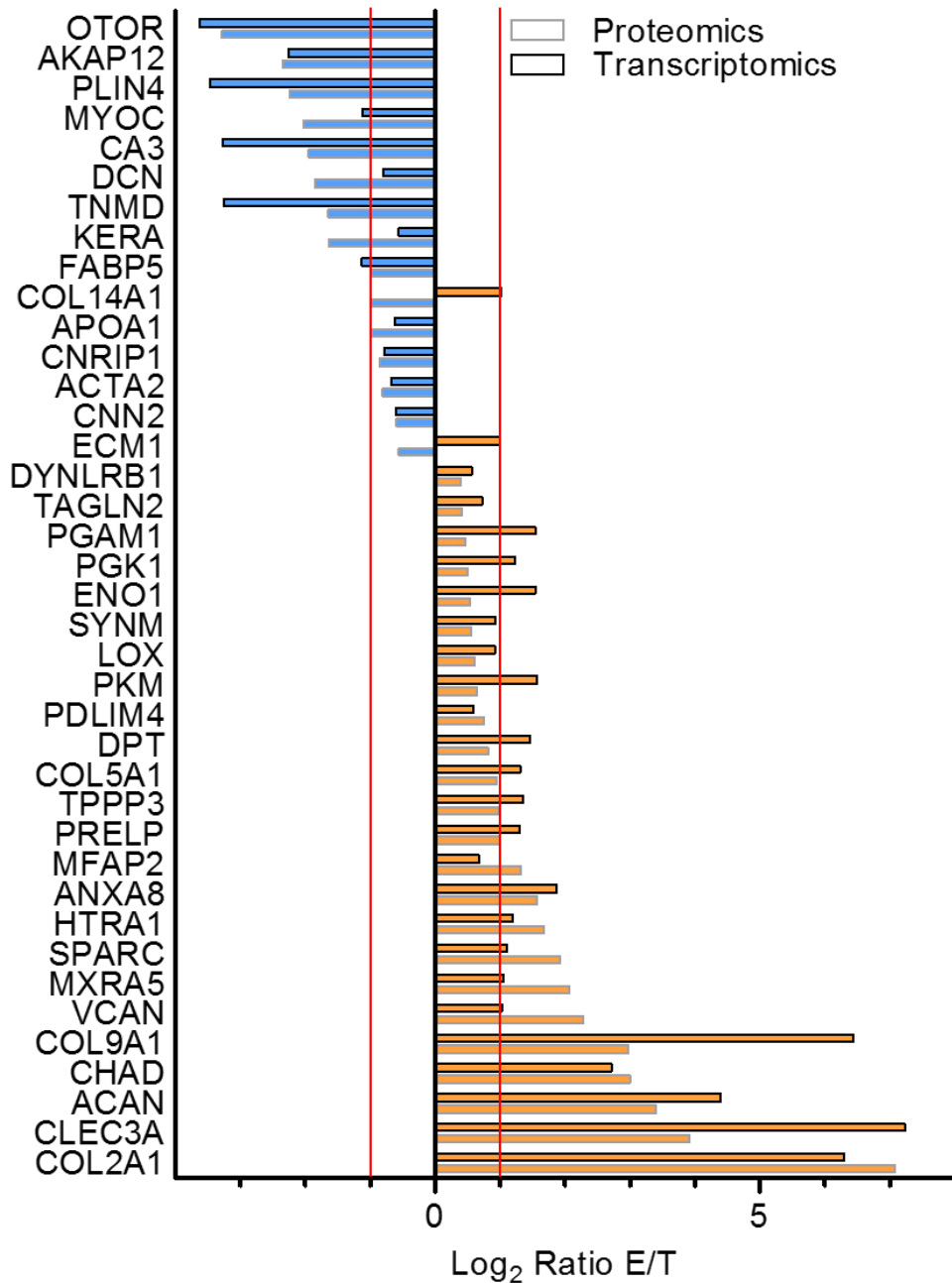


Figure 26: Identified biomarkers of interface region and tendon. Biomarkers are presented which were statistically significant enriched in both proteome and transcriptome of tendon or enthesis. Orange and blue bars represent enrichment in enthesis and tendon, respectively. Gray boxes correspond to enrichment in proteome and black boxes to enrichment in transcriptome. 13 genes were identified as tendon biomarkers (blue) and 24 genes as enthesis biomarkers (orange). Two genes (COL14A1 and ECM1) were identified that were enriched in the tendon proteome and conversely in the enthesis transcriptome.

Of all enriched biomarker candidates, 16 candidates were at least twofold enriched in both transcriptome and proteome (Table 9). Ten of these genes were enriched in the interface region and six of these genes were enriched in the tendon. The respective biomarker candidates as well as their gene products' functions and the corresponding log₂ ratios were listed in Table 9.

Table 9: Biomarkers that were at least twofold enriched in both transcriptome and proteome.

Identified biomarkers as well as the respective functions and log₂ ratios are depicted. Log₂ ratio differences of proteome and transcriptome data sets were calculated for each candidate.

Biomarker	Protein	Function	P* Log ₂ ratio E/T	T* Log ₂ ratio E/T	Δ _(P*-T*) log ₂ ratio E/T
Enthesis					
ACAN	aggrecan	hyalectan proteoglycan, cartilage-specific core protein	3.40	4.40	-1.00
ANXA8	annexin A8	bone-matrix induced protein	1.57	1.88	-0.31
CHAD	chondroadherin	small leucine-rich proteoglycan, interacts with collagen type II	3.00	2.72	0.28
CLEC3A	c-type lectin domain family 3 member a; cartilage derived c-type lectin	cell adhesion	3.92	7.23	-3.31
COL2A1	collagen type II, alpha-1 chain	fibrillar collagen	7.08	6.29	0.79
COL9A1	collagen type IX, alpha-1 chain	cross-links to surface of type II collagen fibrils	2.97	6.44	-3.47
HTRA1	HtrA serine peptidase 1	serine protease targeting extracellular matrix proteins such as fibronectin	1.68	1.19	0.49
MXRA5	matrix-remodelling associated 5	adhesion protein	2.07	1.05	1.02
SPARC	osteonectin	promotes mineral crystal formation	1.92	1.11	0.81
VCAN	versican	hyalectan proteoglycan	2.28	1.03	1.25
Tendon					
AKAP12	A-kinase anchor protein 12	scaffold protein in signal transduction, binds to protein kinase a	-2.35	-2.26	-0.09
CA3	carbonic anhydrase 3	metalloenzyme	-1.94	-3.27	1.33
MYOC	myocilin	cytoskeletal function	-2.02	-1.12	-0.90
OTOR	otoraplin	cartilage development suggested	-3.28	-3.63	0.35

PLIN4	perilipin-4	coats lipid droplets in adipocytes	-2.24	-3.47	1.23
TNMD	tenomodulin	tendon maturation	-1.64	-3.25	1.61

* P: proteome, T: transcriptome

The complete list of log₂ ratio differences between proteome and transcriptome levels of identified biomarkers is located in the appendix (Table 13). As explained in 4.2.2 and 5.2, limitations with regard to precision of interface region sample preparation may result in underestimation of proteomic and transcriptomic differences of tendon and enthesis. The log₂ ratios of the identified biomarkers were thus possibly higher than resolved in this study.

5.3. Discussion

Tissue engineering is a promising and evolving field to tackle the challenge of interface tissue regeneration. Most strategies of tissue engineering involve the use of scaffolds of any sort in combination with cells to biomimic the physiological behavior of the respective tissue. However, in-depth knowledge about the cells present in these tissues and their differential behavior is required to use their full potential for tissue engineering strategies. Tendon cells are relatively well characterized. They are described to be spindle shaped and arranged in long, parallel chains³². Tendon cells, namely tenocytes and tenoblasts, are known to comprise ~ 90 % of the cells within tendon³². The residual ~ 10 % of cells in tendon are, for example, chondrocytes that are located at pressure and insertion sites and vascular cells such as capillary endothelial cells³². However, relatively little is known about the cells present at the interface region between tendon and bone. The morphology of interface cells was observed to differ from the morphology of tendon cells in confocal microscopy (Figure 17), so that the transcriptomes of these cells were compared to identify their differentiation characteristics. Since the proteome analysis identified many cartilage-related cells within the interface region, interface cells were not only compared to tendon cells, but also to cartilage cells of the tibial plateau. We analyzed the expression patterns of cells residing within the tendon-bone interface and compared these expression patterns to cells residing within Achilles tendon and cartilage of the tibial plateau to identify differentiation markers for the respective cells.

A protocol was established to extract high-quality RNA from cryocut sections of shock-frozen tissue samples from Achilles tendon, Achilles tendon enthesis, and tibial plateau cartilage which was challenging due to high density of fibrous materials. A cDNA library was prepared

from extracted high-quality RNA and the transcriptomes were analyzed using next generation sequencing by GATC biotech AG. Expression levels were compared for enthesis and tendon (5.2.1), enthesis and cartilage (5.2.2), as well as tendon and cartilage (5.2.3). Of all sequencing reads that passed quality control, ~ 89 % were mapped to the reference genome Sscrofa10.2, thus information is lost already in the first step of the analysis. Besides the great advantages of using pig as animal model such as availability of samples from an abattoir and physiological similarity to human, it also comes along with several difficulties. Since pig is not as commonly used as animal model as for example, mouse, the commercial availability of test systems such as antibodies or expression microarrays for analysis of pig samples is limited. For example, many antibodies are not available for pig samples, so that antibodies targeted to other species have to be evaluated for their cross specificity for pig before usage in immunofluorescence confocal microscopy. Most importantly, genomic data and genome annotations are not as thoroughly investigated and deep knowledge of the pig transcriptome is limited⁹⁸. This complicated the analysis of porcine transcriptome data and may result in loss of information due to lack of gene annotation data.

Comparison of enthesis and tendon transcriptomes showed that of 3980 enriched transcripts, ~ 50 % were each enriched in enthesis or tendon, indicating that the cells have distinct expression patterns and may undergo different differentiation lineages. The list of genes only expressed in tendon showed overrepresentation of the NCAM1 interaction reactome pathway. NCAM1 is considered to be a cell adhesion mediator¹⁰⁴ and may play a role in the mechanotransduction process that transmits mechanical stimuli onto cells. The list of genes enriched in tendon showed an overrepresentation of biological processes related to immune response, cell migration, and fatty acid metabolism. Biological processes related to fatty acid metabolism were not only identified in the tendon transcriptome, but were also detected in the tendon proteome (4.2.2.2). This is readily explainable with the distribution of fat described in chapter 4.3 indicating interspersed fat deposits in the interfibrillar spaces between tendon fibers. G protein-coupled receptor (GPCR) signaling appears to play an important role in tendon cell signaling, since several reactome pathways related to GPCR were overrepresented.

In the interface region, 35 genes were detected that were not found in tendon. Many of these genes have not yet been annotated thus the respective encoded proteins are still not known. The list of top 10 genes with highest \log_2 fold change in the enthesis compared to tendon included two collagens, namely collagen type II alpha-1 and collagen type IX alpha-1. Interestingly, the two collagens were also enriched in the enthesis proteome (4.2.2.1). The list of

top 10 genes also included MMP13 which is known to be involved in degradation of extracellular matrix¹⁰⁵ and may play a role in the tissue remodeling to adapt to mechanical stresses¹⁰⁶.

The list of all genes enriched in enthesis showed enrichment of processes involved in collagen fibril organization and morphogenesis of a branching structure. The expression of these corresponding genes by cells within the interface region may be a molecular cause for the branched, splayed structures of collagen type II-rich fibers present at the interface region that were presented in 3.1. Furthermore, GO analysis showed many enriched biological processes involved in chondrocyte differentiation. For example, SCRG1, stimulator of chondrogenesis and known to enhance differentiation potential of mesenchymal stem cells, was strongly enriched in the interface region. This indicates that the cells present at the interface region show close similarity to the chondrocytes of cartilage which was further elucidated in the comparison to cartilage (5.2.2).

In the transcriptome comparison of enthesis and cartilage, an asymmetric distribution of enriched genes was observed. As shown in the volcano plot (Figure 23), multiple genes were enriched in cartilage compared to enthesis, but only very few were enriched in enthesis compared to cartilage. This may indicate that the cells present within the interface region derive from chondrocytes, but either remain in a certain differentiation stage or that they are a “reduced” version of a chondrocyte. Only two of the genes enriched in the enthesis compared to cartilage were annotated, therefore no conclusions can be drawn with regard to gene ontology of biological processes. CXCL14 is one of the genes enriched in enthesis, a cytokine known to inhibit angiogenesis¹⁰⁷. Previously it has been suggested that there may be inhibitory molecules expressed by enthesis cells due to the avascularity of entheses³⁰. CXCL14 may be one of these molecules and may play a role in the avascularity of entheses. The genes enriched in cartilage compared to enthesis showed overrepresented biological processes such as chondrocyte differentiation, angiogenesis, morphogenesis of branching epithelium, and cell differentiation. Interestingly, several processes such as chondrocyte differentiation and cartilage development previously shown to be overrepresented in enthesis compared to tendon, were now overrepresented in cartilage compared to enthesis. This may indicate that enthesis cells are much more chondrocyte-like than tendon cells, but not as much differentiated within the chondrocyte lineage as cartilage cells. This would be also consistent with the GO biological process of cell differentiation being overrepresented in the cartilage cells compared to enthesis cells.

The transcriptomes of cartilage and tendon showed symmetric differences as did enthesis and tendon transcriptomes. The top 10 enriched genes in cartilage compared to tendon included cytokine like 1 and matrilin 3, which were also found in the top 10 enriched genes in cartilage compared to enthesis, thus seemingly playing an important role in cartilage. Two collagen type IX chains, namely collagen type IX alpha-1 and collagen type IX alpha-2 were also highly enriched compared to tendon. Collagen type IX alpha-1 was also observed to be enriched in enthesis compared to tendon. Interestingly, CLEC3A was highly elevated in both cartilage and enthesis compared to tendon. CLEC3A is suggested to bind to heparin sulfate proteoglycans on cell surfaces and thus enhancing cell adhesion via integrins¹⁰⁸. The exact function of this molecule within the matrices of cartilage and enthesis have yet to be elucidated. The top 10 enriched genes in tendon compared to cartilage included several genes involved in lipid binding, storage and metabolism. This is, as previously mentioned, readily explainable considering the distribution of fat deposits within the interfibrillar spaces of tendon fibers (4.3). It is to mention that the top 10 genes enriched in tendon compared to enthesis and tendon compared to cartilage completely differ.

Tissue engineering approaches of tendon-bone interfaces rely on deep understanding of the cellular processes occurring at the natural tendon-bone interface. Identification of biomarkers enables the precise characterization of cells cultured on artificial tendon-bone interface scaffolds, such as design-engineered biomaterial scaffolds or decellularized donor scaffolds (6.2) with regard to their differentiation status. The results of proteome and transcriptome studies were compared to identify reliable biomarkers for enthesis cell differentiation. All candidate genes that were statistically significant at least twofold enriched both on protein level (proteome) and the mRNA level (transcriptome) were considered to be strong markers for enthesis cell differentiation. In total, 39 genes were identified that were enriched on both transcript level and protein level. 13 of these genes were enriched in the transcriptome and proteome of tendon and 24 of these genes were enriched in the transcriptome and proteome of the interface region. Interestingly, the remaining two genes showed enrichment in the tendon proteome, but conversely in the enthesis transcriptome. These two candidates were collagen type XIV alpha-1 chain and extracellular matrix protein 1. Collagen type XIV is a FACIT collagen that interacts with collagen fibers, possibly through interaction with small proteoglycans such as decorin and fibromodulin¹⁰⁹. Extracellular matrix protein 1 interacts with a variety of extracellular proteins and is suggested to be involved in various functions¹¹⁰ such as endochondral bone formation and angiogenesis. The observed difference between upregulation in transcriptome and proteome may derive from changing mechanical stimuli that the cells undergo. The half-life of proteins within the extracellular matrix

differs from the half-life of the corresponding mRNA¹¹¹. Therefore, it is conceivable that the observed difference in enrichment may derive from an adaptational process in which the cells respond to an altered demand.

In the integrated analysis of proteome and transcriptome, 16 genes were identified to be statistically significant at least twofold enriched on both protein and transcript level in tendon or enthesis. Six of these genes were enriched in tendon, ten of these genes were enriched in the enthesis. Within the enthesis, cartilage-related biomolecules were identified such as aggrecan, chondroadherin, collagen type II, and versican. Interestingly, several markers of terminal hypertrophic chondrocytes¹⁰⁰ were detected in the cells within the interface region such as runt-related transcription factor 2 (RUNX2), integrin binding sialoprotein (IBSP), and matrix metalloproteinase 13 (MMP13). Conclusively, several biomarkers were identified that can be used to characterize cells on tendon-bone interface scaffolds. This is especially useful with regard to most scientists using mesenchymal stem cells to seed tendon-bone interface scaffolds. Mesenchymal stem cells have the potential to differentiate towards fibroblasts, adipoblasts, chondroblasts, myoblasts, and osteoblasts depending on the stimuli¹¹². By comparing the differentiation of mesenchymal stem cells after cultivation on scaffolds with the biomarkers that were identified here, it can be investigated whether the cells are sufficiently differentiated. Further, by seeding mesenchymal stem cells onto decellularized donor scaffolds, it can be investigated whether the cell microenvironment itself is sufficient to trigger cells towards a given differentiation lineage or whether extensive treatment with growth factors is needed.

6. Regeneration of hard-soft interfaces

Regeneration of junctions between hard and soft tissues, such as cartilage, entheses or integration of endoprotheses, is a key challenge in trauma surgery and orthopedics. In the following paragraphs, two tissue engineering approaches for interface regeneration are discussed. Firstly, an in vivo approach for regeneration of pig knee cartilage after trauma. Secondly, an in vitro scaffold preparation technique to decellularize porcine entheses as tissue engineering scaffolds.

6.1. Cartilage regeneration in vivo using fibrin scaffolds

Cartilage regeneration was histologically investigated as visiting researcher at the Heike Daldrup-Link Laboratory at the Department of Radiology at Stanford University. Briefly, two defects each had been positioned in to knees of minipigs. Mesenchymal stem cells (MSCs) had been labeled with iron oxide nanoparticles for in vivo investigation after implantation using magnetic resonance imaging. The knee cartilage defects had been surgically treated by filling the defects with fibrin scaffolds that contained the labeled mesenchymal stem cells. After 12 weeks, pigs were sacrificed and the cartilage defects were histologically investigated as described in 2.10.

Regular extracellular matrix structure was observed with evenly distributed cells in physiological cartilage samples (Figure 27a). Samples from treated cartilage defects showed structural alteration of the regenerated tissue compared to control cartilage tissue. The defects that had been treated with fibrin scaffolds comprising MSCs showed fibrous tissue within the defect site in hematoxylin and eosin staining (Figure 27b) as well as safranin O staining (Figure 27c). Underlying bone material had been partially resorbed below the defect site. In safranin O stained samples, it was observed that the regenerating defect site contained less glycosaminoglycans than intact cartilage as indicated by the lack of red staining within the defect filling material.

The composition of fibrous tissue that had formed within the defect site was further characterized using immunofluorescent staining of different collagens. Immunofluorescent staining for collagen types I and II showed that the integrity of the collagen type II-rich cartilage layer had not been restored 12 weeks after surgery (Figure 27d). Collagen surrounding the defect depicted the typical collagen type II-rich composition whereas the defect site was primarily composed of collagen type I. Since some collagen type II was detected within the defect site, collagen type III presence was also investigated to analyze whether the remodeling

process was still ongoing. Indeed, double staining of collagen type I and collagen type III identified collagen type III within the defect site. Since collagen type III is involved in wound healing¹¹³, the presence of collagen type III within the defect site indicated that remodeling was still ongoing.

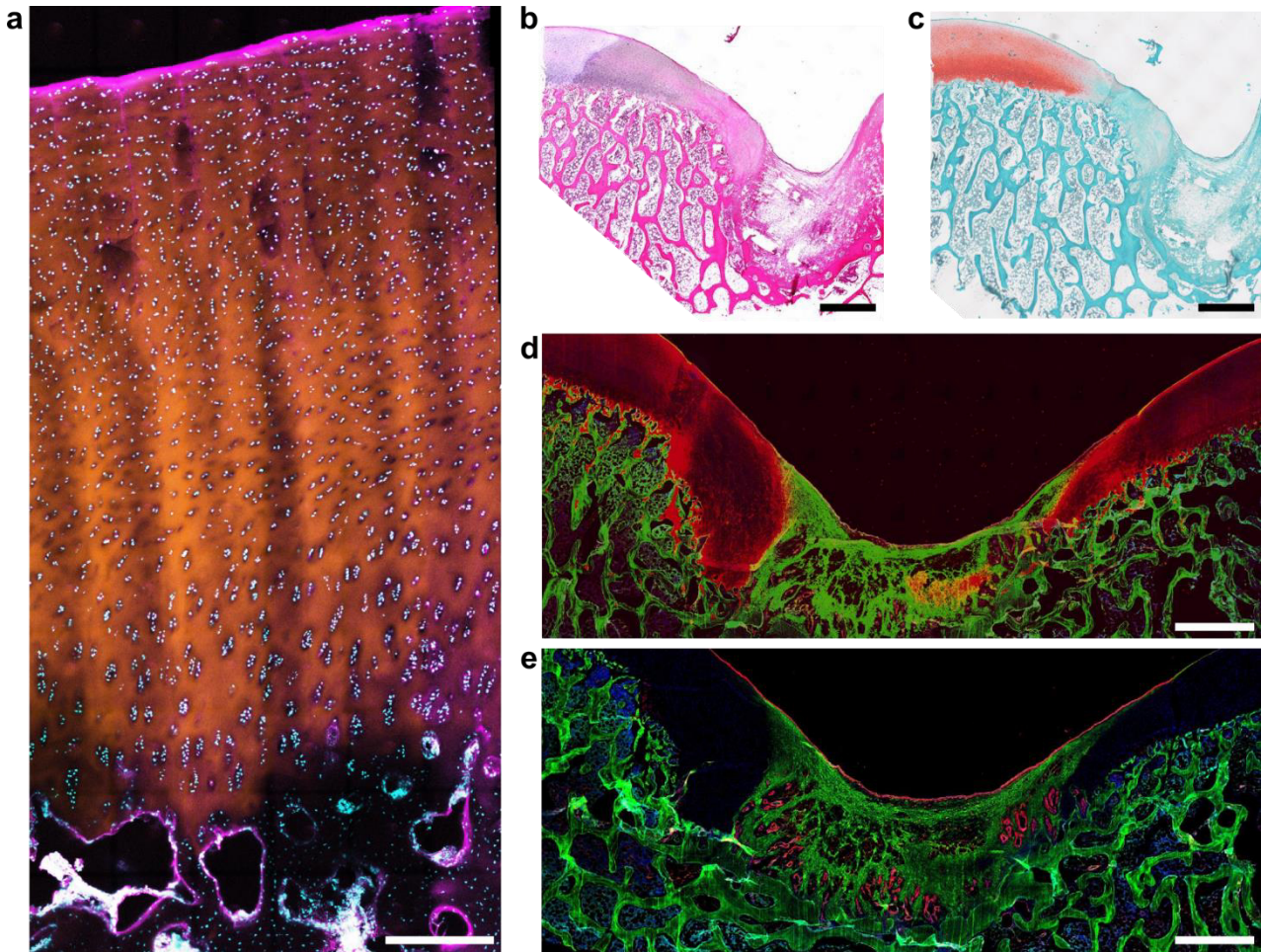


Figure 27: Histological analysis of cartilage regeneration. a, Healthy cartilage imaged using confocal microscopy. Cells, collagen type I, and reflection are depicted in cyan, magenta, and orange, respectively. Scale bar corresponds to 300 μm . b, and c, Partially regenerated cartilage defects that had been treated with fibrin scaffolds were histologically investigated with hematoxylin eosin and safranin O, respectively. The defect was not fully regenerated, but exhibited fibrous tissue within the defect. d, Partially regenerated cartilage defect stained for collagen type II (red), collagen type I (green) and cells (blue). e, Partially regenerated cartilage defect stained for collagen type III (red), collagen type I (green), and cells (blue). The defect was not fully recovered with cartilage-specific collagen type II. Remodeling was still ongoing as indicated by presence of collagen type III. Scale bars in b, c, d, e correspond to 1000 μm .

Conclusively, histological investigation of tissue engineered cartilage defect samples showed that remodeling of the scaffold within the defect into regenerated cartilage tissue was not terminated 12 weeks after surgery. Cartilage regeneration is known to be very challenging²⁶. Positive staining for collagen type III within the defect site indicated that remodeling was still ongoing. Therefore, the presented data show that MSCs may be used for tissue engineering approaches to cartilage recovery. Further modifications of the tissue engineering approach can be investigated to enhance the regenerative potential of the scaffold in the future, such as longer regeneration time and inclusion of growth factors within the scaffold to enhance the regenerative capacity of the MSCs.

6.2. Enthesis regeneration using decellularized scaffolds

There has been an increasing interest in creating scaffolds that may be implanted into defect sites to restore the original function of an enthesis. Biocompatibility and mechanical strength are two important factors that have to be considered. One strategy for regeneration of entheses is the use of decellularized enthesis scaffolds for regeneration via tissue engineering. Due to immunogenicity of antigens that are distributed on cell surfaces, it is crucial that donor tissues are sufficiently decellularized to avoid inflammation and immune rejection after implantation¹¹⁴. A partial denaturation is favored to remove immunogenic molecules from the matrix⁶⁰. We established a protocol to decellularize porcine entheses as scaffolds for enthesis tissue engineering⁵⁶. The systematic investigation of six combinations of different concentrations of sodium dodecyl sulfate (SDS) and Triton X-100 showed that decellularization using 0.5 % SDS with 1 % Triton X-100 for 72 h resulted in the most efficient decellularization. This detergent mixture was combined with different physical treatments showing that additional application of 200 mmHg pressure resulted in the highest decellularization efficiency⁵⁶. Biomechanical tensile testing showed no statistically significant difference in maximum force or Young's modulus in treated groups compared to untreated control. The collagen structure of the enthesis scaffolds was predominantly preserved and the DNA content was statistically significant reduced ($p < 0.001$).

Interestingly, we observed that the interface region featured different decellularization properties than the adjacent tendon and bone regions⁵⁶. The decellularization efficiency at the interface region was statistically significant reduced ($p < 0.05$) compared to the decellularization efficiency of tendon and bone (Figure 28). This may be due to a very dense matrix structure at the fibrocartilaginous interface that resulted in diffusion limitations preventing decellularization chemicals to penetrate deep tissue zones⁵⁶.

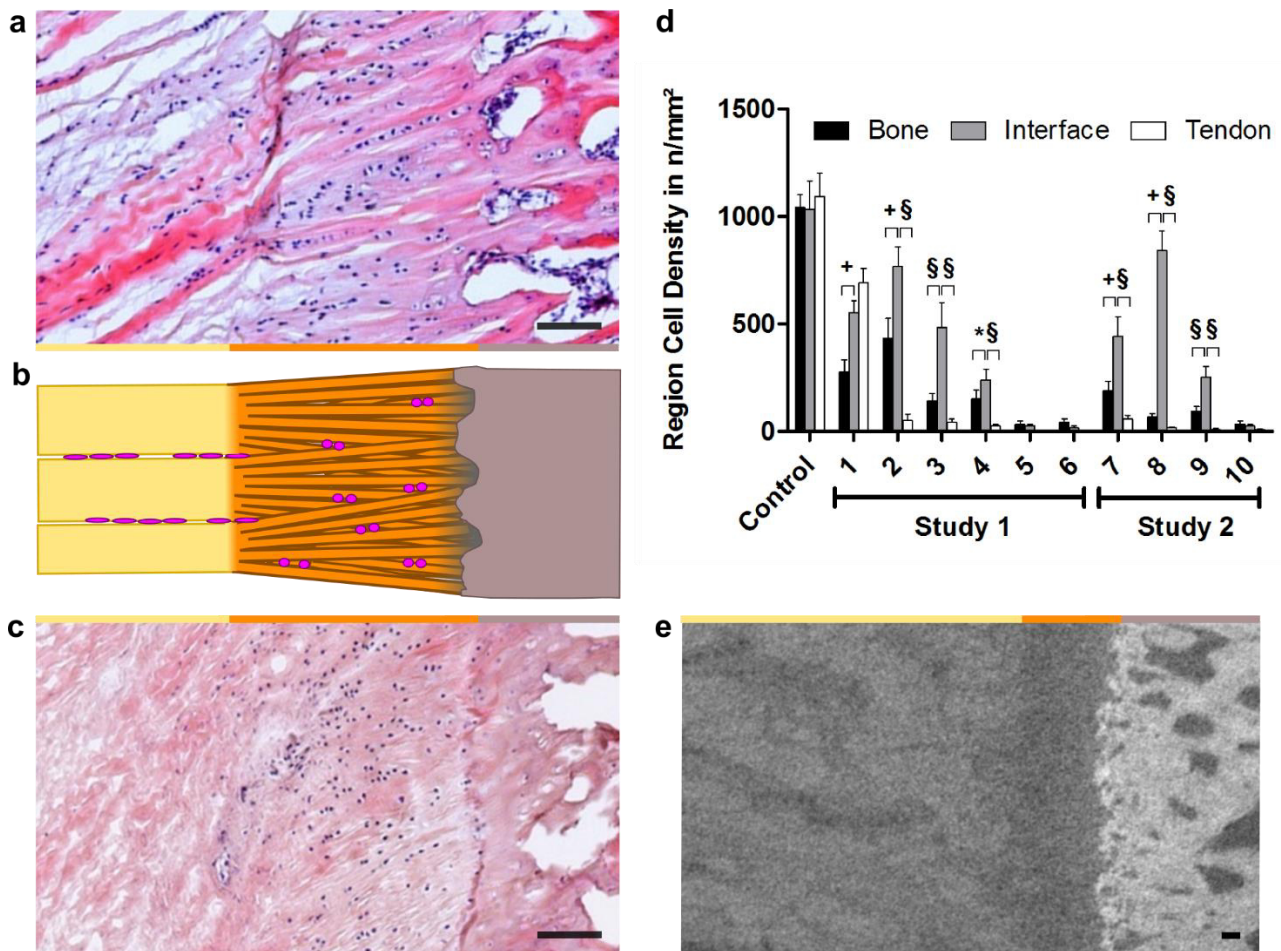


Figure 28: Tissue density and low solute transport may result in the interface region decellularizing less efficiently than tendon and bone. a, Hematoxylin and eosin staining of control group showed that cells are evenly distributed throughout the three regions. b, Scheme of cell morphology and distribution within tendon and the interface. c, The interface decellularized less efficiently than tendon and bone; cells in the interface region appeared to partially withstand the decellularization treatment. Representative image from group 8⁵⁶. d, Cell densities in bone, tendon, and interface region after decellularization using protocols with different concentrations of sodium dodecyl sulfate and Triton X-100 as well as different physical treatments (groups 1-10)⁵⁶. In each group, cell density of the interface region was compared to the cell density of bone and tendon (* $p < 0.05$, + $p > 0.01$, § $p < 0.001$). The interface region decellularized less efficiently than tendon and bone throughout different decellularization groups. e, The interface region showed less absorption than tendon and bone in micro-computed tomography, which may be caused by tissue density and solute transport (chapter 4.2.1). Scale bars correspond to 100 μm . Figure parts a, c, and d adapted from Xu K & Kuntz L, et al.⁵⁶.

The fact that the interface region decellularized less efficiently than tendon and bone, possibly due to diffusion limitations, is particularly interesting with regard to the results of micro-computed tomography. Micro-computed tomography showed less X-ray absorbance at the

interface (4.2.1) that might also be a consequence of contrast agent not sufficiently penetrating the interface region. Thus, both methodologies indicate that the interface region may be a very dense tissue with low diffusive solute transport. It is the combination of different techniques and approaches, in this case the combination of an imaging study and a tissue engineering approach, that leads to better understanding of properties and behavior of a tissue.

Conclusively, a protocol was established to efficiently decellularize 2 mm thick porcine enthesis tissue scaffolds using 0.5 % SDS and 1 % Triton X-100 with 200 mmHg pressure while retaining the biomechanical features of the scaffold. In the ongoing project, decellularized scaffolds will be seeded with mesenchymal stem cells (MSCs). Firstly, proliferation of MSCs on the scaffold will be investigated to ensure proper growth of cells on decellularized scaffolds. Secondly, differentiation of MSCs will be analyzed and compared to the expression patterns of enthesis and tendon cells identified in chapter 5. Hereby, it will be shown whether the extracellular matrix itself is sufficient to target stem cells to a specific differentiation lineage.

6.3. Discussion

Many injuries and diseases in the orthopedic field are related to interfaces between hard and soft materials, such as cartilage-bone defects or defects at the attachment site of ligament/tendon to bone. For example, injuries at the rotator cuff tendon insertion or at the anterior cruciate ligament are very common and their recurrence rate after surgical repair is very high due to mechanical inferiority¹⁵. Tissue engineering is a promising approach to tackle the related challenges and to regenerate these hard-soft interfaces¹⁵. However, interface tissue engineering is particularly challenging due to the intricate multi-tissue biomaterial composite organization¹⁵. Several approaches for tissue engineering of biological hard-soft interface are conceivable.

The most direct approach would be to recreate the native tissue structures, particularly the ones that are linked to the mechanical properties such as collagen fiber structure and composition, mineralization properties, proteoglycan content, as well as the collagen fiber crimp pattern¹⁴. In chapters 3 and 4 we provide guidelines for biomimetic design of artificial enthesis scaffolds by revealing the structural and compositional properties of a functional enthesis. The design principles established in these chapters can be used to produce high-end scaffolds, for example through scaffold bioprinting with biocompatible materials such as spi-

der silk or collagen. Hypothetically, the scaffolds can be seeded with patient cells and implanted into the patient. For this purpose, the transcriptomic analysis in chapter 5 identified biomarkers for interface cells that can be used to characterize the differentiation of cells seeded onto scaffolds with regard to their functional integrity.

A second approach is the use of decellularized donor tissue that could be seeded with patient-derived cells. In chapter 6, we provide a protocol for decellularization of porcine Achilles tendon entheses as scaffolds with potential clinical implication. Successful decellularization allows for subsequent seeding with patient-derived mesenchymal stem cells to prime the scaffold for implantation. Since healing tendon may lose its parallel fiber arrangement and mechanical properties of repaired tendon or the insertion site are mostly not recreated¹⁴, using a decellularized healthy xenograft tissue scaffold may greatly enhance regeneration of tissue function. However, using decellularized scaffolds may have limitations with regard to immune rejection, therefore a thorough decellularization has to be ensured. The evaluated decellularization protocol (chapter 6.2) is a first step in tissue engineering using biological xenograft scaffolds and the recellularization success as well as the *in vivo* behavior have yet to be evaluated.

A third approach is the use of polymerizing gels as scaffolds to transfer cells into the patient. In chapter 6, mesenchymal stem cell seeded fibrin scaffolds for *in vivo* cartilage regeneration were histologically investigated as visiting researcher at the Daldrup-Link Lab at Stanford University. It was observed that cartilage defects were partially recovered three months after implantation of mesenchymal stem cell seeded scaffolds. The defect site exhibited presence of collagen type II, which is a main component of cartilage, but much lower levels than in healthy cartilage. Collagen type I containing fibrous tissue was detected in the defect. The observed collagen type III presence may indicate ongoing remodeling processes¹⁴. The study was therefore extended to provide more healing time for the defect site. Application of these polymerizing gel scaffolds is convenient and very feasible with regard to clinical standards. Therefore, they are very promising for clinical use if the regeneration potential can be enhanced by use of growth factors such as FGF-18, FGF-2 or TGF- β 1²⁶.

The three approaches using biomimetic scaffolds, decellularized donor tissue scaffolds, or polymerizing gel scaffolds have potential for the use in tissue engineering of biological hard-soft interfaces. However, the present studies indicated that an important challenge for tissue engineering is the lack of nutrient supply to cells within a three-dimensional scaffold. For example, different diffusion properties of SDS and Triton X-100 through the interface region

compared to tendon and bone may result in the observed difference in decellularization efficiency between the zones. One of the reasons may be the high amount of hyaluronan proteoglycans present at the interface (chapter 4.2). The large glycosaminoglycan groups of the hyaluronans are negatively charged and may prevent chemicals to enter deeper zones of the tissue due to electrostatic effects and steric hindrance. Lack of diffusion may also play a role in the outcome of the cartilage regeneration study where cells in the inside of the fibrin scaffold might be undersupplied. Additional application of growth factors may accelerate and facilitate remodeling of the scaffold by the cells to obtain functional tissue.

Conclusively, three approaches that show potential for tissue engineering of hard-soft interfaces were discussed, which are biomimetic scaffolds, decellularized donor tissue scaffolds, and polymerizing gel scaffolds. However, tissue engineering of hard-soft interfaces such as cartilage²⁶ and entheses¹⁵ is very sophisticated and still in its infancy.

7. Outlook

The design of resilient interfaces between hard and soft materials evokes challenges in several disciplines, such as engineering and medicine, as interfaces between mechanically dissimilar materials are susceptible to rupture. Biomimicry offers the potential of tackling these challenges by learning and imitating solutions to this complex problem from nature. This thesis aimed at understanding how biological hard-soft interfaces are structured and composed to identify design principles for biomimetic approaches to hard-soft interfaces, with a focus on an exemplary outstanding hard-soft interface, the Achilles tendon bone insertion (enthesis).

Several features were identified that nature uses to reduce stress concentrations at the enthesis. The enthesis is characterized by an interface in which tendon fibers undergo a transition in geometry (chapter 3) and composition (chapter 4) before attaching to bone. The geometrical transition of fibers at the interface leads to reduction of tensile stresses at the interface¹. Compressive stresses are reduced by hyaluronan proteoglycans present within the interface. Cells residing within enthesis, tendon, and cartilage were characterized and biomarkers for differentiation of enthesis cells were identified. Additionally, two tissue engineering approaches for regenerating biological hard-soft interfaces, namely cartilage (6.1) and enthesis (6.2), were presented.

Until now, literature has been ambiguous about the definition and classification of entheses. An “enthesis organ” concept has been proposed as well as the classification into fibrous and fibrocartilaginous entheses⁸⁰. The presence or absence of Sharpey’s fibers at different types of entheses has been controversial¹⁶. The traditionally assumed tidemark has been questioned recently as a graded interface has been proposed for entheses²². The application of the techniques that were established in this thesis to other types of entheses – such as the rotator cuff enthesis or the anterior cruciate ligament enthesis – as well as the transfer to human samples will shed light on to whether the observed structural and compositional features are ubiquitous enthesis design principles or a unique feature of the Achilles tendon enthesis. Finally, this could lead to the identification of explicit enthesis classifications.

This thesis identified several biomolecular key structures of the porcine Achilles tendon bone interface to pave the way for biomimetic approaches to hard-soft interfaces. The presented understanding of the structural and compositional transition of the material at the interface as well as the cellular biomarkers can be utilized for biomimetic strategies aimed at designing hard-soft interfaces.

8. References

- 1 Rossetti, L. & Kuntz, L. *et al.* The microstructure and micromechanics of the tendon-bone insertion. *Nature materials*, doi:10.1038/nmat4863 (2017).
- 2 Thomopoulos, S., Birman, V. & Genin, G. M. in *Structural Interfaces and Attachments in Biology* (ed Thomopoulos) (Springer Science+Business Media, 2013).
- 3 Genin, G. M. & Liu, Y. in *Structural Interfaces and Attachments in Biology* (ed Thomopoulos) (Springer Science+Business Media, 2013).
- 4 Lu, H. H. & Thomopoulos, S. Functional attachment of soft tissues to bone: development, healing, and tissue engineering. *Annual review of biomedical engineering* **15**, 201-226, doi:10.1146/annurev-bioeng-071910-124656 (2013).
- 5 Birman, V., Keil, T. & Hosder, S. in *Structural Interfaces and Attachments in Biology* (ed Thomopoulos) (Springer Science+Business Media 2013).
- 6 Deymier, A. C. *et al.* Micro-mechanical Properties of the Tendon-to-Bone Attachment. *Acta biomaterialia*, doi:10.1016/j.actbio.2017.01.037 (2017).
- 7 Ho, S. P., Marshall, S. J., Ryder, M. I. & Marshall, G. W. The tooth attachment mechanism defined by structure, chemical composition and mechanical properties of collagen fibers in the periodontium. *Biomaterials* **28**, 5238-5245, doi:10.1016/j.biomaterials.2007.08.031 (2007).
- 8 Lee, B. P., Messersmith, P. B., Israelachvili, J. N. & Waite, J. H. Mussel-Inspired Adhesives and Coatings. *Annual Review of Materials Research* **41**, 99-132, doi:10.1146/annurev-matsci-062910-100429 (2011).
- 9 Bhushan, B. Biomimetics: lessons from nature-an overview. *Philosophical Transactions of the Royal Society A Mathematical, Physical and Engineering Sciences* **367**, 1445-1486, doi:10.1098/rsta.2009.0011 (2009).
- 10 Sanchez, C., Arribart, H. & Guille, M. M. G. Biomimetism and bioinspiration as tools for the design of innovative materials and systems. *Nature materials* **4**, 277-288, doi:10.1038/nmat1339 (2005).
- 11 Qu, D., Mosher, C. Z., Boushell, M. K. & Lu, H. H. Engineering complex orthopaedic tissues via strategic biomimicry. *Annals of biomedical engineering* **43**, 697-717, doi:10.1007/s10439-014-1190-6 (2015).
- 12 Lei, J. & Temenoff, J. S. in *Structural Interfaces and Attachments in Biology* (ed Thomopoulos) (Springer Science+Business Media, 2013).
- 13 Benjamin, M. & McGonagle, D. Entheses: tendon and ligament attachment sites. *Scandinavian journal of medicine & science in sports* **19**, 520-527, doi:10.1111/j.1600-0838.2009.00906.x (2009).
- 14 Connizzo, B. K., Yannascoli, S. M. & Soslowsky, L. J. Structure-function relationships of postnatal tendon development: a parallel to healing. *Matrix biology : journal of the International Society for Matrix Biology* **32**, 106-116, doi:10.1016/j.matbio.2013.01.007 (2013).
- 15 Font Tellado, S., Balmayor, E. R. & Van Griensven, M. Strategies to engineer tendon/ligament-to-bone interface: Biomaterials, cells and growth factors. *Advanced drug delivery reviews*, doi:10.1016/j.addr.2015.03.004 (2015).
- 16 Benjamin, M. *et al.* The skeletal attachment of tendons--tendon "enthesees". *Comparative biochemistry and physiology. Part A, Molecular & integrative physiology* **133**, 931-945 (2002).
- 17 Thomopoulos, S. The role of mechanobiology in the attachment of tendon to bone. *IBMS BoneKEy* **8**, 271-285, doi:10.1138/20110515 (2011).

- 18 Thomopoulos, S. *et al.* The localized expression of extracellular matrix components in healing tendon insertion sites: an in situ hybridization study. *Journal of orthopaedic research* **20**, 454-463, doi:10.1016/S0736-0266(01)00144-9 (2002).
- 19 Shaw, H. M. & Benjamin, M. Structure-function relationships of entheses in relation to mechanical load and exercise. *Scandinavian journal of medicine & science in sports* **17**, 303-315, doi:10.1111/j.1600-0838.2007.00689.x (2007).
- 20 Yoon, J. H. & Halper, J. Tendon proteoglycans: biochemistry and function. *Journal of musculoskeletal & neuronal interactions* **5**, 22-34 (2005).
- 21 Hu, Y. *et al.* Stochastic Interdigitation as a Toughening Mechanism at the Interface between Tendon and Bone. *Biophysical journal* **108**, 431-437, doi:10.1016/j.bpj.2014.09.049 (2015).
- 22 Genin, G. M. *et al.* Functional grading of mineral and collagen in the attachment of tendon to bone. *Biophysical journal* **97**, 976-985, doi:10.1016/j.bpj.2009.05.043 (2009).
- 23 Thomopoulos, S., Marquez, J. P., Weinberger, B., Birman, V. & Genin, G. M. Collagen fiber orientation at the tendon to bone insertion and its influence on stress concentrations. *Journal of biomechanics* **39**, 1842-1851, doi:10.1016/j.jbiomech.2005.05.021 (2006).
- 24 Sophia Fox, A. J., Bedi, A. & Rodeo, S. A. The basic science of articular cartilage: structure, composition, and function. *Sports health* **1**, 461-468, doi:10.1177/1941738109350438 (2009).
- 25 Guilak, F., Butler, D., Goldstein, S. & Mooney, D. *Functional Tissue Engineering*. (Springer, 2003).
- 26 Huey, D. J., Hu, J. C. & Athanasiou, K. A. Unlike bone, cartilage regeneration remains elusive. *Science* **338**, 917-921, doi:10.1126/science.1222454 (2012).
- 27 Mohan, N. & Detamore, M. in *Structural Interfaces and Attachments in Biology* (ed thomopoulos) (Springer Science+Business Media, 2013).
- 28 Mouw, J. K., Ou, G. & Weaver, V. M. Extracellular matrix assembly: a multiscale deconstruction. *Nature Reviews Molecular Cell Biology* **15**, 771-785, doi:10.1038/nrm3902 (2014).
- 29 Tresoldi, I. *et al.* Tendon's ultrastructure. *Muscles, ligaments and tendons journal* **3**, 2-6, doi:10.11138/mltj/2013.3.1.002 (2013).
- 30 Benjamin, M., Kaiser, E. & Milz, S. Structure-function relationships in tendons: a review. *Journal of anatomy* **212**, 211-228, doi:10.1111/j.1469-7580.2008.00864.x (2008).
- 31 Kjaer, M. Role of extracellular matrix in adaptation of tendon and skeletal muscle to mechanical loading. *Physiological reviews* **84**, 649-698, doi:10.1152/physrev.00031.2003 (2004).
- 32 Kannus, P. Structure of the tendon connective tissue. *Scandinavian journal of medicine & science in sports* **10**, 312-320 (2000).
- 33 Wang, J. H. Mechanobiology of tendon. *Journal of biomechanics* **39**, 1563-1582, doi:10.1016/j.jbiomech.2005.05.011 (2006).
- 34 Screen, H. R. C. *et al.* An investigation into the effects of the hierarchical structure of tendon fascicles on micromechanical properties. *Proceedings of the Institution of Mechanical Engineers, Part H: Journal of Engineering in Medicine* **218**(2),109-19 (2004).

- 35 Orgel, J. P., Irving, T. C., Miller, A. & Wess, T. J. Microfibrillar structure of type I collagen in situ. *Proceedings of the National Academy of Sciences of the United States of America* **103**, 9001-9005, doi:10.1073/pnas.0502718103 (2006).
- 36 Brinckmann, J. in *Collagen: Primer in Structure, Processing and Assembly* (eds Jürgen Brinckmann, Holger Notbohm, & P. K. Müller) 1-6 (Springer Berlin Heidelberg, 2005).
- 37 Koide, T. & Nagata, K. in *Collagen: Primer in Structure, Processing and Assembly* (eds Jürgen Brinckmann, Holger Notbohm, & P. K. Müller) 85-114 (Springer Berlin Heidelberg, 2005).
- 38 Birk, D. E. & Bruckner, P. in *Collagen: Primer in Structure, Processing and Assembly* (eds Jürgen Brinckmann, Holger Notbohm, & P. K. Müller) 185-205 (Springer Berlin Heidelberg, 2005).
- 39 Kielty, C.M. & Grant, M.E. in *Connective Tissue and Its Heritable Disorders: Molecular, Genetic, and Medical Aspects* (eds Royce & Steinmann) 159-221 (John Wiley & Sons, 2002).
- 40 Kadler, K. E., Holmes, D. F., Trotter, J. A. & Chapman, J. A. Collagen fibril formation. *The Biochemical journal* **316** (Pt 1), 1-11 (1996).
- 41 Buehler, M. J. Nature designs tough collagen: explaining the nanostructure of collagen fibrils. *Proceedings of the National Academy of Sciences of the United States of America* **103**, 12285-12290, doi:10.1073/pnas.0603216103 (2006).
- 42 Bozec, L., van der Heijden, G. & Horton, M. Collagen fibrils: nanoscale ropes. *Biophysical journal* **92**, 70-75, doi:10.1529/biophysj.106.085704 (2007).
- 43 Petruska, J. A. & Hodge, A. J. A Subunit Model for the Tropocollagen Macromolecule. *Proceedings of the National Academy of Sciences of the United States of America* **51**, 871-876 (1964).
- 44 Hulmes, D. J. Building collagen molecules, fibrils, and suprafibrillar structures. *Journal of structural biology* **137**, 2-10, doi:10.1006/jsbi.2002.4450 (2002).
- 45 Hulmes, D. J. & Miller, A. Quasi-hexagonal molecular packing in collagen fibrils. *Nature* **282**, 878-880 (1979).
- 46 Hulmes, D. J. S., Jesior, J. C., Miller, A., Berthetcolominas, C. & Wolff, C. Electron-Microscopy Shows Periodic Structure in Collagen Fibril Cross-Sections. *Proceedings of the National Academy of Sciences of the United States of America* **78**, 3567-3571, doi:DOI 10.1073/pnas.78.6.3567 (1981).
- 47 Antipova, O. & Orgel, J. P. In situ D-periodic molecular structure of type II collagen. *The Journal of biological chemistry* **285**, 7087-7096, doi:10.1074/jbc.M109.060400 (2010).
- 48 Eyre, D. R. & Wu, J.-J. in *Collagen: Primer in Structure, Processing and Assembly* (eds Jürgen Brinckmann, Holger Notbohm, & P. K. Müller) 207-229 (Springer Berlin Heidelberg, 2005).
- 49 Wang, C. *et al.* Identification of amino acids important for the catalytic activity of the collagen glucosyltransferase associated with the multifunctional lysyl hydroxylase 3 (LH3). *The Journal of biological chemistry* **277**, 18568-18573, doi:10.1074/jbc.M201389200 (2002).
- 50 Kuettner, K. E. & Kimura, J. H. Proteoglycans: an overview. *Journal of cellular biochemistry* **27**, 327-336, doi:10.1002/jcb.240270403 (1985).
- 51 Iozzo, R. V. & Schaefer, L. Proteoglycan form and function: A comprehensive nomenclature of proteoglycans. *Matrix biology: journal of the International Society for Matrix Biology* **42**, 11-55, doi:10.1016/j.matbio.2015.02.003 (2015).

- 52 Robbins, J. R., Evanko, S. P. & Vogel, K. G. Mechanical loading and TGF-beta regulate proteoglycan synthesis in tendon. *Archives of Biochemistry and Biophysics* **342**, 203-211, doi:10.1006/abbi.1997.0102 (1997).
- 53 Midwood, K. S., Williams, L. V. & Schwarzbauer, J. E. Tissue repair and the dynamics of the extracellular matrix. *The international journal of biochemistry & cell biology* **36**, 1031-1037, doi:10.1016/j.biocel.2003.12.003 (2004).
- 54 Kjaer, M. in *Collagen: Structure and Mechanics* (ed Fratzl) 249-267 (Springer Science+Business Media, LLC, 2008).
- 55 Neal, R. A. *et al.* Three-dimensional elastomeric scaffolds designed with cardiac-mimetic structural and mechanical features. *Tissue engineering. Part A* **19**, 793-807, doi:10.1089/ten.tea.2012.0330 (2013).
- 56 Xu, K. & Kuntz, L. *et al.* Efficient decellularization for tissue engineering of the tendon-bone interface with preservation of biomechanics. *PloS one* **12**, e0171577, doi:10.1371/journal.pone.0171577 (2017).
- 57 Dohmen, P. M., Lembcke, A., Holinski, S., Pruss, A. & Konertz, W. Ten Years of Clinical Results With a Tissue-Engineered Pulmonary Valve. *The Annals of Thoracic Surgery* **92**, 1308-1314 (2011).
- 58 Mazza, G. *et al.* Decellularized human liver as a natural 3D-scaffold for liver bioengineering and transplantation. *Scientific reports* **5**, 13079, doi:10.1038/srep13079 (2015).
- 59 Peloso, A. *et al.* Current achievements and future perspectives in whole-organ bioengineering. *Stem Cell Research & Therapy* **6**, 107, doi:10.1186/s13287-015-0089-y (2015).
- 60 Burgkart, R. *et al.* Decellularized kidney matrix for perfused bone engineering. *Tissue engineering. Part C, Methods*, doi:10.1089/ten.TEC.2013.0270 (2013).
- 61 Schneider, C. A., Rasband, W. S. & Eliceiri, K. W. NIH Image to ImageJ: 25 years of image analysis. *Nature methods* **9**, 671-675 (2012).
- 62 *Romeis - Mikroskopische Technik*. (Spektrum Akademischer Verlag, 2010).
- 63 Boersema, P. J., Raijmakers, R., Lemeer, S., Mohammed, S. & Heck, A. J. Multiplex peptide stable isotope dimethyl labeling for quantitative proteomics. *Nature protocols* **4**, 484-494, doi:10.1038/nprot.2009.21 (2009).
- 64 Mi, H., Muruganujan, A., Casagrande, J. T. & Thomas, P. D. Large-scale gene function analysis with the PANTHER classification system. *Nature Protocols* **8**, 1551-1566, doi:10.1038/nprot.2013.092 (2013).
- 65 Langmead, B., Trapnell, C., Pop, M. & Salzberg, S. L. Ultrafast and memory-efficient alignment of short DNA sequences to the human genome. *Genome biology* **10**, R25, doi:10.1186/gb-2009-10-3-r25 (2009).
- 66 Mi, H. *et al.* PANTHER version 11: expanded annotation data from Gene Ontology and Reactome pathways, and data analysis tool enhancements. *Nucleic Acids Research* **45**, D183-D189, doi:10.1093/nar/gkw1138 (2017).
- 67 Huang da, W., Sherman, B. T. & Lempicki, R. A. Systematic and integrative analysis of large gene lists using DAVID bioinformatics resources. *Nature protocols* **4**, 44-57, doi:10.1038/nprot.2008.211 (2009).
- 68 Franceschini, A. *et al.* STRING v9.1: protein-protein interaction networks, with increased coverage and integration. *Nucleic Acids Res* **41**, D808-815, doi:10.1093/nar/gks1094 (2013).

- 69 Szklarczyk, D. *et al.* STRING v10: protein-protein interaction networks, integrated over the tree of life. *Nucleic Acids Res* **43**, D447-452, doi:10.1093/nar/gku1003 (2015).
- 70 de S. e Silva, J. M. *et al.* Three-dimensional non-destructive soft-tissue visualization with X-ray staining micro-tomography. *Scientific reports* **5**, 14088, doi:10.1038/srep14088 (2015).
- 71 Franchi, M. *et al.* Different crimp patterns in collagen fibrils relate to the subfibrillar arrangement. *Connective tissue research* **49**, 85-91, doi:10.1080/03008200801913635 (2008).
- 72 Franchi, M. *et al.* Crimp morphology in relaxed and stretched rat Achilles tendon. *Journal of anatomy* **210**, 1-7, doi:10.1111/j.1469-7580.2006.00666.x (2007).
- 73 Fratzl, P. *et al.* Fibrillar structure and mechanical properties of collagen. *Journal of structural biology* **122**, 119-122, doi:10.1006/jsbi.1998.3966 (1998).
- 74 Rigozzi, S., Müller, R., Stemmer, A. & Snedeker, J. G. Tendon glycosaminoglycan proteoglycan sidechains promote collagen fibril sliding—AFM observations at the nanoscale. *Journal of biomechanics* **46**, 813-818, doi:10.1016/j.jbiomech.2012.11.017 (2013).
- 75 *Collagen: Structure and Mechanics*. (ed Fratzl) (Springer Science+Business Media, LLC, 2008).
- 76 Bushberg, J. T., Seibert, J. A., Leidholdt, E. M. & Boone, J. M. *The Essential Physics of Medical Imaging*. (Wolters Kluwer Health, 2011).
- 77 Evans, R. C. & Quinn, T. M. Solute diffusivity correlates with mechanical properties and matrix density of compressed articular cartilage. *Archives of Biochemistry and Biophysics* **442**, 1-10, doi:10.1016/j.abb.2005.07.025 (2005).
- 78 Shafieyan, Y., Khosravi, N., Moeini, M. & Quinn, T. M. Diffusion of MRI and CT contrast agents in articular cartilage under static compression. *Biophysical journal* **107**, 485-492, doi:10.1016/j.bpj.2014.04.041 (2014).
- 79 Maroudas, A. Distribution and diffusion of solutes in articular cartilage. *Biophysical journal* **10**, 365-379, doi:10.1016/S0006-3495(70)86307-X (1970).
- 80 Benjamin, M. *et al.* Where tendons and ligaments meet bone: attachment sites ('entheses') in relation to exercise and/or mechanical load. *Journal of anatomy* **208**, 471-490, doi:10.1111/j.1469-7580.2006.00540.x (2006).
- 81 Peffers, M. J. *et al.* Proteomic analysis reveals age-related changes in tendon matrix composition, with age- and injury-specific matrix fragmentation. *The Journal of biological chemistry* **289**, 25867-25878, doi:10.1074/jbc.M114.566554 (2014).
- 82 Little, D. *et al.* Proteomic differences between male and female anterior cruciate ligament and patellar tendon. *PloS one* **9**, e96526, doi:10.1371/journal.pone.0096526 (2014).
- 83 Wopenka, B., Kent, A., Pasteris, J. D., Yoon, Y. & Thomopoulos, S. The tendon-to-bone transition of the rotator cuff: a preliminary Raman spectroscopic study documenting the gradual mineralization across the insertion in rat tissue samples. *Applied Spectroscopy* **62**, 1285-1294, doi:10.1366/000370208786822179 (2008).
- 84 Schwartz, A. G., Pasteris, J. D., Genin, G. M., Daulton, T. L. & Thomopoulos, S. Mineral distributions at the developing tendon enthesis. *PloS one* **7**, e48630, doi:10.1371/journal.pone.0048630 (2012).
- 85 Liu, Y. *et al.* Modelling the mechanics of partially mineralized collagen fibrils, fibres and tissue. *Journal of the Royal Society, Interface/the Royal Society* **11**, 20130835, doi:10.1098/rsif.2013.0835 (2014).

- 86 Kim, J. H. *et al.* Matrix cross-linking-mediated mechanotransduction promotes posttraumatic osteoarthritis. *Proceedings of the National Academy of Sciences of the United States of America* **112**, 9424-9429, doi:10.1073/pnas.1505700112 (2015).
- 87 Hubmacher, D. & Apte, S. S. ADAMTS proteins as modulators of microfibril formation and function. *Matrix biology: journal of the International Society for Matrix Biology* **47**, 34-43, doi:10.1016/j.matbio.2015.05.004 (2015).
- 88 Buchanan, C. I. & Marsh, R. L. Effects of long-term exercise on the biomechanical properties of the Achilles tendon of guinea fowl. *Journal of applied physiology* **90**, 164-171 (2001).
- 89 Kannus, P., Jozsa, L., Natri, A. & Jarvinen, M. Effects of training, immobilization and remobilization on tendons. *Scandinavian journal of medicine & science in sports* **7**, 67-71 (1997).
- 90 Michna, H. & Hartmann, G. Adaptation of tendon collagen to exercise. *International orthopaedics* **13**, 161-165 (1989).
- 91 Shaw, H. M., Santer, R. M., Watson, A. H. & Benjamin, M. Adipose tissue at entheses: the innervation and cell composition of the retromalleolar fat pad associated with the rat Achilles tendon. *Journal of anatomy* **211**, 436-443, doi:10.1111/j.1469-7580.2007.00791.x (2007).
- 92 Han, W. M. *et al.* Microstructural heterogeneity directs micromechanics and mechanobiology in native and engineered fibrocartilage. *Nature materials*, doi:10.1038/nmat4520 (2016).
- 93 Thorpe, C. T., Birch, H. L., Clegg, P. D. & Screen, H. R. The role of the non-collagenous matrix in tendon function. *International journal of experimental pathology* **94**, 248-259, doi:10.1111/iep.12027 (2013).
- 94 Majd, S. E. *et al.* Both hyaluronan and collagen type II keep proteoglycan 4 (lubricin) at the cartilage surface in a condition that provides low friction during boundary lubrication. *Langmuir* **30**, 14566-14572, doi:10.1021/la504345c (2014).
- 95 Gattazzo, F., Urciuolo, A. & Bonaldo, P. Extracellular matrix: A dynamic microenvironment for stem cell niche. *Biochimica et biophysica acta* **1840**, 2506-2519, doi:10.1016/j.bbagen.2014.01.010 (2014).
- 96 Pirooznia, M., Nagarajan, V. & Deng, Y. GeneVenn - A web application for comparing gene lists using Venn diagrams. *Bioinformatics* **1**, 420-422 (2007).
- 97 Groenen, M. A. *et al.* Analyses of pig genomes provide insight into porcine demography and evolution. *Nature* **491**, 393-398, doi:10.1038/nature11622 (2012).
- 98 Freeman, T. C. *et al.* A gene expression atlas of the domestic pig. *BMC biology* **10**, 90, doi:10.1186/1741-7007-10-90 (2012).
- 99 Aken, B. L. *et al.* The Ensembl gene annotation system. *Database* **2016**, baw093-baw093, doi:10.1093/database/baw093 (2016).
- 100 Komori, T. Regulation of bone development and extracellular matrix protein genes by RUNX2. *Cell and tissue research* **339**, 189-195, doi:10.1007/s00441-009-0832-8 (2010).
- 101 Komori, T. Signaling networks in RUNX2-dependent bone development. *Journal of cellular biochemistry* **112**, 750-755, doi:10.1002/jcb.22994 (2011).
- 102 Takimoto, A., Oro, M., Hiraki, Y. & Shukunami, C. Direct conversion of tenocytes into chondrocytes by Sox9. *Experimental cell research* **318**, 1492-1507, doi:10.1016/j.yexcr.2012.04.002 (2012).

- 103 Salazar, V. S., Gamer, L. W. & Rosen, V. BMP signalling in skeletal development, disease and repair. *Nature Reviews Endocrinology* **12**, 203-221, doi:10.1038/nrendo.2016.12 (2016).
- 104 Walmod, P. S., Kolkova, K., Berezin, V. & Bock, E. Zippers make signals: NCAM-mediated molecular interactions and signal transduction. *Neurochemical research* **29**, 2015-2035 (2004).
- 105 Page-McCaw, A., Ewald, A. J. & Werb, Z. Matrix metalloproteinases and the regulation of tissue remodelling. *Nature reviews Molecular cell biology* **8**, 221-233, doi:10.1038/nrm2125 (2007).
- 106 Schwartz & Thomopoulos. in *Structural Interfaces and Attachments in Biology* (ed Thomopoulos) (Springer Science+Business Media, 2013).
- 107 Shellenberger, T. D. *et al.* BRAK/CXCL14 is a potent inhibitor of angiogenesis and a chemotactic factor for immature dendritic cells. *Cancer research* **64**, 8262-8270, doi:10.1158/0008-5472.can-04-2056 (2004).
- 108 Tsunozumi, J., Higashi, S. & Miyazaki, K. Matrilysin (MMP-7) cleaves C-type lectin domain family 3 member A (CLEC3A) on tumor cell surface and modulates its cell adhesion activity. *Journal of cellular biochemistry* **106**, 693-702, doi:10.1002/jcb.22062 (2009).
- 109 Ricard-Blum, S., Ruggiero, F. & Van der Rest, M. in *Collagen: Primer in Structure, Processing and Assembly* (eds Jürgen Brinckmann, Holger Notbohm, & P. K. Müller) 35-84 (Springer Berlin Heidelberg, 2005).
- 110 Li, Y. *et al.* Production and characterization of domain-specific monoclonal antibodies against human ECM1. *Protein expression and purification* **121**, 103-111, doi:10.1016/j.pep.2016.01.011 (2016).
- 111 Schwanhauser, B. *et al.* Global quantification of mammalian gene expression control. *Nature* **473**, 337-342 (2011).
- 112 Almalki, S. G. & Agrawal, D. K. Key transcription factors in the differentiation of mesenchymal stem cells. *Differentiation* **92**, 41-51, doi:10.1016/j.diff.2016.02.005 (2016).
- 113 Juneja, S. C., Schwarz, E. M., O'Keefe, R. J. & Awad, H. A. Cellular and molecular factors in flexor tendon repair and adhesions: a histological and gene expression analysis. *Connective tissue research* **54**, 218-226, doi:10.3109/03008207.2013.787418 (2013).
- 114 Cheng, C. W., Solorio, L. D. & Alsberg, E. Decellularized tissue and cell-derived extracellular matrices as scaffolds for orthopaedic tissue engineering. *Biotechnology advances* **32**, 462-484, doi:10.1016/j.biotechadv.2013.12.012 (2014).

9. Appendix

9.1. Identified transcription factors and growth factors

9.1.1. Enthesis

Candidates with transcription factor or growth factor activity were identified within the transcripts that were enriched in the enthesis compared to tendon.

Table 10: Candidates with transcription factor or growth factor activity enriched in enthesis compared to tendon.

ID	Gene Name	GO molecular function terms (selected) or InterPro domain
Transcription factors		
ENSSSCG00000003974	Cbp/p300 interacting transactivator with Glu/Asp rich carboxy-terminal domain 4 (CITED4)	GO:0000988~transcription factor activity
ENSSSCG000000022096	POU class 3 homeobox 3 (POU3F3)	GO:0001071~nucleic acid binding transcription factor activity
ENSSSCG000000011704	WW domain containing transcription regulator 1 (WWTR1)	GO:0000988~transcription factor activity
ENSSSCG000000025551	runt-related transcription factor 2, RUNX2 (LOC100737965)	
ENSSSCG00000000443	DNA-binding GLI family zinc finger 1 (GLI1)	GO:0003676~nucleic acid binding
ATP8B1	ATPase phospholipid transporting 8B1	GO:0045892~negative regulation of transcription
BARX1	BARX homeobox 1	GO:0006357~regulation of transcription from RNA polymerase II promoter
CKS2	CDC28 protein kinase regulatory subunit 2	GO:0045893~positive regulation of transcription
COPS2	COP9 signalosome subunit 2	GO:0045892~negative regulation of transcription
E2F1	E2F transcription factor 1	GO:0000122~negative regulation of transcription from RNA polymerase II promoter
ETV4	ETS variant 4	GO:0006357~regulation of transcription from RNA polymerase II promoter
F2RL1	F2R like trypsin receptor 1	GO:0000187~activation of MAPK activity
GLI2	GLI family zinc finger 2	GO:0000122~negative regulation of transcription from RNA polymerase II promote
KLF4	Kruppel like factor 4	GO:0032088~negative regulation of NF-kappaB transcription factor activity

MDFI	MyoD family inhibitor	GO:0045892~negative regulation of transcription
NDP	NDP, norrin cystine knot growth factor	GO:0045893~positive regulation of transcription
RAB7B	RAB7B, member RAS oncogene family(RAB7B)	GO:0051092~positive regulation of NF-kappaB transcription factor activity
SMYD2	SET and MYND domain containing 2	GO:0000122~negative regulation of transcription from RNA polymerase II promoter
SOX7	SRY-box 7	GO:0001706~endoderm formation
SOX9	SRY-box 9	GO:0001502~cartilage condensation
SP7	Sp7 transcription factor	GO:0001649~osteoblast differentiation
THAP7	THAP domain containing 7	GO:0045892~negative regulation of transcriptio
WWP2	WW domain containing E3 ubiquitin protein ligase 2	GO:0043433~negative regulation of sequence-specific DNA binding transcription factor activity
ZIC1	Zic family member 1	GO:0007389~pattern specification process,
AIRE	autoimmune regulator	GO:0045944~positive regulation of transcription from RNA polymerase II promoter,
BHLHE41	basic helix-loop-helix family member e41	GO:0006351~transcription
CMKLR1	chemerin chemokine-like receptor 1	GO:0045600~positive regulation of fat cell differentiation
F2R	coagulation factor II thrombin receptor	GO:0000187~activation of MAPK activity
CYTL1	cytokine like 1	GO:0002062~chondrocyte differentiation
DLL4	delta like canonical Notch ligand 4	GO:0000122~negative regulation of transcription from RNA polymerase II promoter
ENO1	enolase 1	GO:0045892~negative regulation of transcription
ECM1	extracellular matrix protein 1	GO:0006357~regulation of transcription from RNA polymerase II promoter
FOXA3	forkhead box A3	GO:0045944~positive regulation of transcription from RNA polymerase II promoter,
GREM1	gremlin 1, DAN family BMP antagonist	GO:0051092~positive regulation of NF-kappaB transcription factor activity
HR	hair growth associated	GO:0006355~regulation of transcription

HOXA1	homeobox A1	GO:0006355~regulation of transcription
HIF1A	hypoxia inducible factor 1, alpha subunit (basic helix-loop-helix transcription factor)	GO:0051216~cartilage development
INHBA	inhibin beta A subunit	GO:0006357~regulation of transcription from RNA polymerase II promoter
ID2	inhibitor of DNA binding 2, HLH protein	GO:0000122~negative regulation of transcription from RNA polymerase II promoter
IRX3	iroquois homeobox 3	GO:0006355~regulation of transcription, DNA-templated
NPAS2	neuronal PAS domain protein 2	GO:0006351~transcription
NAMPT	nicotinamide phosphoribosyl-transferase	GO:0045944~positive regulation of transcription from RNA polymerase II promoter
PTCH1	patched 1	GO:0000122~negative regulation of transcription from RNA polymerase II promoter
RHOA	ras homolog family member A	GO:0043124~negative regulation of I-kappaB kinase/NF-kappaB signaling
RGCC	regulator of cell cycle	GO:0045944~positive regulation of transcription from RNA polymerase II promoter
STAT4	signal transducer and activator of transcription 4	GO:0006351~transcription
SNAPC1	small nuclear RNA activating complex polypeptide 1	GO:0042795~snRNA transcription from RNA polymerase II promoter
SNAI2	snail family transcriptional repressor 2	GO:0003676~nucleic acid binding
SLC38A3	solute carrier family 38 member 3	GO:0061402~positive regulation of transcription from RNA polymerase II promoter in response to acidic pH
TXN	thioredoxin	GO:0000122~negative regulation of transcription from RNA polymerase II promoter
MYCN	v-myc avian myelocytomatosis viral oncogene neuroblastoma derived homolog	GO:0045944~positive regulation of transcription from RNA polymerase II promoter
VDR	vitamin D (1,25-dihydroxyvitamin D3) receptor	GO:0000122~negative regulation of transcription from RNA polymerase II promoter
ZBTB11	zinc finger and BTB domain containing 11	GO:0006355~regulation of transcription
Growth factor activity		
ENSSSCG00000030998	WNT inhibitory factor 1 (WIF1)	IPR000742:Epidermal growth factor-like domain

ENSSSCG00000010698	fibroblast growth factor receptor 2 (FGFR2)	GO:0000166~nucleotide binding,
ENSSSCG00000005494	tenascin C (TNC)	IPR000742:Epidermal growth factor-like domain
ENSSSCG00000001695	vascular endothelial growth factor A (VEGFA).	GO:0005102~receptor binding
CD109	CD109 molecule	GO:0030512~negative regulation of transforming growth factor beta receptor signaling pathway
HTRA1	HtrA serine peptidase 1	GO:0030512~negative regulation of transforming growth factor beta receptor signaling pathway
LRP8	LDL receptor related protein 8	IPR000742:Epidermal growth factor-like domain
NDP	NDP, norrin cystine knot growth factor	GO:0045893~positive regulation of transcription
CHST11	carbohydrate sulfotransferase 11	GO:0002063~chondrocyte development
COMP	cartilage oligomeric matrix protein	IPR000742:Epidermal growth factor-like domain
FURIN	furin, paired basic amino acid cleaving enzyme	GO:0032902~nerve growth factor production
GPC1	glypican 1	GO:0040037~negative regulation of fibroblast growth factor receptor signaling pathway
HHIP	hedgehog interacting protein	GO:0040036~regulation of fibroblast growth factor receptor signaling pathway
MMP9	matrix metalloproteinase 9	GO:0045742~positive regulation of epidermal growth factor receptor signaling pathway
MFGE8	milk fat globule-EGF factor 8 protein	IPR000742:Epidermal growth factor-like domain
PGF	placental growth factor	GO:0048010~vascular endothelial growth factor receptor signaling pathway
PDGFRB	platelet-derived growth factor receptor, beta polypeptide	GO:0038091~positive regulation of cell proliferation by VEGF-activated platelet derived growth factor receptor signaling pathway
RGCC	regulator of cell cycle	GO:0072537~fibroblast activation GO:0090272~negative regulation of fibroblast growth factor production
SHISA2	shisa family member 2	GO:0040037~negative regulation of fibroblast growth factor receptor signaling pathway
THBD	Thrombomodulin	IPR000742:Epidermal growth factor-like domain
THBS3	thrombospondin 3	IPR000742:Epidermal growth factor-like domain

TGFBI	transforming growth factor, beta-induced, 68kDa	
VCAN	Versican	IPR000742:Epidermal growth factor-like domain

9.1.2. Tendon

Candidates with transcription factor or growth factor activity were identified within the transcripts that were enriched in tendon compared to enthesis.

Table 11: Transcription factors and growth factors identified to be enriched in tendon compared to enthesis.

ID	Gene Name	GO molecular function terms (selected) or InterPro domain
Transcription factors		
ENSSSCG00000016795	brain abundant membrane attached signal protein 1 (BASP1)	GO:0003714~transcription corepressor activity
ENSSSCG00000028635	general transcription factor II-I repeat domain-containing protein 2 (LOC100620992)	GO:0000981~RNA polymerase II transcription factor activity
ENSSSCG00000013511	hepatoma-derived growth factor-related protein 2 (LOC100526035)	GO:0003677~DNA binding
ENSSSCG00000008624	lipin 1 (LPIN1)	GO:0003713~transcription coactivator activity
ENSSSCG00000027115	transcription initiation factor TFIID subunit 1-like (LOC100620926)	GO:0043565~sequence-specific DNA binding
CEBPA	CCAAT/enhancer binding protein alpha	GO:0000975~regulatory region DNA binding
CD3D	CD3d molecule	GO:0003712~transcription cofactor activity
ERCC3	ERCC excision repair 3, TFIIH core complex helicase subunit	GO:0000166~nucleotide binding
EYA2	EYA transcriptional coactivator and phosphatase 2	GO:0004721~phosphoprotein phosphatase activity
ISL1	ISL LIM homeobox 1	GO:0000988~transcription factor activity, protein binding
KLF11	Kruppel like factor 11	GO:0000975~regulatory region DNA binding
MLXIPL	MLX interacting protein like	GO:0000976~transcription regulatory region sequence-specific DNA binding
SATB1	SATB homeobox 1	GO:0000976~transcription regulatory region sequence-specific DNA binding
YBX3	Y-box binding protein 3	GO:0000976~transcription regulatory region sequence-specific DNA binding
ZFP37	ZFP37 zinc finger protein	GO:0001071~nucleic acid binding transcription factor activity

ATF3	activating transcription factor 3	GO:0000975~regulatory region DNA binding
ATOH8	atonal bHLH transcription factor 8	GO:0001071~nucleic acid binding transcription factor activity
BATF	basic leucine zipper ATF-like transcription factor	GO:0000975~regulatory region DNA binding
CRYM	crystallin mu	GO:0000988~transcription factor activity
CUX2	cut like homeobox 2	GO:0000975~regulatory region DNA binding
ESRRB	estrogen related receptor beta	GO:0001071~nucleic acid binding transcription factor activity
FOXP2	forkhead box P2	GO:0000975~regulatory region DNA binding
HIF3A	hypoxia inducible factor 3 alpha subunit	GO:0000981~RNA polymerase II transcription factor activity
IRF5	interferon regulatory factor 5	GO:0000975~regulatory region DNA binding
MED7	mediator complex subunit 7	GO:0000988~transcription factor activity
MYOC	myocilin	GO:0000988~transcription factor activity
NR2F1	nuclear receptor subfamily 2 group F member 1	GO:0000981~RNA polymerase II transcription factor activity
NR4A3	nuclear receptor subfamily 4 group A member 3	GO:0000975~regulatory region DNA binding,
PPARG	peroxisome proliferator activated receptor gamma	GO:0000989~transcription factor activity
PROX1	prospero homeobox 1	GO:0000975~regulatory region DNA binding
TSHZ2	teashirt zinc finger homeobox 2	GO:0000981 RNA polymerase II transcription factor activity
ZNF711	zinc finger protein 711	GO:0000976 transcription regulatory region sequence-specific DNA binding

Growth factor activity

ENSSSCG00000013511	hepatoma-derived growth factor-related protein 2 (LOC100526035)	GO:0003677~DNA binding
ADAM19	ADAM metallopeptidase domain 19	IPR000742:Epidermal growth factor-like domain
ADAM22	ADAM metallopeptidase domain 22	IPR000742:Epidermal growth factor-like domain
EPHA3	EPH receptor A3	IPR009030:Insulin-like growth factor binding protein
EPHA5	EPH receptor A5	IPR009030:Insulin-like growth factor binding protein
FAT3	FAT atypical cadherin 3	IPR000742:Epidermal growth factor-like domain

KAZALD1	Kazal type serine peptidase inhibitor domain 1	IPR000867:Insulin-like growth factor-binding protein
RSPO2	R-spondin 2	IPR009030:Insulin-like growth factor binding protein
HMCN2	hemicentin 2	IPR000742:Epidermal growth factor-like domain
HGF	hepatocyte growth factor	IPR027284:Hepatocyte growth factor
IGFBP4	insulin like growth factor binding protein 4	GO:0005520~insulin-like growth factor binding
IGFALS	insulin like growth factor binding protein acid labile subunit	GO:0019838~growth factor binding
IGFBP5	insulin-like growth factor binding protein 5	GO:0019838~growth factor binding
LEP	leptin	GO:0008083~growth factor activity
MMRN1	multimerin 1	IPR000742:Epidermal growth factor-like domain
OIT3	oncprotein induced transcript 3	IPR000742:Epidermal growth factor-like domain
PLAU	plasminogen activator, urokinase	IPR000742:Epidermal growth factor-like domain
PDGFRB	platelet-derived growth factor receptor, beta polypeptide	GO:0005017~platelet-derived growth factor-activated receptor activity
PTGS1	prostaglandin-endoperoxide synthase 1	IPR000742:Epidermal growth factor-like domain
PTGS2	prostaglandin-endoperoxide synthase 2	IPR000742:Epidermal growth factor-like domain
SCUBE2	signal peptide, CUB domain and EGF like domain containing 2	IPR000742:Epidermal growth factor-like domain
SLIT2	slit guidance ligand 2	IPR000742:Epidermal growth factor-like domain
SVEP1	sushi, von Willebrand factor type A, EGF and pentraxin domain containing 1	IPR000742:Epidermal growth factor-like domain
TENM1	teneurin transmembrane protein 1	IPR000742:Epidermal growth factor-like domain
TENM3	teneurin transmembrane protein 3	IPR000742:Epidermal growth factor-like domain
VEGFD	vascular endothelial growth factor D	GO:0008083~growth factor activity
VWCE	von Willebrand factor C and EGF domains	IPR000742:Epidermal growth factor-like domain

9.1.3. Cartilage

Candidates with transcription factor or growth factor activity were identified within the transcripts that were enriched in cartilage compared to enthesis.

Table 12: Transcription factors and growth factors that are enriched in cartilage compared to enthesis.

ID	Gene Name	GO molecular function terms (selected) or InterPro domain
Transcription factors		
ENSSSCG00000013049	REST corepressor 2 (RCOR2)	GO:0001071~nucleic acid binding transcription factor activity
GLIS1	GLIS family zinc finger 1	GO:0003702~RNA polymerase II transcription factor activity
NKX3-2	NK3 homeobox 2	GO:0003700~transcription factor activity
NKX6-1	NK6 homeobox 1	GO:0003700~transcription factor activity
CYTL1	cytokine-like 1	GO:0016563~transcription activator activity
SATB1	SATB homeobox 1	GO:0003700~transcription factor activity
DLX3	distal-less homeobox 3	GO:0003700~transcription factor activity
EGR2	early growth response 2	GO:0003700~transcription factor activity
EGR3	early growth response 3	GO:0030528~transcription regulator activity
ETV5	ets variant 5	GO:0003700~transcription factor activity
FOXA3	forkhead box A3	GO:0003700~transcription factor activity
Growth factors		
ENSSSCG00000030998	WNT inhibitory factor 1 (WIF1)	IPR000742:Epidermal growth factor-like domain
ENSSSCG00000027367	fibroblast growth factor receptor 2 (FGFR2)	GO:0005007~fibroblast growth factor-activated receptor activity
ENSSSCG00000001536	signal peptide, CUB and EGF-like domain-containing protein 3 (LOC100152993)	IPR000742:Epidermal growth factor-like domain
ENSSSCG00000001695	vascular endothelial growth factor A (VEGFA)	GO:0070851~growth factor receptor binding
WISP3	WNT1 inducible signaling pathway protein 3	GO:0008083~growth factor activity
BMP7	bone morphogenetic protein 7	GO:0008083~growth factor activity
FGF1	fibroblast growth factor 1 (acidic)	GO:0008083~growth factor activity

FGFR4	fibroblast growth factor receptor 4	GO:0005007~fibroblast growth factor receptor activity
GDF5	growth differentiation factor 5	GO:0008083~growth factor activity
IGFBP5	insulin-like growth factor binding protein 5	GO:0019838~growth factor binding
LIF	leukemia inhibitory factor (cholinergic differentiation factor)	GO:0008083~growth factor activity,
MACC1	metastasis associated in colon cancer 1	GO:0008083~growth factor activity
TGFA	transforming growth factor, alpha	GO:0008083~growth factor activity

9.2. Biomarker differences between proteome and transcriptome

Differences of \log_2 ratios in proteome and transcriptome were calculated for all identified biomarkers.

Table 13: Difference of \log_2 ratios E/T between proteome and transcriptome. \log_2 ratios E/T were compared between proteome and transcriptome data sets by subtraction of \log_2 ratios E/T detected in transcriptomics from \log_2 ratios E/T detected in proteomics.

Gene name	Proteome \log_2 ratio E/T	Transcriptome \log_2 ratio E/T	Δ (Proteome-Transcriptome) \log_2 ratio E/T
TNMD	-1.64	-3.25	1.61
CA3	-1.94	-3.27	1.32
VCAN	2.28	1.03	1.25
PLIN4	-2.24	-3.47	1.23
MXRA5	2.07	1.05	1.02
SPARC	1.92	1.11	0.81
COL2A1	7.08	6.29	0.79
MFAP2	1.32	0.68	0.64
HTRA1	1.68	1.19	0.49
OTOR	-3.28	-3.63	0.36
CHAD	3.00	2.72	0.28
PDLIM4	0.76	0.59	0.16
FABP5	-0.98	-1.13	0.14
CNN2	-0.59	-0.60	0.01
CNRIP1	-0.86	-0.78	-0.08
AKAP12	-2.35	-2.26	-0.10
ACTA2	-0.81	-0.67	-0.14
DYNLRB1	0.39	0.57	-0.18
PRELP	1.00	1.30	-0.30
TAGLN2	0.42	0.72	-0.31
ANXA8	1.57	1.88	-0.31
LOX	0.61	0.92	-0.32
APOA1	-0.97	-0.63	-0.35
COL5A1	0.94	1.31	-0.37
SYNM	0.56	0.93	-0.37
TPPP3	0.98	1.36	-0.38
DPT	0.81	1.47	-0.66
PGK1	0.51	1.23	-0.72
MYOC	-2.02	-1.12	-0.90
PKM	0.65	1.57	-0.92
ACAN	3.40	4.40	-1.00

ENO1	0.54	1.54	-1.00
DCN	-1.85	-0.80	-1.06
KERA	-1.63	-0.56	-1.07
PGAM1	0.47	1.54	-1.08
ECM1	-0.56	1.00	-1.56
COL14A1	-0.98	1.02	-2.00
CLEC3A	3.92	7.23	-3.31
COL9A1	2.97	6.44	-3.47

9.3. Buffers and Solutions

9.3.1. Phosphate Buffered Saline (PBS, 10x)

Phosphate buffered saline (10x) was prepared by dissolving NaCl (115 mM), Na₂HPO₄ (16 mM), KH₂PO₄ (4 mM) in distilled water. The pH was adjusted to pH = 7.4. For further use, the buffer was 1:10 diluted in distilled water.

9.3.2. Phosphate Buffered Saline – Tween[®] 20

PBS (10x) concentrate (9.3.1) was diluted 1:10 in distilled water. 100 µl Tween[®] 20 (Sigma) was added to 1000 ml PBS (1x).

9.3.3. Decalcification Solution

A phosphate buffered solution was prepared by dissolving 87 g NaCl, 12.46 g Na₂HPO₄ × 2 H₂O, and 4.37 g NaH₂PO₄ × 2 H₂O in 10 l distilled water to obtain final concentrations of 0.15 M, 0.007 M, and 0.0028 M, respectively. 1000 g Titriplex and 218.75 g citric acid monohydrate were added and dissolved by heating to 35 °C. The pH was adjusted to pH 7.2 using sodium hydroxide. Samples were incubated with decalcification solution for 4 to 6 weeks on a shaker and decalcification success was estimated with needle puncture.

9.4. Antibody list

The following table lists all primary and secondary antibodies that were used for immunofluorescence stainings.

Table 14: List of primary and secondary antibodies (AB).

Target	Antibody	Manufacturer	Dilution
Primary AB			
Collagen type I*	mouse monoclonal, ab90395	Abcam	1:1000
Collagen type II*	rabbit polyclonal, ab34712	Abcam	1:1000
Collagen type III*	rabbit polyclonal, ab7778	Abcam	1:100
Mouse isotype	Normal mouse IgG, 500-M00	Peprotech	Conc. as primary AB
Mouse isotype	Mouse IgM isotype	eBioscience	Conc. as primary AB
Mouse isotype	Mouse IgG1k isotype	eBioscience	Conc. as primary AB
Rabbit isotype	Normal rabbit IgG, 500-P00	Peprotech	Conc. as primary AB
Rabbit isotype	Rabbit IgG isotype, 02-6102	ThermoFisher Scientific	Conc. as primary AB
Secondary AB			
Anti-rabbit	Atto 647n anti-rabbit IgG, 40839	Sigma	1:200
Anti-rabbit	Alexa Fluor® 647 anti-rabbit IgG, A-21245	ThermoFisher Scientific	1:200
Anti-mouse	Alexa Fluor® 594 anti-mouse IgG, 115-587-003	Dianova	1:200
Anti-mouse	Alexa Fluor® 488 anti-mouse IgG, 115-545-062	Dianova	1:200
Anti-mouse	Alexa Fluor® 488 anti-mouse IgG, A-11001	ThermoFisher Scientific	1:200

*antibodies were 1:1 diluted with glycerol upon arrival